MOLECULAR MECHANISMS CONTROLLING NEUROVASCULAR PATTERNING

CHARLOTTE MADEN

Thesis submitted in fulfilment of the requirements for the degree of

Doctor of Philosophy

University College London

Institute of Ophthalmology

Supervisor: Dr Christiana Ruhrberg

DECLARATION

I, Charlotte Maden, confirm that the work presented in this thesis is my own. Where information has been derived from other sources, I confirm that this has been indicated in the thesis.

ACKNOWLEDGEMENTS

I would like to thank my supervisor Christiana Ruhrberg for her support, guidance and enthusiasm. The rest of the Ruhrberg lab have been amazing, including current members - Alex Fantin, Fran Mackenzie, Brett Hosking and the superb PCR shop keepers, Kathryn Davidson and Laura Denti - as well as old members - Quenten Schwarz, Joey Vieira and Ivan Wall. The office is always a fun place to be, mainly thanks to Mike, Natalie and biscuits. And thank you anyone in Cell Biology I have ever pestered! Also thanks to the Medical Research Council for funding my studies.

A massive thank you to my family - to Mum for constant encouragement, to Dad for his help and making me get on with it, to Tom for cheering me up - and to Nick for getting me through it.

ABSTRACT

The vascular system delivers oxygen and nutrients to tissues throughout the developing organism, including the nervous system. Vice versa, the nervous system innervates resistance arteries to modulate vascular function. The two systems share several guidance cues and cell-surface receptors. One receptor is neuropilin 1 (NRP1), which is present on blood vessels and neurons.

The sympathetic nervous system is a neural crest cell (NCC)-derived structure that innervates the heart and blood vessels to modulate heart rate and vasoconstriction. Semaphorin3A (SEMA3A) signals through NRP1 to pattern the axonal projections of sympathetic nerves. I show here that this signalling pathway also controls the earliest stage of sympathetic nervous system development - sympathetic NCC migration through the somites. Accordingly, sympathetic NCCs stray into ectopic territories and differentiate into sympathetic neurons in mice with disrupted NRP1/SEMA3A signalling. I also show that NRP2/SEMA3F signalling provides a backup pathway for NRP1/SEMA3A signalling in sympathetic NCC guidance. I further show defective sympathetic innervation of the heart and dorsal aorta in postnatal mice with disrupted NRP1/SEMA3A signalling and describe a previously unidentified role for NRP2 in sympathetic axon guidance. I found that the recently discovered SEMA3G does not play a part in sympathetic axon guidance to target arteries, despite its unique arterial expression.

The alternative NRP1 ligand, a vascular endothelial growth factor isoform termed VEGF164, is essential for the sprouting of new blood vessels from existing ones in a process called angiogenesis. A large body of *in vitro* evidence suggests that heparan sulphate proteoglycans (HSPGs) are required for VEGF164-driven angiogenesis by promoting its interaction with its receptors VEGFR1, VEGFR2 and NRP1. *In vivo* data supporting the idea that HSPGs are essential for angiogenesis, however, are sparse. I here found that mouse embryos lacking enzymes required for the sulphation of HSPGs, or lacking enzymes essential for HSPG production in specific cells, had no obvious vascular branching defects in the hindbrain and do not phenocopy mutants lacking VEGF164. These observations suggest that HSPGs are not essential for VEGF164-driven angiogenesis. In contrast, I found that the VEGF164/NRP1 guided migration of facial branchiomotor neurons was dependent on the presence of HSPGs. Taken together, these results provide evidence for the differential requirement of HSPGs in VEGF164-driven neural, but not endothelial cell patterning in the hindbrain.

TABLE OF CONTENTS

LIST OF FIGURES

LIST OF TABLES

ABBREVIATIONS

aCasp3	activated Caspase3
AP	Alkaline phosphatase
β-Gal	β-galactosidase
BCIP	5-bromo-4-chloro-3-indolyl phosphate
BMP	Bone morphogenetic protein
BSA	Bovine serum albumin
CASH1	Chick achaete-scute homolog 1
CNS	Central nervous system
DAB	Diaminobenzidine
DCC	Deleted in colorectal cancer
DIG	Digoxigenin
DMSO	Dimethylsulfoxide
dNTP	Deoxyribonucleotide triphosphate
cDNA	Complementary deoxyribonucleic acid
DNase	Deoxyribonuclease
dpc	Days post coitum
DRG	Dorsal root ganglia
ECM	Extracellular matrix
EDTA	Ethyldiaminotetraacetic acid, disodium salt
EMT	Epithelial-to-mesenchymal transition
EXT	Exostosin
FBM	Facial branchiomotor (neuron)
FGF	Fibroblast growth factor
FLK1	Fetal liver kinase 1 (VEGFR2)
FLT1	Fms-like tyrosine kinase 1 (VEGFR1)
GAG	Glycosaminoglycan
Gal	Galactose
GDNF	Glial cell line-derived neurotrophic factors
GlcA	*D*-glucuronic acid
GlcNAc	*N*-acetyl glucosamine

GlcNS	*N*-sulphated glucosamine
GPI	glycosylphosphatidylinositol
HRP	horseradish peroxidase
HS2ST	Heparan sulphate 2-*O*-sulphotransferase
HS3ST1-3	Heparan sulphate 3-*O*-sulphotransferase
HS6ST1-3	Heparan sulphate 6-*O*-sulphotransferase
HSPG	Heparan sulphate proteoglycan
IB4	*Bandeirae simplicifolia* BS-I isolectin B4
IdoA	Iduronic acid
Ig	Immunoglobulin
Isl1	Islet1
ITAM	Immuno-receptor tyrosine-based activation motif
MASH1	mammalian achaete-scute homolog 1
mRNA	Messenger ribonucleic acid
N-CAM	N-cell adhesion molecule
NBT	4-Nitro-blue-tetrazoliumchloride
NDST	*N*-deacetylase/*N*-sulphotransferase
NF	Neurofilament
NGF	Nerve growth factor
NGS	Normal goat serum
NIP1	Neuropilin interacting protein 1
NRP	Neuropilin
NRS	Normal rabbit serum
NTMT	NaCl, Tris-HCl, $MgCl_2$, Tween-20 buffer
PBS	Phosphate buffered saline
PBT	PBS and TritonX100
PCP	Planar cell polarity
PCR	Polymerase chain reaction
PDZ	Postsynaptic density-95/Discs large/Zona occludens
PECAM	Platelet-endothelial cell adhesion molecule
PFA	Paraformaldehyde
PNS	Peripheral nervous system

r	Rhombomere
RNase	Ribonuclease
RT	Room temperature
SCG	Superior cervical ganglia
SDS	Sodium dodecyl sulphate
SEMA3	Class 3 semaphorin
SMA	Smooth muscle actin
SULF	Sulphatase
TAE	Tris acetate EDTA buffer
TBE	Tris borate EDTA buffer
TBS	Tris buffered saline
TBST	TBS and Tween20
TE	Tris-EDTA buffer
TH	Tyrosine hydroxylase
VEGF	Vascular endothelial growth factor
VEGFR	VEGF receptor
VIIn	Facial nuclei
Vn	Trigeminal nuclei
XIIn	Hypoglossal nuclei
X-Gal	5-bromo-4-chloro-3-beta-D-galactopyranoside

CHAPTER 1. INTRODUCTION

The vascular system is essential for development of the vertebrate embryo. It delivers oxygen and nutrients to allow growth of all of the tissues in the organism, including the nervous system. Vice versa, the nervous system innervates resistance arteries to modulate vasculature function. In this thesis, I have firstly investigated the molecular control of the development of the sympathetic nervous system, which innervates the heart and arteries of the vascular system. I have paid particular attention to the neuropilins, signalling receptors involved in both angiogenesis and neurogenesis that bind both semaphorins and vascular endothelial growth factor (VEGF). Secondly, I have assessed the role of heparan sulphate proteoglycans in VEGF-driven vascularisation and motor neuron migration in the developing mouse hindbrain.

1.1 Molecular mechanisms controlling the development of the sympathetic nervous system

The sympathetic nervous system innervates a wide variety of targets, including exocrine and endocrine glands and ducts, smooth muscle layers of the intestine and pilomotor muscles, as well as smooth muscle layers of the blood vessels and the cardiac muscles and nodes of the heart, to initiate changes in response to stress. It consists of preganglionic and postganglionic neurons – the former being neuroectoderm-derived nerves synapsing the central nervous system (CNS) to the latter. From here on, I will refer to the postganglionic sympathetic neurons simply as sympathetic neurons. They have cell bodies in aggregations known as sympathetic ganglia, and extend axons to distal locations. The paravertebral ganglia lie in bilateral chain formations in the trunk region, parallel to the vertebral column, and the prevertebral ganglia, forming the superior cervical ganglia, are in the cranium. Also part of the sympathetic nervous system are the chromaffin cells of the adrenal medulla. All sympathetic neurons are derived from neural crest cells.

1.1.1 The Neural Crest

The cells of the neural crest (NC) were first described in 1868 by the Swiss embryologist Wilhelm His, who initially named them 'Zwischenstrang' – the intermediate cord. They are a transient population of multipotent cells fundamental and specific to developing vertebrates and give rise to a diverse range of cell types.

Different subpopulations of neural crest cells (NCCs) exist, which are classified by the pattern of their emergence from the neural tube and the organ systems they contribute to:

- Cranial neural crest emerge from the hindbrain and give rise to neurons, glia and melanocytes, as well as cranial bones and connective tissue, of the head
- Cardiac neural crest emerge between the otic vesicle and the third somite in the mouse and give rise to autonomic neurons and glia, smooth muscle cells of the great vessels and melanocytes
- Trunk neural crest emerge from the spinal cord, between somites 7 and 28 in the mouse and give rise to sensory and sympathetic neurons, glia, chromaffin cells and melanocytes
- Vagal neural crest emerge in the neck, between somites 1 and 7 in the mouse and give rise to enteric neurons of the gut, glia and melanocytes
- Sacral neural crest emerge from the spinal cord, between somites 7 and 28 in the mouse and give rise to enteric neurons of the hindgut, glia and melanocytes

1.1.2 Induction of Neural Crest

1.1.2.1 Neurulation

NCCs form in the neural tube. In early development, at around embryonic day (E) 7.25 in the mouse, neuroectoderm is induced from the ectodermal germ layer and forms the neural plate. During a process called neurulation, the neural plate progressively folds in on itself, creating the neural folds at the borders between non-neural ectoderm and neuroectoderm (Fig. 1.1). The ventral midline of the neural plate aligns with the notochord and the neural folds conjoin to form the dorsal aspect of the neural tube – the site of NCC formation. Closure of the neural tube occurs in a rostrocaudal, or anteroposterior, sequence; i.e. neural tube closure in the trunk proceeds from the older, anterior end to the younger, posterior end. This direction of anteroposterior development is echoed throughout trunk development, for example in somitogenesis (for review (Gridley, 2006)).

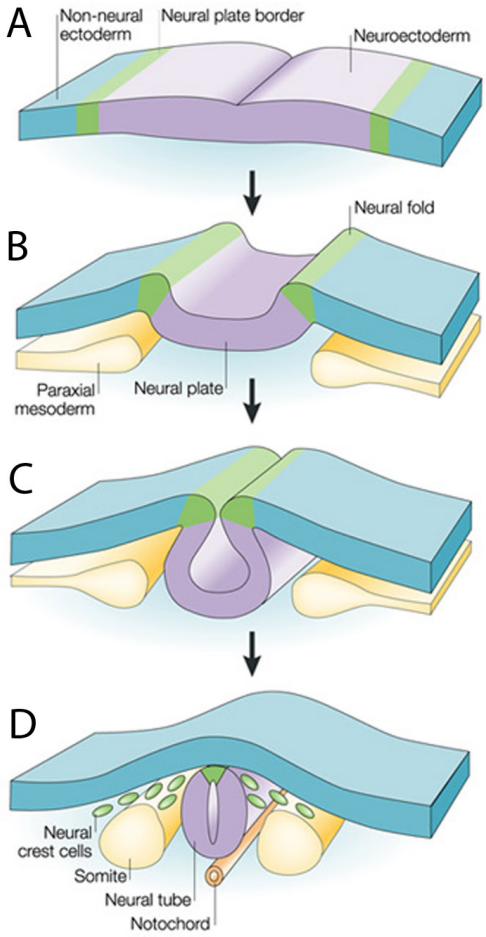

Figure 1.1: Development of the neural tube.

(A) The ectoderm is flat with defined areas of neural tissue (neuroectoderm, purple), non-neural tissue (ectoderm, blue) and neural plate border (green). (B) At the beginning of neural induction, the neuroectoderm folds and the neural plate is induced. Paraxial mesoderm is formed. (C) The neural folds come together and the neural tube begins to form. (D) The neural tube has closed, separated from the overlaying epidermis and aligned with the notochord. NCCs are induced from neural folds at dorsal aspect of neural tube, and are shown here delaminating. The somites have also formed from paraxial mesoderm (Diagram adapted from (Gammill and Bronner-Fraser, 2003)).

Signalling between the epidermal ectoderm and the newly formed neural tube initiates NCC induction soon after neural tube closure. Signals from the underlying mesoderm have also been implicated in the process, although are not thought to be essential, as ectoderm is able to compensate for loss of signals in the absence of mesoderm, shown by studies in zebrafish (Ragland and Raible, 2004). Several morphogens are implicated in NC induction, including WNTs, bone morphogenetic proteins (BMPs) and fibroblast growth factors (FGFs), which act in concert.

1.1.2.2 Morphogenetic induction signals

WNTs: WNTs are multifunctional secreted signalling proteins that bind to receptors from the frizzled family (see (Schmidt, 2008) for review) and are involved in two signalling pathways. The first is the canonical WNT pathway, which, briefly, involves activation of β-catenin to stimulate TCF/LEF transcription factors. The second is the non-canonical WNT pathway, which is β-catenin independent. WNTs are expressed in the dorsal neural tube and are necessary and sufficient for NCC induction (Wu et al., 2003). It has recently been suggested that the specific family member required for this role is WNT6 in chick (Schmidt et al., 2007).

BMPs: BMPs are multifunctional secreted proteins best known for their function in dorsoventral patterning. BMP2, 4 and 7, are expressed in epidermal ectoderm and are involved in neural crest formation (Liem et al., 1995). A BMP gradient develops through BMP interaction with antagonists, such as noggin, in the ectoderm that specifies dorsoventral patterning, with the neural plate border cells, NCCs, forming at intermediate levels of BMP signalling. The specific role for BMPs in NCC induction itself, however, is still debated. A recent study provides evidence for the interplay between WNTs and BMP signalling in neural crest induction: an initial stage of induction requires WNT activation alongside BMP inhibition, then a second stage requires the activation of both pathways for the maintenance of the process (Steventon et al., 2009).

FGFs: FGFs are multifunctional secreted proteins widely involved in embryonic development, growth regulation and morphogenesis. They are known to function in the induction of NCCs, albeit indirectly as modifiers of the WNT pathway, and FGF8 in particular is implicated (Monsoro-Burq et al., 2005).

Notch ligands: Serrate and Delta protein ligands bind to Notch receptors to regulate cell fate decisions. In contrast to WNT/BMP/FGF signalling, Notch signalling results from direct cell-cell contact and downstream signalling occurs in adjacent cells only. The Notch signalling pathway has two suggested roles in NCC development; firstly in induction, although a specific role in mouse trunk NCC is yet to be shown, and later in cell fate diversification (Cornell and Eisen, 2005).

Retinoic acid: Retinoic acid has also been suggested to have a role in NCC induction as it is able to induce NCCs from neural fold tissue in an *in vitro* induction model (Villanueva et al., 2002).

1.1.2.3 NC-specifying transcription factors

The induction of NCCs by morphogenetic signals is followed by expression of NC-specifying transcription factors, which promote continuing NCC generation. These are discussed below.

SNAIL/SLUG: SNAIL (SNAI1), a zinc finger transcription factor, and its close relative SLUG (SNAI2) are involved at several stages in NCC development, such as specification and induction via the WNT pathway. They are expressed specifically in NCCs and can therefore be utilised as NC markers (Hemavathy et al., 2000).

FOXD3: FOXD3 is a winged-helix transcription factor also specific to NCCs, and has been shown to function as a transcriptional activator for genes involved in cell multipotency. (Dottori et al., 2001; Kos et al., 2001)

SOX9/SOX10: The group E Sox proteins, SOX8, 9 and 10, are high-mobility group (HMG)-domain transcriptional activators with multiple and overlapping functions in development. In particular, SOX9 is required for NCC induction and delamination and subsequent survival (Cheung et al., 2005) and SOX10 is required for NCC induction, specification and differentiation (Carney et al., 2006; Kelsh, 2006; Southard-Smith et al., 1998). Later, SOX9 and SOX10 synergise with other transcription factors to initiate differentiation in NCCs (Cheung and Briscoe, 2003).

PAX: The PAX transcriptional activators are stimulated at this point, although they are not NCC- specific as they are also expressed in the neural plate environment (Wang et al., 2008).

ZIC: The Zic family of zinc-finger transcription factors, also expressed in NCCs and the neural plate, are thought to be involved in proliferation and specification of NCCs (Nakata et al., 1998).

AP2: There are some additional NCC markers that are also expressed in the non-neural ectoderm, such as the transcription factor Ap2 (Mitchell et al., 1991).

1.1.3 Delamination

Once NCCs have been fully induced, they are situated in the dorsal neural tube as epithelial-like cells and adopt a regular and elongated shape. Delamination is the process by which the NCCs leave the dorsal neural tube at around E8.5 of mouse development.

They undergo epithelial-to-mesenchymal transition (EMT), literally a transition of the cells from a two-dimensional organisation in the neural epithelium into a three-dimensional mesenchymal-like organisation (Nakaya and Sheng, 2008). EMT occurs in many other processes, both in normal embryogenesis and adulthood, for example tissue repair and tumour metastasis. EMT in delaminating NCCs is tightly controlled, primarily, although not exclusively, by SNAIL and SLUG. SOX9 and FOXD3 are involved in EMT activation, working synergistically with SNAIL and SLUG (Cheung et al., 2005; Sakai et al., 2006). BMPs also take part, most prominently BMP4 in chick, which acts through the upregulation of RhoB, a RhoGTPase that modulates cell dynamics (Groysman et al., 2008). Together these proteins bring about EMT by breaking adherens and tight junctions through regulation of adhesion proteins on NCCs. Thus, a switch in the expression mixture of integrins and cell adhesion molecules on the NCCs takes place, with the down-regulation of N-CAM, N-cadherin and E-cadherin, and a concomitant down-regulation of cadherin-6b and up-regulation of cadherin-7 in chick (Taneyhill et al., 2007). Claudins and occludin are also repressed, according to cell culture work (Ikenouchi et al., 2003). These changes allow the NCCs to completely dissociate from the epithelial sheet. The neural tube epithelium, however, does not seem to be disrupted by EMT; it remains intact, which further demonstrates the tight regulation of the process (for review (Duband, 2006)). During delamination, the morphology of the NCCs changes dramatically, and they become irregular in shape and extend filopodia at the leading edge.

1.1.4 Migration

Once trunk NCCs have emerged from the neural tube, they aggregate in an extracellular matrix-rich area called the migration staging area, located between the neural tube, the dorsal somite and the surface epithelium (Weston, 1991). From here the NCCs undergo significant migratory movements, commencing just before E9.0 in the mouse, which are highly directional and ordered. It has been proposed that NCCs migrate by 'contact inhibition' that is controlled by WNT proteins and their frizzled receptors via the non-canonical planar cell polarity (PCP) pathway, in which PCP factors polarise a field of cells along an axis, and cause cytoskeletal changes that lead to migration through the small GTPases RhoA and Rac (for review (Alfandari et al., 2010)). WNT11 in particular has been implicated in *Xenopus* (De Calisto et al., 2005), and syndecan4, a heparan sulphate proteoglycan, also contributes to PCP-controlled directional migration by influencing the orientation of cell protrusions (Matthews et al., 2008).

By this stage in development, the somites have formed. These are paired masses of mesoderm that are segmentally arranged along the anteroposterior axis of the early

vertebrate embryo. Somites are composed of three layers: sclerotome, which forms vertebral structures, myotome, which forms muscle, and dermotome, which forms dermis.

1.1.4.1 Migration patterns

Live imaging of NC migration (for example (Kasemeier-Kulesa et al., 2005)) has shown that NCCs initially emerge from the neural tube in an unsegmented manner, but subsequently migrate in distinct streams along different paths through the embryo (Fig. 1.2). The first group of trunk NC begins migration at about E8.75 and travels ventrally and medially along a 'ventromedial' pathway, avoiding the more superficial dermotome and myotome (dermomyotome) layers. These are referred to as **early wave NCCs**, and move between adjacent somites, in the intersomitic boundary, following the intersomitic blood vessels. The bulk of the NCCs on the ventromedial path migrates slightly later and travels through the anterior half of the sclerotome of each somite, avoiding the posterior half and the dermomyotome layers (Bronner-Fraser, 1986; Rickmann et al., 1985). These are referred to as **intermediate wave NCCs**. The remainder of the cells, having delaminated later or waited in the migration staging area for about one day of development, form the **late wave of migrating NCCs**. They move on the dorsolateral pathway in close proximity to the overlying ectoderm, and will form the melanocytes of the skin (Erickson et al., 1992).

Of the early wave of migrating trunk NC, the cells travelling the furthest arrest migration near the dorsal aorta and will later differentiate into the neurons and glia of the sympathetic nervous system. The remainder of the early migrating cells will arrest further dorsally in the somite and become the sensory neurons and glia of the dorsal root ganglia (DRG). When I started my thesis research, it was debated if the fate of each NCC depends on signals from their local environment once they have delaminated and migrated, but gathering evidence supports that NCC fate is predetermined at the time of delamination. For example, a lineage tracing study in chick provided evidence for fate being defined by the dorsoventral position of the pre-migratory NCC in the neural tube and the timing of their delamination. Based on this, when neural-fated NCCs were extracted and reinserted into the melanocyte-fated NCC migratory stream, they were still able to differentiate into a neural fate (Krispin et al., 2010).

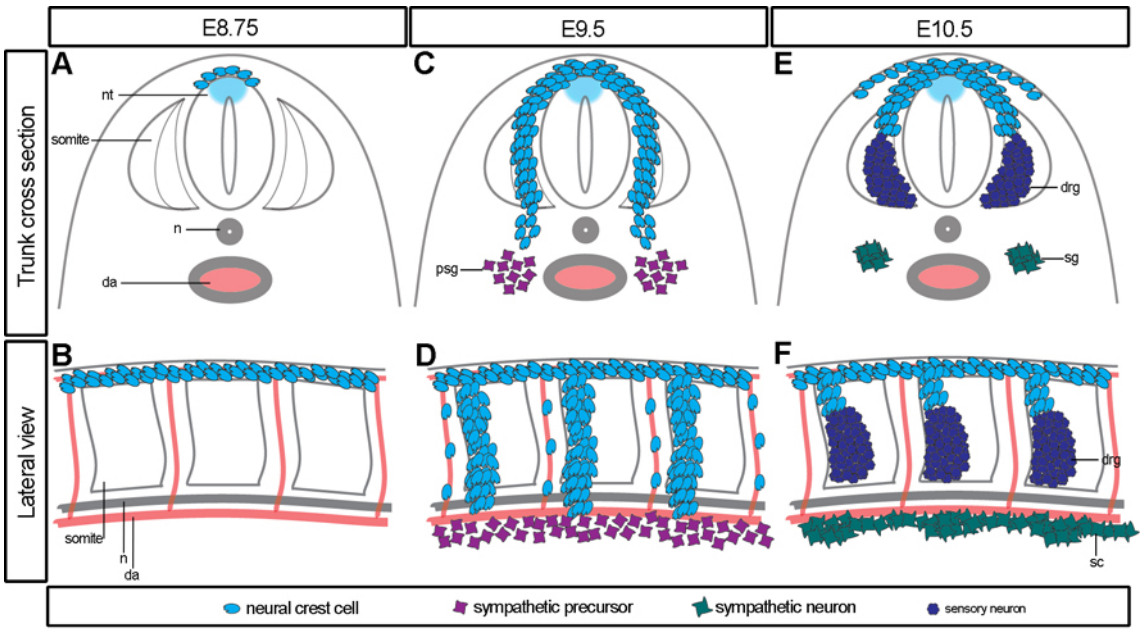

Figure 1.2: Stages and patterns of NCC migration.

At E8.75, the early wave of NCCs have delaminated from the neural tube (nt; A) into the migration staging area along the dorsal neural tube (B). At E9.0, they begin to migrate through the ventromedial pathway (as in C), a few along the intersomitic boundary but mostly through the anterior half of each somite, with the posterior somite and dermomyotome layers kept NCC-free (as in D). The earliest of these NCCs arrest migration at the dorsal aorta (da) at E9.5 to seed the primary sympathetic ganglia (psg), and differentiate into sympathetic precursors (C,D). At E10.5, the sympathetic precursors undergo a secondary migratory movement away from the dorsal aorta (E), differentiate into mature sympathetic neurons and form the sympathetic ganglia (sg) of the sympathetic chain (sc; F). Other NCCs on the ventromedial pathway arrest further dorsally to form the dorsal root ganglia (drg). n, notochord.

The segmental migration pattern of the trunk NC through the anterior sclerotome places the NCCs in the correct location for further development into neurons of the sympathetic ganglia or sensory neurons of the DRG. Similarly, but independently of NCCs, once motor neuron axons emerge from the neural tube, they enter only the anterior half of each somite (Keynes and Stern, 1984; Rickmann et al., 1985). The significance of this segmental migration pattern on DRG formation was initially illustrated by grafting experiments in chick; correct morphogenesis and segmentation of the DRG does not occur when the anteroposterior migration pattern is disrupted by transplantation (Kalcheim and Teillet, 1989).

1.1.4.2 Transcriptional control

A complex network of signals regulates NCC migration (for review (Kulesa et al., 2009)). Fundamental co-ordinators for NCC migration are the previously described transcription factors SOX10 and FOXD3. In the mouse, whereas SOX9 is specific to pre-migratory NCC (Cheung et al., 2005), SOX10 is expressed in migratory NCC as it is required for multipotency and specification of the different NCC fates (Carney et al., 2006; Cheng et al., 2000; Kelsh, 2006). FOXD3 regulates the expression of cell-cell adhesion molecules required for migration (Cheung et al., 2005), for example cadherins and integrins.

1.1.4.3 Migration guidance cues

Both permissive and inhibitory signals from the extracellular matrix guide migration, for example fibronectin (Rovasio et al., 1983) and F-spondin (Debby-Brafman et al., 1999), respectively. Additionally, a host of mesenchymally-derived proteins, initially known for their axon guidance functions, have now been shown to provide attractive or repulsive cues to guide NCC migration through their respective receptors expressed by trunk NCCs (for review (Kuriyama and Mayor, 2008)). These are discussed below.

Ephrins/Ephs: Based on research showing the action of ephrins and their Eph receptors in repulsive axon guidance, ephrin ligands secreted by the caudal half of each somite were found to repel migrating trunk NCCs *in vitro*, which express Eph receptors (Wang and Anderson, 1997). *In vivo* work in chick demonstrated that transmembrane ephrinB1, expressed in the caudal sclerotome, prevents NCCs that express its receptor Eph-B3 from entering the caudal somite (Krull et al., 1997). EphrinB ligands also prevent early ventrally migrating NCCs from entering the dorsolateral pathway through their Eph-B receptors, but conversely, then promote migration of melanocyte-fated NCCs along the dorsolateral pathway (Santiago and Erickson, 2002).

Semaphorins/neuropilins: Class 3 semaphorins are well-established axonal guidance molecules. Semaphorin3A (SEMA3A) signalling through its neuropilin 1 (NRP1) receptor has been implicated as a repulsive cue in NCC migration in *in vitro* assays (Eickholt et al.,

1999), and SEMA3A/NRP1 signalling acts as a repulsive cue for cranial NCC migration in chick (McLennan and Kulesa, 2007; Osborne et al., 2005) and mouse (Schwarz et al., 2008a), but was reported to have no effect in mouse trunk NCC migration (Kawasaki et al., 2002). SEMA3F, expressed in the caudal sclerotome, prevents trunk NCCs expressing NRP2 from entering the rostral somite (Gammill et al., 2006). Semaphorins and their neuropilin receptors will be discussed in more detail later in the chapter, as their role in mouse NCC migration was a major focus of this thesis.

Slits/Robos: In chick, Slit2 is produced by mesenchyme surrounding the gut, and acts as a chemorepellant, preventing trunk NCCs which express Robo1 and Robo2 receptors from entering the gut (De Bellard et al., 2003). It also speeds up their migration away from the Slit2-positive area. Vagal NCCs destined for the enteric nervous system do not express Robo1 and Robo2 and can therefore penetrate the gut and migrate its entire length to populate it (De Bellard et al., 2003). Additionally, Slit2 is produced in the dermomyotome during early NCC migration, and predominantly through the Robo1 receptor helps confine early migrating NCCs to their ventromedial pathway. Experiments in chick found ectopic NCC migration along the dorsolateral route at early stages when a dominant negative Robo1 receptor was expressed in early NCC (Jia et al., 2005).

Stromal cell derived factor (SDF)-1/CXCR4: The chemokine SDF-1 acts as an attractive cue for CXCR4-expressing sympathetic NCCs to migrate ventrally towards the dorsal aorta, segregating them from NCCs destined for the dorsal root ganglia in chick (Kasemeier-Kulesa et al., 2010). In mice, CXCR4 is thought to be expressed by sensory NC populations destined for the DRG, and DRGs in mice lacking CXCR4 are disorganised, however the sympathetic ganglia were not examined (Belmadani et al., 2005). It has been suggested that *in vitro* SDF-1 also modulates semaphorin signalling in axons (Chalasani et al., 2003), which may provide a mechanism for NCC migration through SEMA3A-expressing mesenchyme.

Netrins/DCC: Netrins have been shown to attract migrating NCCs through the DCC receptor in vagal regions of the chick and mouse (Jiang et al., 2003), although there is currently no evidence for a role for netrins in migrating NCCs in the trunk region.

Neuregulin-1/ErbB2/3: Sympathetic-fated NCCs require mesenchymally-expressed Neuregulin-1 signalling through its tyrosine kinase receptor complex ErbB2/ErbB3 for correct migration of NCCs and for aggregation of sufficient numbers of NCCs at the dorsal aorta (Britsch et al., 1998). Mice lacking neuregulin-1, ErbB2 or ErbB3 therefore have hypoplasia of the sympathetic nervous system.

1.1.5 Sympathetic Nervous System Development

1.1.5.1 Differentiation into sympathetic precursors

As previously mentioned, the first of the early wave trunk NCCs migrating along the ventromedial pathway are destined to become sympathetic neurons and aggregate proximal to the dorsal aorta. Once arrived, at around E9.5 in the mouse, it is thought that dorsal aorta-derived BMP2, 4 and 7 signalling initiates differentiation of these NCCs into sympathetic precursors (Schneider et al., 1999; Shah et al., 1996). However, studying this process is difficult, as BMP knockout mice die early in development (for example (Luo et al., 1995)). In mice lacking ALK3 in NCCs, a BMP receptor, sympathetic NCCs differentiate but die at E10, providing evidence for BMPs not inducing differentiation, but being survival factors for NCCs (Morikawa et al., 2009). Consistent with this, CASH1, a sympathetic NCC specifier in chick, is switched on in NCCs before BMP4 in chick, suggesting that BMPs are not essential for differentiation into a sympathetic fate (McPherson et al., 2000).

NCC differentiation is achieved via activation of a complex interplay of transcription factors in NCC (Huber, 2006; Reissmann et al., 1996; Schneider et al., 1999) (Fig. 1.3). These include the mammalian achaete-scute homolog 1 (MASH1), the paired homeodomain proteins PHOX2B (Pattyn et al., 1999) and PHOX2A (Morin et al., 1997), basic helix-loop-helix factor HAND2 (Morikawa et al., 2007) and zinc-finger factor GATA3 (Tsarovina et al., 2004). MASH1 and PHOX2B are essential for autonomic differentiation and are markers for the precursory sympathetic neuronal state. Briefly, it is thought that PHOX2B activates or maintains MASH1; together, they both activate PHOX2A, and through separate pathways also aid in the progression towards a sympathetic neuronal cell fate via HAND2 and GATA3 (for review (Huber, 2006)). The sympathetic precursors form two primary sympathetic chains, loosely arranged ganglia bilaterally flanking the dorsal aorta.

1.1.5.2 Further migration and differentiation

After induction into sympathetic precursors, a secondary migration step takes place in which the precursors migrate away slightly from the dorsal aorta and differentiate into either sympathetic neurons or chromaffin cells of the adrenal medulla, depending on their location in the trunk (Anderson et al., 1991; Ernsberger et al., 1995) (Fig. 1.3). The mature sympathetic neurons become more closely associated and form the ganglia of the sympathetic chain, and begin to express neuronal and catecholaminergic markers (Cochard et al., 1978). Tyrosine hydroxylase (TH), an enzyme required for the synthesis of noradrenalin by neurons, is produced, as well as dopamine beta-hydroxylase. General neuronal markers also start to be expressed at this time, such as neurofilaments (NF), intermediate filaments specific to neurons, and SCG10, a membrane-bound protein

specific to neurons (Wuenschell et al., 1990). Chromaffin cells of the adrenal medulla downregulate neuronal markers and induce adrenaline synthesising enzymes.

The sympathetic neurons remain dynamic at this point. Some neurons migrate further anteriorly to become part of the prevertebral ganglia and the superior cervical ganglion (SCG). Additionally, some neurons begin to extend axonal processes along the chain in an anteroposterior fashion, joining the ganglia to complete the chain-like structure. Axon extension from cell bodies stretching outside of the chain towards target organs commences at around E13 in the mouse. For example, the internal and external carotid arteries have sympathetic axons associated with them by E13.5 (Makita et al., 2008).

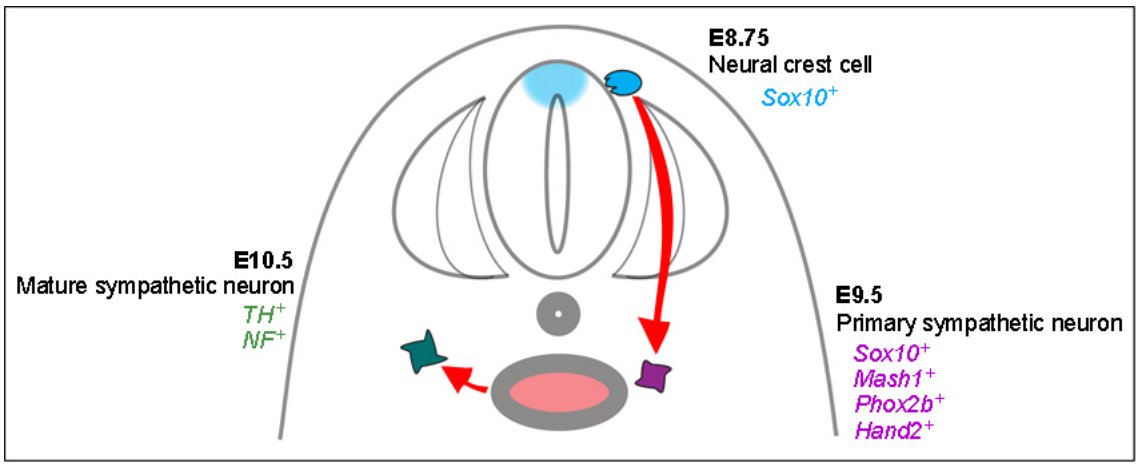

Figure 1.3: Transcription factors and markers involved in sympathetic neuron development from NCCs.

Sox10 is expressed by sympathetic NCCs once they delaminate from the neural tube at E8.75 and expression is continued during NCC migration through the somite. Sympathetic NCCs arrest migration at the dorsal aorta at E9.5, where they differentiate into primary sympathetic anlagen and express *Mash1*, *Phox2b* and later *Hand2* whilst still expressing *Sox10*. At E10.5 the sympathetic anlagen migrate away from the dorsal aorta and mature into sympathetic neurons. The *Sox10, Mash1*, *Phox2b* and *Hand2* transcription factors are switched off and the neurons express sympathetic-specific tyrosine hydroxylase (TH) and neuronal markers such as neurofilament (NF).

1.1.5.3 Target innervation: the heart

One of the target organs innervated by the sympathetic nervous system is the heart, which is also extensively innervated by other autonomic nerves. Surprisingly little is known about the development of sympathetic innervation of the heart. It is thought that sympathetic nerves augment cardiac performance by modulating heart rate, conduction velocity, myocardial contraction and relaxation in response to stress, and several studies have suggested that the pattern of sympathetic innervation is critical for effective cardiac performance in humans (for example (Cao et al., 2000a; Cao et al., 2000b)). Sympathetic axons from the stellate ganglia, a prevertebral ganglion, extend to the base of the heart, descend the pulmonary arteries and innervate the left and right atria and ventricles of the heart, which was elucidated by studies in dog and human (Crick et al., 1994; Randall et al., 1968). Sympathetic fibres are also present in the atrioventricular and sinus nodes, but not in the nerve bundles of the human conduction system (Chow et al., 1993). Sympathetic nerve fibres reside mainly in the epicardial surface of the heart, with fibres entering deeper layers of myocardium in decreasing numbers. During mouse embryonic development, sympathetic fibres remain on the surface epicardium. At birth, they begin to penetrate the endocardium, and by early adulthood an epicardial-to-endocardial gradient of sympathetic fibres is apparent (Ieda et al., 2004; Ieda et al., 2007). SEMA3A expression in the subepicardium maintains this gradient (Ieda et al., 2007), as discussed later (Chapter 1.1.7.3).

1.1.6 Patterning of the sympathetic nervous system

1.1.6.1 Vascular signals

Axonal outgrowth from the sympathetic chain often occurs in close proximity to blood vessels, and most sympathetic trunks travel along blood vessels thereafter (Makita et al., 2008). This has led to the suggestion that cues from blood vessels regulate sympathetic nervous system growth. In agreement with this, vascular-derived signals act as sympathetic axon growth or survival factors, despite not being required for initial sympathetic development.

Endothelins: A member of the endothelin family, Edn3, released from external carotid arteries and signals through the endothelin receptor EdnrA to guide a subset of sympathetic axons expressing the receptor towards their target in mice, the external carotid arteries (Makita et al., 2008).

Glial cell line-derived neurotrophic factors (GDNF) family ligands/RET receptors: Artemin, neurturin and persephin are vascular-derived GDNF family members. Mice deficient in

artemin/RET signalling have less sympathetic proliferation, mis-routed sympathetic axons and accelerated sympathetic neuronal death (Andres et al., 2001; Enomoto et al., 2001; Honma et al., 2002).

1.1.6.2 Non-vascular derived signals:

Neurotrophins/nerve growth factor (NGF): The classic neurotrophin, NGF, is a chemoattractant required for proper sympathetic innervation of target organs. Mice with deficient NGF signalling have no sympathetic innervation of heart ventricles and submaxillary and parotid glands, although proximal projections are preserved (Glebova and Ginty, 2004). Overexpression of neurotrophin 3 increases the number of sympathetic neurons (Albers et al., 1996).

Semaphorins/neuropilins: Semaphorins are implicated in sympathetic nervous system patterning through their neuropilin receptors, as discussed below.

1.1.7 Semaphorins and neuropilins

1.1.7.1 Semaphorins

Semaphorins are a diverse family of secreted, transmembrane or glycosylphosphatidylinositol (GPI)-linked signalling proteins, characterised by a 500 amino acid sema domain. There are over 20 known semaphorins, belonging to eight classes according to classification based on structure and amino-acid sequence (for review (Yazdani and Terman, 2006)). With the exception of class 2 semaphorins, all semaphorins bind the plexin family of transmembrane receptors. Plexins are grouped into four categories (A-D), and contain a sema domain to mediate the interaction with SEMAs. Relevant to this study are the vertebrate-specific secreted class 3 semaphorins (SEMA3s), which have a stretch of highly basic amino acids in their carboxy-terminal region. To date seven class 3 semaphorins have been identified, named SEMA3A to SEMA3G. SEMA3s are best known for their role in nervous system development as repulsive axon guidance cues, due to their ability to collapse growth cones of developing neurons by redistribution of the cytoskeleton and endocytosis of the growth cone cell membrane, hence SEMA3A was in fact originally named collapsin-1 (Luo et al., 1993). SEMA3 molecules require binding of neuropilins to activate plexins, with the exception of SEMA3E, which can bind neuropilin or signal directly through PlexinD1 (Gu et al., 2005).

1.1.7.2 Neuropilins

The two neuropilins, NRP1 and NRP2, are single-pass transmembrane proteins consisting of 923 and 926 amino acids, respectively. They share an overall amino acid homology of only 44%. Their large extracellular domain contains different domains: two CUB domains

(for complement proteins C1r/C1s, UEGF and BMP1) called a1/a2, two factor V/VIII homology domains called b1/b2, and a MAM domain (for meprin/A-5 protein/receptor protein-tyrosine phosphatase μ) called c (Fig. 1.4). The MAM domain promotes dimerisation and oligomerisation with other cell surface receptors. Neuropilins also have short cytoplasmic domains containing a PDZ-binding motif. This mediates binding to GIPC, a protein involved in protein trafficking that also contains a PDZ-domain (De Vries et al., 1998) and is identical to synectin (Gao et al., 2000) or NIP1 (NRP-interacting protein 1) (Cai and Reed, 1999) (Wang et al., 2006). The exact function of the cytoplasmic domains remains to be elucidated, but the fact that they are highly conserved between mice and humans indicate they may have an important role. An alternative splice form of NRP2 exists, called NRP2a, which also contains a partial consensus ITAM (immuno-receptor tyrosine-based activation motif) in its cytoplasmic domain that is not present in NRP1 or NRP2 (Rossignol et al., 2000).

NRP1, initially called A5, was identified as an adhesion molecule in the nervous system of *Xenopus* embryos (Fujisawa et al., 1995). Having been renamed NRP and then NRP1, it was found to bind SEMA3A. At the same time, NRP2 was identified (Chen et al., 1997; He and Tessier-Lavigne, 1997; Kolodkin et al., 1997). Subsequently, NRP1 and NRP2 were found to bind an isoform of vascular endothelial growth factor-A (VEGF-A), VEGF165 (VEGF164 in mice) (Gluzman-Poltorak et al., 2000; Soker et al., 1998). Thus, the NRPs have the unusual ability to bind two structurally and functionally distinct ligands, and have roles dependent on their localisation and ligand binding. NRPs also directly bind heparin *in vitro* (Mamluk et al., 2002), which is thought to indicate an ability to bind heparan sulphate proteoglycans (HSPGs) *in vivo*. VEGF165 is a heparin-binding molecule, and NRP1 also interacts with other heparin-binding molecules, such as FGFs, to potentiate their activity with their receptors (West et al., 2005).

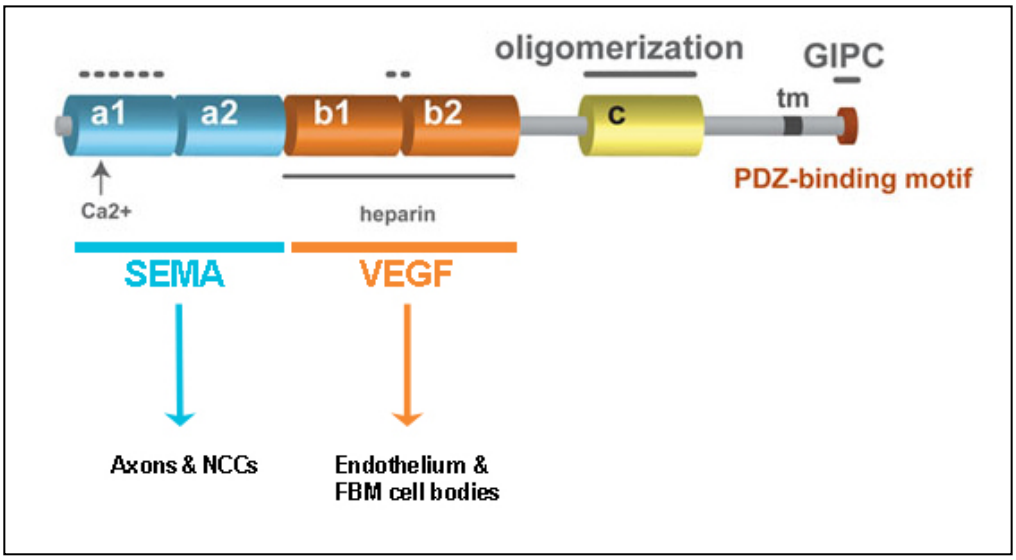

Figure 1.4: Structure and ligand binding of NRP1.

NRP1 binds SEMA3 through its a1/a2 domains in axons and NCCs. It binds VEGF165 through its b1/b2 domains, where it also binds heparin, in endothelium and facial branchiomotor (FBM) neuron cell bodies. It has a c domain for oligomerisaton, a short transmembrane (tm) domain, and a small cytoplasmic domain containing a PDZ-binding motif for binding with GIPC. Localisation (i.e. axons/NCCs vs. endothelium) and ligand binding (i.e. SEMA vs. VEGF165) dictate its mechanism of action. (Diagram adapted from (Schwarz and Ruhrberg, 2010)).

1.1.7.3 NRP/SEMA signalling in the nervous system

Neuropilins recruit plexins to form a receptor complex in which the NRP is required for ligand binding and the plexin transduces signals (Kitsukawa et al., 1997). NRP1 is best known for binding SEMA3A to aid fasciculation and regulate branching of axons. It can also bind SEMA3B and SEMA3C, although with no growth cone collapse ability, as well as SEMA3D, SEMA3E, and SEMA3F with much lower affinity (Chen et al., 1997; Feiner et al., 1997; Takahashi et al., 1998). NRP2 preferentially binds SEMA3F (Giger et al., 2000), but it can also bind SEMA3B, SEMA3C and SEMA3G (Chen et al., 1997; Takahashi et al., 1998; Taniguchi et al., 2005). NRP1 is expressed on particular classes of neurons in the peripheral nervous system (PNS) and CNS, including the trigeminal, facial, glossopharyngeal, vagus, spinal sensory and motor neurons (Kawakami et al., 1996). Mice lacking SEMA3A have severely disrupted nerve patterns in the PNS (Taniguchi et al., 1997), which is phenocopied in mice lacking NRP1 (Kitsukawa et al., 1997) and when the SEMA-binding domain of NRP1 is disrupted (Gu et al., 2003). NRP2/SEMA3F signalling aids in fasciculation and branching of cranial nerves (Giger et al., 2000; Sahay et al., 2003), and also in patterning, for example of the olfactory nerve (Walz et al., 2007).

Importantly for this thesis, NRP1/SEMA3A signalling is required for correct aggregation of sympathetic neurons into primary sympathetic ganglia. Mice lacking NRP1 have mislocated sympathetic neurons and disorganised sympathetic chains, but NCC migration is believed to be normal (Kawasaki et al., 2002). Another study showed that mice lacking PlexinA4, but not PlexinA3, have sympathetic axon guidance defects, but mice lacking both plexins have defects worse than each single mutant. This suggests that PlexinA4 conveys SEMA3A/NRP1 signals, but that the plexins are functionally redundant (Waimey et al., 2008). Additionally, this study claims that NRP2 is not required for sympathetic development.

As previously mentioned, NRP1/SEMA3A signalling is thought to be a repulsive guidance cue for cranial NCC migration (McLennan and Kulesa, 2007; Osborne et al., 2005; Schwarz et al., 2008a), but may not act in trunk NCC migration *in vivo* (Kawasaki et al., 2002), despite data showing that SEMA3A repels trunk NCC *in vitro* (Eickholt et al., 1999). However, a publication I co-authored during the undertaking of this thesis showed that NRP1/SEMA3A signalling does indeed coordinate trunk NCC guidance, and mice lacking NRP1 have increased NCC migration along the intersomitic boundary between the somites and in the dermomyotome layer instead of the sclerotome (Schwarz et al., 2009b). In mice lacking SEMA3F/NRP2 signalling, NCCs migrate uniformly through the anterior and posterior sclerotome, due to a cell-autonomous defect in NCCs, not defective somite polarity. However, normal development of the sympathetic nervous system and a segmented peripheral nervous system were reported (Gammill et al., 2006). The mice

lacking PlexinA3 and PlexinA4 that had sympathetic nervous system defects did not have sympathetic NCC migration or aggregation defects (Waimey et al., 2008). A summary of what is known of the control of trunk NCC migration by SEMA3A and SEMA3F signalling is illustrated in Fig. 1.5.

Continuing from the necessity for SEMA3A/NRP1 signalling in sympathetic axon guidance, SEMA3A is also required for correct sympathetic innervation patterning in the heart of postnatal mice. By acting as a chemorepellant for sympathetic axons, SEMA3A ensures these axons remain on the epicardial surface in embryonic mice and do not penetrate the myocardium (Ieda et al., 2007). Loss of SEMA3A results in disruption of the epicardial-to-endocardial gradient of sympathetic axons in postnatal mice, which results in sinus bradycardia and abrupt sinus slowing (Ieda et al., 2007).

SEMA3G is the most recently discovered semaphorin (Taniguchi et al., 2005). It is described as having 46% identity similarity to SEMA3A and 44.5% to SEMA3F, but despite this, it was found to bind NRP2, not NRP1 (Taniguchi et al., 2005). It was also found to repel sympathetic axons *in vitro*, but not DRG axons (Taniguchi et al., 2005). Embryonic expression of SEMA3G was initially reported as mainly in the kidney and dorsal root ganglia, and at low levels in the brain (Taniguchi et al., 2005). Whilst work for this thesis was underway, a publication showed with a *LacZ* reporter mouse that SEMA3G is expressed in the major arteries and small branching arteries in all organs of mouse embryos, and in arteries with smooth muscle coats in postnatal mice at diminishing levels with age (Kutschera et al., 2011). This study suggested that SEMA3G has a paracrine effect on smooth muscle cells, causing increased smooth muscle cell migration in an *in vitro* assay (Kutschera et al., 2011). Surprisingly, an *in vivo* role for SEMA3G was not identified in this study even though the mouse reporter line used caused a total loss of SEMA3G.

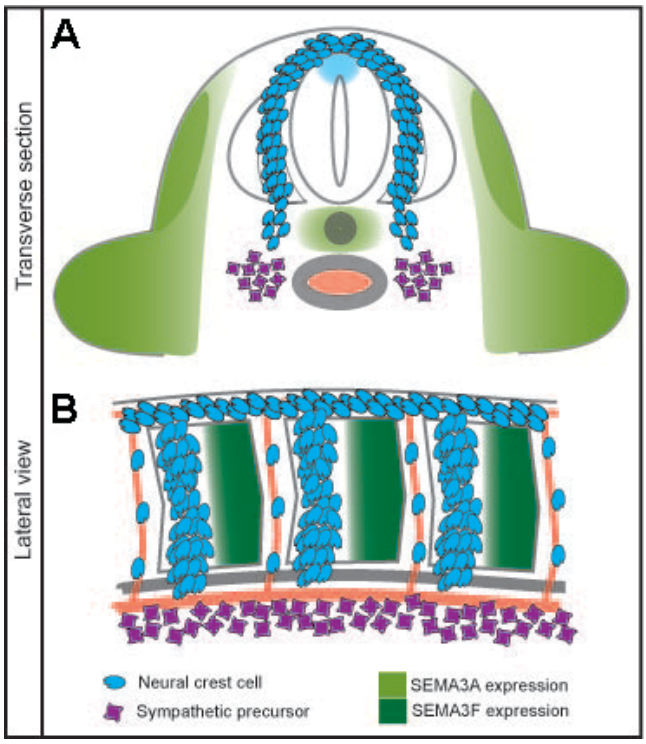

Figure 1.5: Semaphorin expression and NCC migration control.

Schematic of a transverse section through the trunk region of an E9.5 mouse embryo, with areas in forelimb, dermomyotome and around the notocord indicated where SEMA3A is expressed (light green, A). This contributes to confining NRP1-expressing NCCs to the ventromedial migration path. Lateral view of the embryo indicates SEMA3F expression in the posterior half of each somite (dark green, B). This contributes to confining NRP2-expressing migratory NCCs to the anterior half of each somite.

1.1.7.4 NRP/VEGF signalling in vascular system

Mice lacking NRP1 have greatly reduced vessel growth, particularly in the CNS (Kawasaki et al., 1999), although the phenotype is different to that observed in mice lacking the VEGF164 isoform (Gerhardt et al., 2004; Ruhrberg et al., 2002), which is discussed in detail later (Chapter 1.2.4). The role of NRP1 in the vasculature is independent of any form of SEMA signalling (Vieira et al., 2007). NRP1 has been proposed to act as a co-receptor to the VEGF-A receptor VEGFR2, thereby potentiating VEGF165 signalling through VEGFR2 (for example (Soker et al., 1998)). However, the exact role for NRP1 in the developing vasculature remains to be defined, as discussed in a review I co-authored (Fantin et al., 2009). NRP2 has also been implicated in VEGF-A isoform binding, as it binds VEGF165 (although with lower affinity than NRP1) and the shorter isoform VEGF145 (Neufeld et al., 2002).

1.1.7.5 VEGF signalling in the sympathetic nervous system

Some evidence for a potential role for VEGF-A in sympathetic nervous system development exists, as *in vitro* data suggests that VEGF164 stimulates growth of sympathetic axon and growth cone spreading through its tyrosine kinase receptor VEGFR1 (Marko and Damon, 2008). Moreover, VEGF-A is produced by sympathetic targets, such as carotid arteries, and may help control neurite outgrowth *in vivo* (Long et al., 2009). VEGF-A also patterns other parts of the nervous system, such as the facial branchiomotor neurons, and this will be discussed in more detail later (Chapter 1.2.4.3).

1.2 The role of HSPGs in VEGF-A signalling

In this part of the thesis, I will explore whether heparan sulphate proteoglycans (HSPGs) are involved in VEGF-A driven vascularisation of the brain and neuronal migration. HSPGs are membrane-bound proteins carrying sugar side chains that are related to heparin, a highly sulphated glycosaminoglycan made in granular mast cells. Heparin is released only at sites of injury in the vasculature, whereas the lower sulphated heparan sulphate (HS) chains are found ubiquitously on all animal cell surfaces and interact with a plethora of proteins. This interaction diversity is made possible by variation in the structure and sulphation patterns of HS chains themselves and also by variation of the core protein. Many processes are dependent on HSPGs, such as growth factor signalling, morphogenesis and pathology. For example, *Drosophila* HSPGs Dally and Dlp help establish *Wingless* (Wg) gradients in the developing wing bud (Han et al., 2005) and HSPGs promote FGF signalling during gastrulation in the mouse (Garcia-Garcia and Anderson, 2003). Besides WNTs and FGFs, HSPGs also modulate Hedgehog and BMP signalling (reviewed by (Lin, 2004)). I will therefore explore the hypothesis that HSPGs play a role in the signalling of another growth factor, VEGF-A, in sprouting angiogenesis and neuronal patterning.

1.2.1 HSPG structure

1.2.1.1 Core proteins

There are three main families of proteoglycan core proteins carrying HS chains: the transmembrane syndecans (syndecan-1 to -4) and GPI-linked glypicans (gypican-1 to -6), and the basement membrane proteins perlecan, agrin and collagen type XVIII. Other proteins that can associate with HS include betaglycan and a CD44 splice variant (for review (Esko and Selleck, 2002)). The core proteins are expressed in a cell type specific manner. The structure of HS chains is independent of expression of the core protein, but depends on the presence of specific enzymes that are also expressed in a cell type-specific fashion. Between one and four HS chains are attached to each protein core.

1.2.1.2.Heparan sulphate chain structure

HS belongs to a family of unbranched polysaccharides called glycosaminoglycans, which are composed of repeating disaccharide units of hexuronic acid and amino sugars. Other members of the glycosaminoglycan family are chondroitin sulphate, dermatan sulphate and keratan sulphate. In HS, the hexuronic acid can either be *D*-glucuronic acid (GlcA), GlcA sulphated at C-2 (GlcA2S), *L*-iduronic acid (IdoA) or IdoA2S, and the amino sugar is a form of glucosamine; *N*-acetylglucosamine (GlcNAc), *N*-sulphated glucosamine (GlcNS) or unsubstituted glucosamine ($GlcNH_3$), which can all be variably *O*-sulphated. From these

components, 48 disaccharide combinations are possible, but only 23 disaccharides have been identified in HS *in vivo* (Esko and Selleck, 2002). HS chains typically consist of domains rich in GlcA/GlcNAc disaccharide units (*N*-acetylated domains) and domains containing IdoA/GlcNS disaccharide units (*N*-sulphated domains), or some domains with alternating GlcA/GlcNAc and IdoA/GlcNS disaccharide units (*N*-acetylated/*N*-sulphated domains). In contrast, chondroitin sulphate consists of repeating GlcA and *N*-acetylgalactosamine, dermatan sulphate of IdoA and *N*-acetylgalactosamine and keratan sulphate of galactose and *N*-acetylgalactosamine.

1.2.2 HSPG biosynthesis

1.2.2.1 HS chain polymerisation

HS chains are synthesised in the Golgi body by a series of enzymes (Fig. 1.6) (Nuwayhid et al., 1986). Synthesis commences with the attachment of a xylose residue to a specific serine amino acid in the core protein by xylotransferase, then the addition of two *D*-galactose (Gal) residues by galactosyltransferase I and II and a GlcA residue by glucuronosyltransferase I. This forms the tetrasaccharide linkage complex required for chain elongation of HS, as well as for chondroitin, dermatan and keratan sulphates and heparin. The synthesis processes for different glycosaminoglycans subsequently diverge, dependent on the addition of the next residue.

Polymerisation of HS is initiated by addition of one GlcNAc residue to the tetrasaccharide by a GlcNAc transferase, which acts only on tetrasaccharides destined to become HS. Polymerisation is then catalysed by EXT1 and EXT2. These enzymes are two members of the exostosin gene family that were given their name because mutations in either the *Ext1* or *Ext2* gene in humans have been identified in the skeletal dysplasia hereditary multiple exostoses (for review (Nadanaka and Kitagawa, 2008)). EXT1 and EXT2 contain a large globular luminal domain (Colley, 1997) with two catalytic sites: one for GlcNAc transferase and another for Glc transferase activity (Lind et al., 1998), enabling the same enzyme to add alternating residues to the polysaccharide chain. EXT1 and EXT2 have very low activity separately, but form a heterodimer *in vivo* that has substantially higher glycosyltransferase activity than the separate monomers. This results in the loss of function of both enzymes if only one is mutated (McCormick et al., 2000).

It was originally thought that chain polymerisation occurs before any other modifications, but glycosyltransferase activity has been shown to increase with concomitant *N*-sulphation of the chain, suggesting simultaneous polymerisation by EXT enzymes and chain modification by other enzymes (Lidholt and Lindahl, 1992; Lindahl et al., 1989).

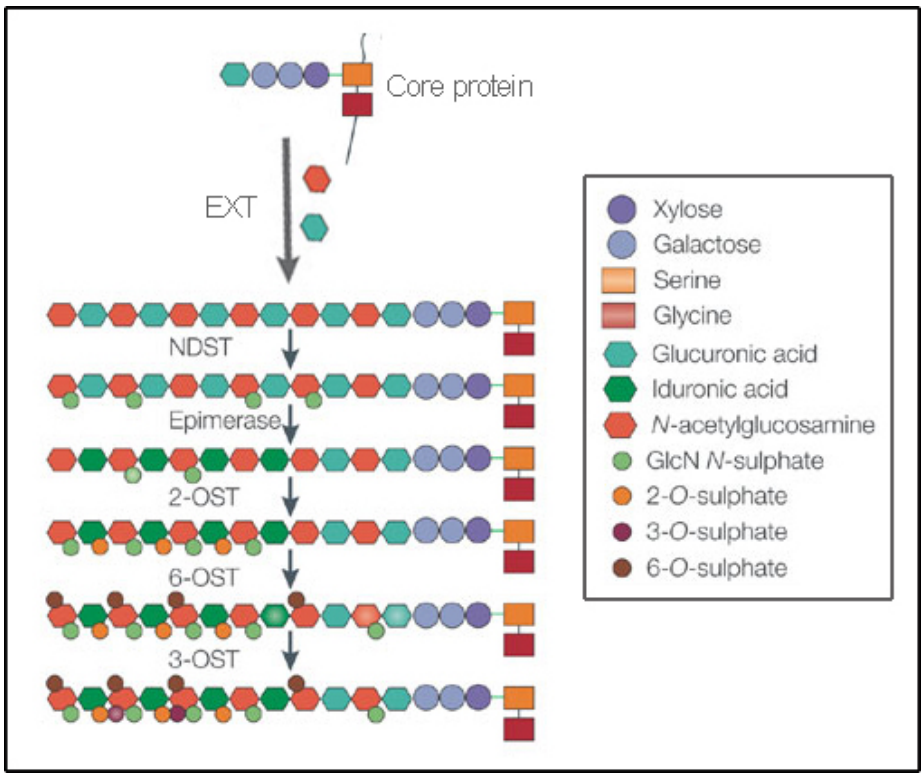

Figure 1.6: Biosynthesis of HSPGs.

Synthesis is initiated in the Golgi body by the binding of the tetrasaccharide linkage complex to a serine residue of the core protein. Polymerisation is then catalysed by the EXT enzymes, EXT1 and EXT2. The HS chain can be modified by *N*-deacetylase/*N*-sulphotransferase (NDST)-1 and -2, C5-epimerase, 2-*O*-sulphotransferase (HS2ST / 2OST), 6-*O*-sulphotransferases (HS6ST1-3 / 6OST1-3) and 3-*O*-sulphotransferases (HS3ST1-4 / 3OST1-4). The enzymes do not necessarily act in this order. For example, EXT1/2 and NDST1/2 can work simultaneously, but NDST1/2 must act before HS2ST. HSPGs are then transported to the cell surface, where sulphatases (SULF) 1 and 2 can act on HSPGs to remove specific 6-*O*-sulphate groups. In this way, a wide variety of HSPGs are produced (diagram adapted from (Hacker et al., 2005)).

1.2.2.2 HS chain modifications

The first HS chain modification, which is a prerequisite for later modifications, is the removal of *N*-acetyl groups from selected GlcNAc residues and subsequent replacement with sulphate, carried out by bi-functional *N*-deacetylase/*N*-sulphotransferase (NDST) enzymes. There are four mammalian NDST enzymes grouped into two subtypes: NDST1/2 and NDST3/4 (Aikawa et al., 2001). NDST1 and 2, the best characterised NDSTs, are abundantly and ubiquitously expressed, consistent with being involved in HS synthesis, and exhibit distinctive functions. In contrast, NDST3 and 4 have a restricted expression pattern and may act on previously modified HS chains (Aikawa et al., 2001). NDST2 has higher *N*-deacetylase than *N*-sulphation activity compared to NDST1, which has a higher *N*-sulphation activity. These properties and the relative expression of each enzyme define the degree of *N*-sulphation of the HS chain (Pikas et al., 2000).

C5-epimerase acts on GlcA residues that are adjacent to GlcNS, turning them into *L*-IdoA, the 5' epimer of *D*-GlcA present at ligand binding sites of HS. IdoA can exist in various conformations, adding flexibility to the chain and creating varying ligand specificities (Raman et al., 2003). That it does not act on *O*-sulphated GlcA, or GlcA adjacent to *O*-sulphated GlcNS, suggests that epimerisation comes after *N*-deacetylation/*N*-sulphation, but before any *O*-sulphation (Hagner-McWhirter et al., 2000).

2-*O*-sulphotransferase (HS2ST) catalyses the transfer of a sulphate group to C-2 of the hexuronic acid, acting preferentially on IdoA, but also on GlcA, and mainly in *N*-sulphated domains (Kusche and Lindahl, 1990). 2-*O*-sulphated IdoA residues are a universal component of HS, with between 50 and 90% of IdoA residues being 2-*O*-sulphated (Safaiyan et al., 2000).

6-*O*-sulphotransferases (HS6ST) catalyse the addition of sulphate groups to C-6 of glucosamine residues. Three isozymes exist, HS6ST1-3, which have differential specificity for the hexuronic acid adjacent to the targeted *N*-sulphated glucosamine. HS6ST1 prefers IdoA-GlcNS units, but also acts on GlcNAc; HS6ST2 acts on both GlcA-GlcNS and IdoA-GlcNS dependent on substrate concentration; and HS6ST3 acts on either with no preference (Habuchi et al., 2000). An alternative splice form of HS6ST2 has been described (Habuchi et al., 2003). Consistent with the idea that the isoforms target different HS chains for varying functions *in vivo*, HS6ST enzymes exhibit differential expression patterns (Sedita et al., 2004).

3-*O*-sulphostransferases (HS3ST) catalyse the addition of sulphate groups to C-3 of glucosamine residues. They exist in at least six forms (Shworak et al., 1999; Xia et al., 2002). The best characterised is HS3ST1, since 3-*O*-sulphation of GlcA-GlcNS and GlcA-GlcNS6S is essential for the binding site of antithrombin (Atha et al., 1985). HS3ST1 can

also act on IdoA-GlcNS and IdoA-GlcNS6S, but only in the absence of 2-*O*-sulphation of hexuronic acid, which blocks HS3ST1 action. HS3ST2 acts on GlcNS residues with 2-*O*-sulphated hexuronic acids. HS3ST3A and B act on IdoA2S-GlcNS and IdoA2S-GlcNH2.

Relatively recently described are a new group of enzymes, the sulphatases (SULFs), which are active on the cell surface and in the ECM, rather than intracellularly. They modulate HS by removal of 6-*O*-sulphate groups from the chain (Lamanna et al., 2006).

1.2.3 Gene targeting to study HSPG function

Targeted disruption of genes of interest and analysis of the resulting developmental phenotype can be used to identify essential HSPG functions. One possible approach is to mutate the core protein of particular HSPGs. However, other HS chains still present on the cell surface might compensate. An alternative approach would be the targeted disruption of genes encoding the enzymes required for HSPG biosynthesis. For example, mice lacking EXT enzymes do not produce HS, and accordingly die at gastrulation due to failure to organise mesoderm or extraembryonic tissue (Lin et al., 2000). Disrupting the expression of enzymes required for HS chain modification rather than initial polymerisation would result in altered HS fine structure and is less lethal. Below, I discuss various findings from such knockout studies.

Ndst1-null mice have severe HS structural defects, with dramatically decreased levels of *N*-sulphation in most tissues (Ringvall et al., 2000). Although the ensuing phenotypes are not fully penetrant, embryos die perinatally, with craniofacial skeletal defects, particularly in mandibular development (Yasuda et al., 2010). *Ndst1*-null mice also have defects in pericyte recruitment during vascular development (Abramsson et al., 2007) (see Chapter 1.2.4). Visual inspection of the published images suggests that blood vessels grow and branch properly in these animals. *Ndst2*-null mice have a mast cell defect caused by a lack of sulphated heparin, although no structural HS defects are observed in any other tissues (Forsberg et al., 1999). The observation that *Ndst2, 3* and *4* are upregulated in the lungs of *Ndst1*-null mice suggests functional compensation (Hu et al., 2009).

A mutation in the *Hsepi* gene, encoding C5-epimerase, results in highly *N*-sulphated HS devoid of IdoA residues (Li et al., 2003). *Hsepi*-null mice die at birth due to respiratory failure and also exhibit renal agenesis and skeletal defects, although many other developmental processes appear to proceed relatively normally. On closer inspection, IdoA-containing HS are also required for pericyte recruitment in the developing vasculature (Abramsson et al., 2007).

Mice lacking HS2ST die neonatally due to renal agenesis, and also exhibit eye and skeletal defects, such as decreased long bone size, craniofacial abnormalities and polydactyly, and a slight decrease in neural progenitor proliferation (Bullock et al., 1998). Despite these, most tissues with high *Hs2st* expression develop normally. This may be because *Hs2st*-null mice have more extensively 6-*O*-sulphated HS, suggestive of compensation (Merry et al., 2001).

Hs6st1-null mice are embryonic lethal between E15.5 and birth and exhibit a decrease in placental microvessels, smaller skeleton size and a lung morphology defect (Habuchi et al., 2007). A very slight upregulation in *Hs6st3* and *Hs2st* mRNA was reported in the mutants. Mouse knockout data for the other *Hs6st2* and *Hs6st3* genes have not yet been published. In zebrafish, morpholino knockdown of *Hs6st2* decreases vessel branching in the caudal vein tail, causing pooling of blood in the tail (Chen et al., 2005).

Hs3st1-null embryos appear healthy and exhibit none of the expected coagulation defects, but they have intrauterine growth retardation and embryonic lethality, depending on genetic background (HajMohammadi et al., 2003). Knockout data for the other *Hs3st* genes have not yet been published.

1.2.4 VEGFA-driven angiogenesis and neuronal patterning

1.2.4.1 Angiogenesis

Angiogenesis is the process by which new blood vessels grow from pre-existing major vessels, which are themselves formed during vasculogenesis (for reviews (Flamme et al., 1997; Risau, 1997)). Angiogenesis is preceded by breakdown of the surrounding extracellular matrix (ECM). Specific endothelial cells then become 'tip cells', which lead the angiogenic sprout by extending filopodia into areas of high VEGF-A concentration and migrating towards it (Gerhardt et al., 2003; Ruhrberg et al., 2002). Endothelial cells behind them, termed 'stalk cells', proliferate and the resulting branch is made into a vessel by lumenisation (Fig. 1.7) (Gerhardt et al., 2003). Branching and anastomosis repeat, and a capillary plexus is formed. The new vessels are then pruned, remodelled and patterned into a vascular hierarchy of arteries, arterioles, capillaries, vein and venuoles. Finally, vessels are stabilised by recruitment of perivascular smooth muscle cells, called pericytes in smaller vessels, and the endothelial cells become quiescent (Lindblom et al., 2003). Angiogenesis forms the functional vascular system in the embryo that is essential for life, but also takes place in pathogenesis, for example in retinopathy and tumour angiogenesis in cancer (for a review (Ferrara, 2000)).

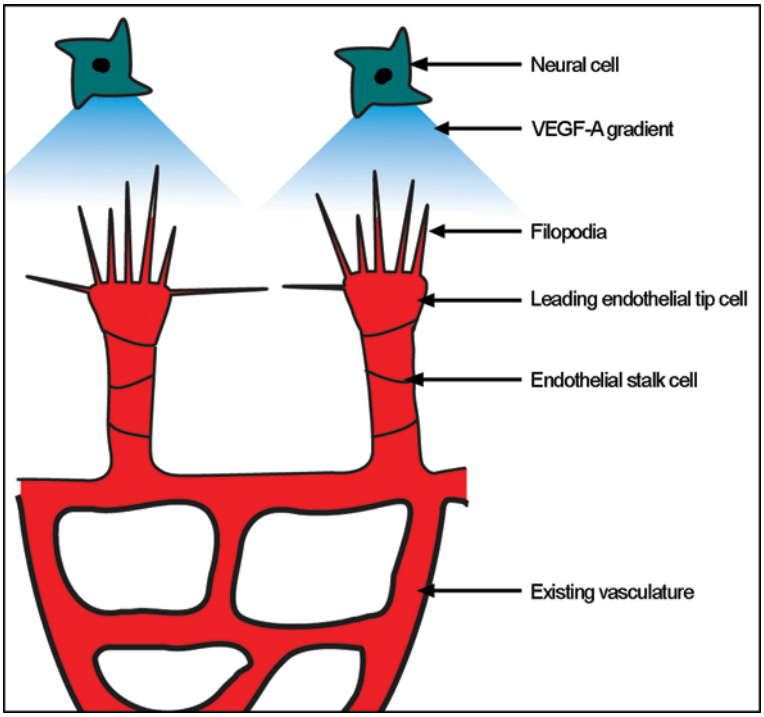

Figure 1.7: Sprouting angiogenesis in the brain.

New vessels sprout from a pre-existing vasculature. VEGF-A produced by neural progenitor cells is retained in a gradient by the extracellular matrix. Endothelial tip cells at the leading edge of the vascular plexus extend filopodia into an area of high VEGF-A concentration and migrate towards it, leading endothelial stalk cells, which proliferate and form a new vessel.

VEGF-A is a potent stimulator of angiogenesis and regulates most, if not all, steps in the angiogenic process, including endothelial cell recruitment, migration, proliferation and apoptosis. The importance of VEGF-A is illustrated by mice lacking even a single allele of the *Vegfa* gene, which die before E10.5 due to cardiovascular defects (Carmeliet et al., 1996). Cells in areas of hypoxia, which need to attract new blood vessels, produce VEGF-A.

A good model to study angiogenesis is the developing vessel plexus in the brainstem of the mouse, where the process occurs in a stepwise fashion that is readily visualised (Fig. 1.8). New vessels sprout into the brain from existing vessels in the pial membrane at around E9.5 in the mouse. The sprouts invade the hindbrain, extending ventricularly and reaching the subventricular zone at around E10.25. Here, the vessels sprout outwards and fuse into the subventricular vessel plexus at E12. Between E12 and E13, the capillary plexus is remodelled. Neural progenitor cells in the subventricular zone produce the VEGF-A that guides the angiogenic process (Raab et al., 2004). Dissecting and flatmounting the mouse hindbrain at particular developmental ages allows visualisation of brain vascularisation (Fig. 1.8B,C) (Ruhrberg et al., 2002). Disruptions to the process are easily identifiable by under or over-branching or altered morphology of the vessels in the subventricular plexus.

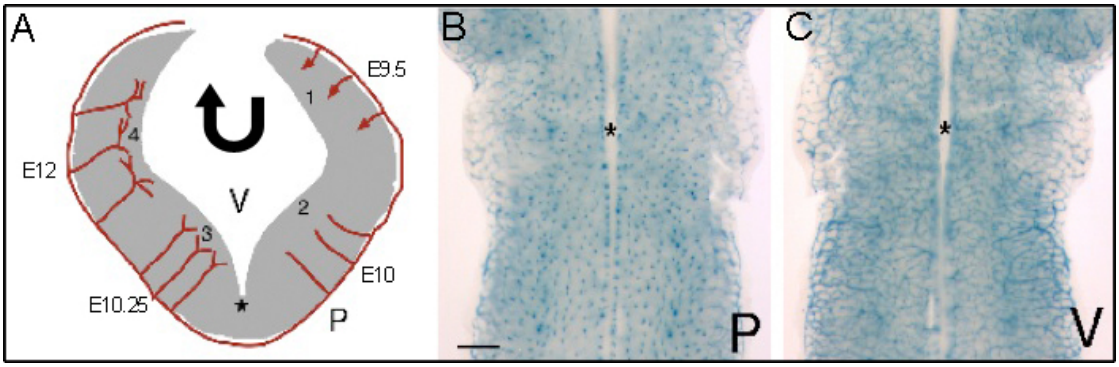

Figure 1.8: The mouse embryonic hindbrain as a model for studying sprouting angiogenesis.

(A) Step-wise process of vessel growth in the developing hindbrain. Vessels invade the hindbrain from the pial (P) membrane at E9.5 (1) and grow towards the ventricular (V) zone (2). At E10.25 vessels reach the subventricular zone and begin to branch (3) to form the subventricular vascular plexus at E12 (4). (B) E12.5 hindbrain viewed from pial (P) side with vessels labelled with a *Tie2 LacZ* reporter to visualise vessel sprouts. (C) The same hindbrain viewed from the ventricular (V) side to visualise vessel branches. Either the sprouts on the pial side or the branches on the ventricular side can be quantified to study angiogenic processes. * indicates the midline (diagram adapted from (Ruhrberg et al., 2002)).

1.2.4.2 VEGF-A

VEGF-A exists in several isoforms, which are produced by alternative mRNA splicing of a transcript from the single *Vegfa* gene. Multiple isoforms have been identified in humans, the most common being VEGF189, VEGF165, VEGF145 and VEGF121, so-called due to the number of amino acids in the mature protein. The murine homologues each lack one amino acid, and contain 188, 164, 144 and 120 amino acids, respectively (Fig. 1.9). All isoforms share the same N-terminus, encoded by exons 1 to 5. Exons 6 and 7 encode heparin-binding domains, which confer HS-binding *in vitro*, and VEGF189, the longest isoform, contains both of these domains. It therefore has the highest heparin-binding affinity, and is always membrane or ECM-bound. VEGF121, the shortest isoform lacking both exon 6 and 7, does not bind heparin and is fully diffusible once secreted. VEGF165 contains exon 7, but not 6, and therefore has intermediate heparin-binding affinity. This isoform is the most abundant *in vivo* and the most important for angiogenesis (Park et al., 1993).

VEGF165 signalling is directed through two type III receptor tyrosine kinases, VEGF receptor-1 [VEGFR1; Fms-like tyrosine kinase 1 (FLT1) in mice] and VEGFR2 [kinase insert domain receptor (KDR) in humans; fetal liver kinase 1 (FLK1) in mice] (de Vries et al., 1992; Terman et al., 1992). Also involved in VEGF165 signalling are the neuropilins, specifically NRP1 (Soker et al., 1996; Soker et al., 1998). All VEGF receptors are also heparin-binding proteins.

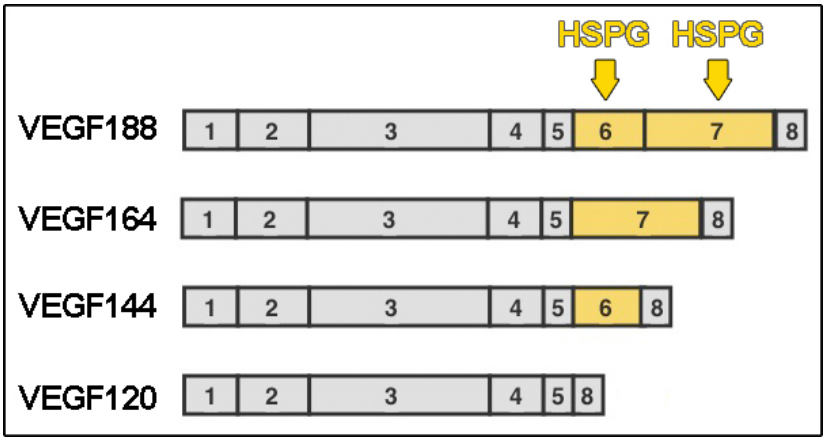

Figure 1.9: Isoforms of murine VEGF-A.

VEGF-A exists as multiple isoforms that arise from alternative splicing of the gene product of 8 exons. All isoforms contain exons 1-5 and exon 8, with exons 6 and 7 alternatively spliced. Exons 6 and 7 are the heparin-binding domains, which confer HS-binding *in vitro*. The inclusion or exclusion of these exons results in the varying heparin-binding efficiency of each isoform. (Diagram adapted from (Ruhrberg et al., 2002)).

1.2.4.3 VEGF-A guided neural patterning

Mice lacking VEGF164 appear to have normal axon fasciculation and nerve patterning in the PNS (Schwarz et al., 2004; Vieira et al., 2007). However, several findings *in vitro* suggest that VEGF165 is required in the developing nervous system, and in mice VEGF164 contributes to neural patterning in the CNS by controlling migration of the facial branchiomotor (FBM) neurons, discussed below (Schwarz et al., 2004). More recently, it was shown that VEGF-A gradients also control granule cell migration in the cerebellum of the developing mouse brain, independently of defects in vascularisation (Ruiz de Almodovar et al., 2010). The role of HSPGs in neuronal VEGF-A signals was not examined.

FBM neurons are born bilaterally in the ventricular hindbrain in a segment called rhombomere (r) 4, and their somata undergo a specific, directed migration movement between E12 and E14 in the mouse (Fig. 1.10A). They migrate caudally and tangentially at the ventricular surface through r5 to r6, and then dive down to the pial side of the hindbrain where they arrest migration in rounded aggregates, which become the paired nuclei of the facial nerve (Auclair et al., 1996). Concurrently, FBM neurons extend axons out of the hindbrain into the 2nd branchial arch to form the facial nerve. FBM neurons express NRP1 and their axons are guided in part by SEMA3A signalling through a NRP1/PlexinA4 receptor complex. In contrast, FBM soma migration is controlled by VEGF164 signalling through NRP1, not by SEMA3A (Schwarz et al., 2004). *Vegfa* is expressed ventricularly at the midline and at the site of facial nucleus formation on the pial side of the hindbrain (Fig. 1.10B,C). In mice lacking VEGF164, FBM somata were misguided, with many invading r5, and the facial nuclei were misshapen and in anterior positions (Fig. 1.10,D-G). Mice expressing only VEGF164 and no other VEGF-A isoforms have no FBM migration defects (Schwarz et al., 2004).

It is thought that VEGF164 signalling through NRP1 requires a co-receptor for signal transduction, as SEMA signalling through NRP1 normally requires plexins (Feiner et al., 1997; Takahashi et al., 1999). Previous work in the lab has therefore aimed at identifying a co-receptor required for this signalling. Quenten Schwarz assessed embryos lacking PlexinA1-4, the kinase domain of VEGFR1 or VEGFR2 in the neuronal lineage, but found that none of these had FBM neuronal migration defects (Q. Schwarz & C. Ruhrberg, unpublished data). It was then hypothesised that NRP1 may transduce the signal itself through its cytoplasmic domain, the function of which has not yet been found. Quenten Schwarz generated a mouse in which the cytoplasmic domain of NRP1 was disrupted but the ligand binding and transmembrane domains were still functional. In this thesis, I will investigate these mice to define whether the cytoplasmic domain of NRP1 or another co-receptor is required for VEGF164/NRP1 signalling in FBM neurons.

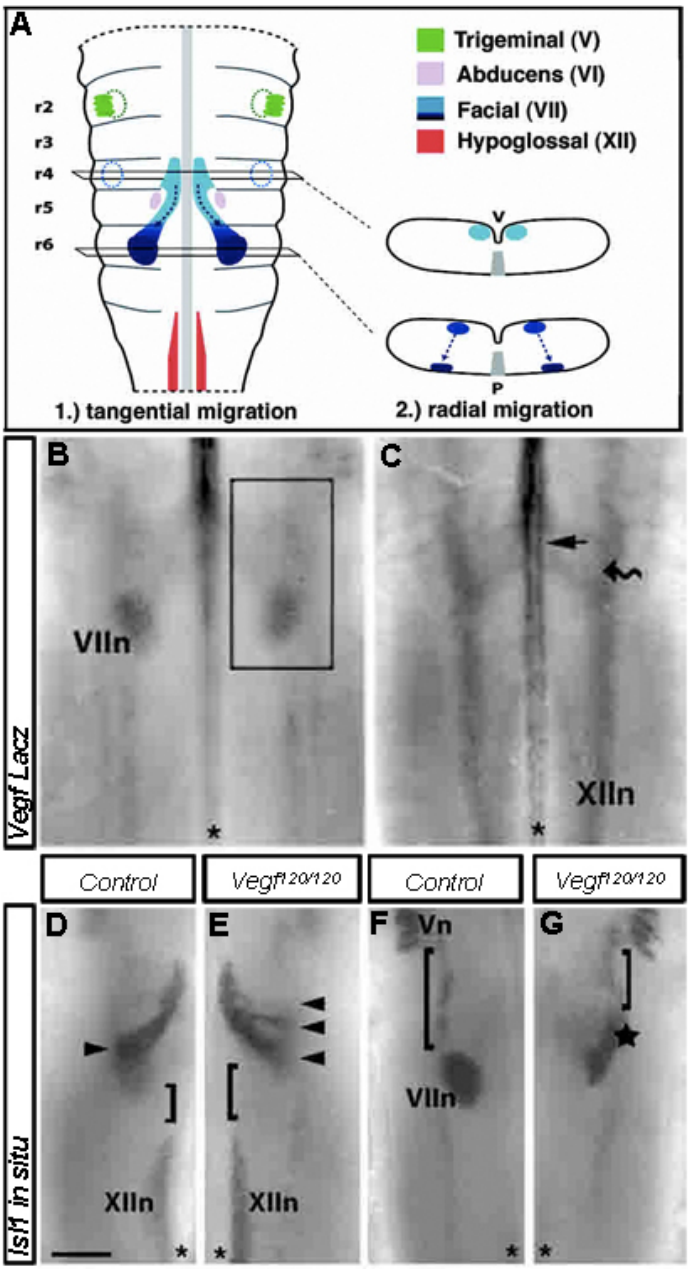

Figure 1.10: Migration of FBM neurons in the hindbrain is disrupted in the absence of VEGF164.

(A) Schematic representation of positioning of the trigeminal, abducens, facial and glossopharyngeal motor neuron nuclei in the mouse hindbrain at E12.5, with rhombomere (r)2 to r6 labelled. Hatched circles represent the position of the exit points for the axons from the facial and trigeminal neurons. The facial neurons migrate from r4 tangentially to r6. The top cross section represents the ventricular (v) position of the facial neurons at r4, and the bottom shows the radial migration of the facial neurons at r6 to the pial (p) side. (B,C) Expression of a *Vegfa LacZ* reporter in E12.5 hindbrain reveals *Vegfa* is expressed at the site of facial nucleus (VIIn) formation on the pial side (B); on the ventricular side, Vegfa is expressed at the midline (arrow), in sets of stripes (wavy arrow) and in the area where the hypoglossal nuclei (XIIn) form (C). (D-G) E13.25 control hindbrains subjected to *in situ* hybridisation with Isl1 probe to allow

visualisation of migrating FBM somata from r4 on the ventricular side (D, arrowhead) to r6, close to the hypoglossal nuclei (XIIn), where they dive down to the pial side and form facial nuclei (VIIn, F) posterior to the trigeminal nuclei (Vn). In absence of VEGF164, FBM somata migrate in multiple streams (E, arrowheads) further anteriorly from the hypoglossal nuclei than in control (compare brackets in D,E). Misshapen facial nuclei form (star in G) closer to the trigeminal nuclei than in control hindbrains (compare brackets in F,G). Scale bars: 250 μm. * indicates midline. Images and schematic adapted with permission from (Schwarz et al., 2004).

1.2.5 Function of HSPGs in angiogenesis and neural development

It is hypothesised that HSPGs may be required in a similar way to the well-documented FGF model, in which basic FGF (bFGF or FGF2) cannot bind its tyrosine kinase receptor in the absence of HSPGs (Yayon et al., 1991), and sequestering cell surface HSPGs therefore prevents FGF-signalling (Rapraeger et al., 1991). Accordingly, mice lacking an enzyme required to synthesise the hexuronic acid components of HS cannot undergo FGF-driven gastrulation (Garcia-Garcia and Anderson, 2003).

1.2.5.1 HSPGs in angiogenesis

The theory that HSPGs are involved in VEGF-A guided angiogenesis is based on three lines of evidence. Firstly, the heparin-binding affinities of VEGF165 and VEGF189 vary dependent on the presence of the heparin-binding domains, shown *in vitro* (Park et al., 1993). This was supported by *in vivo* studies, which showed that loss of heparin-binding VEGF-A disrupts VEGF-A gradients in the ECM (Gerhardt et al., 2003; Ruhrberg et al., 2002). Accordingly, mice that express solely the secreted, non heparin-binding VEGF120 isoform have vascular defects in the brain, with impaired filopodia extension from tip cells, leading to fewer branch points and large luminal diameters (Fig. 1.11). Conversely, mice expressing only heparin-binding VEGF-A, i.e. VEGF188, exhibited an opposing phenotype, with ectopic branching and formation of thin microvessels. A model was proposed in which the isoforms of VEGF-A are differentially localised and retained by HSPGs in a gradient dependent on their varying HS-binding abilities, to control blood vessel branching. However, it was never directly investigated if HSPGs are indeed essential for retaining VEGF-A in the ECM.

Secondly, *in vitro* work suggests that HS promotes VEGF165 binding to VEGFR1 and VEGFR2 (Gitay-Goren et al., 1992; Tessler et al., 1994), as well as to NRP1 (Soker et al., 1998). These observations suggest that HSPGs play a role in presenting VEGF165 to its receptors. Consistent with this idea, neither VEGFR2-deficient stem cell cultures nor HS-deficient stem cell cultures can develop a vasculature upon VEGF165 stimulation where wildtype stem cell cultures can. In co-cultures, however, endothelial cell VEGFR2 (derived from HS-deficient cells) can be activated in *trans* by HSPGs produced by pericytes (derived from VEGFR2-deficient cells) (Jakobsson et al., 2006). The authors propose a model by which cell surface HSPGs also modulate VEGFR2 turnover by trapping it at the cell surface rather than being internalised and recycled.

Thirdly, recent *in vitro* work using human umbilical vein endothelial cells showed that 2-*O*- and 6-*O*-sulphated groups on HS are required for VEGF165 mitogenic activity and endothelial tube formation *in vitro* (Ashikari-Hada et al., 2005), and 6-*O*-sulphation seems to be particularly important (Robinson et al., 2006).

Yet, there has been little *in vivo* evidence supporting the requirement for HSPGs in angiogenesis. A notable example is a zebrafish study using *Hs6st2* morpholino knockdown that resulted in caudal vein plexus defects (Chen et al., 2005). However, the phenotype was mild compared to VEGF or VEGF receptor knockouts (for example (Nasevicius et al., 2000)).

1.2.5.2 HSPGs in the nervous system

There are also many examples of HSPGs functioning in brain patterning and axon guidance in the developing nervous system, indicating that they are produced in the brain. For example, mice lacking HSPGs specifically in neural tissues have midbrain/hindbrain patterning defects, and lack the inferior colliculus (originating from midbrain) and cerebellum (originating from hindbrain), due to defective FGF8 distribution (Inatani et al., 2003). Also, axon guidance at the optic chiasm requires HSPGs for Slit2 signalling (Pratt et al., 2006).

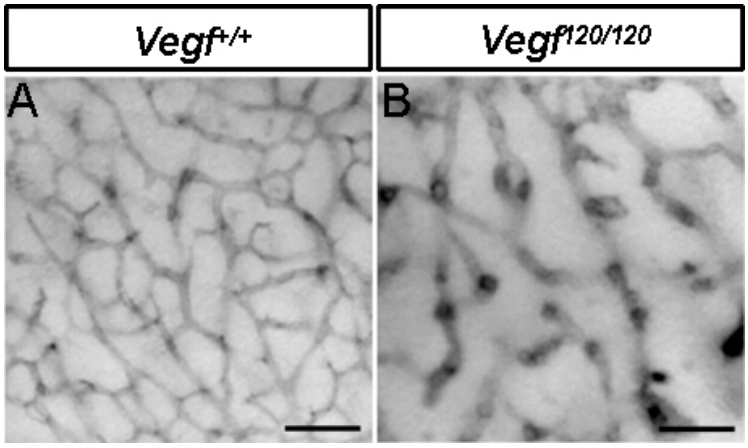

Figure 1.11: Loss of heparin-binding VEGF164 decreases vessel branching.

E12.5 hindbrains immunolabelled with the endothelial marker PECAM to visualise the developing vasculature. Wildtype hindbrains (A) have a complex network of branched microvessels. In embryos producing only the non-heparin-binding isoform of VEGF-A (*Vegf*$^{120/120}$, B), the hindbrain vessels are less branched, and have larger diameters and bulbous vessel ends. Images kindly provided by Joaquim Vieira and Christiana Ruhrberg. Scale bar: 200μm.

1.3 Aims

In the first part of this thesis I examined sympathetic innervation of the cardiovascular system. My aim was to investigate how NRP1 and NRP2 and their SEMA ligands control the early steps in the development of the sympathetic nervous system from sympathetic NCCs in the mouse. I also aimed to assess how NRP1 patterns sympathetic axon extension in target organs by investigating heart innervation, and to investigate if the novel semaphorin, SEMA3G, helps pattern the sympathetic nervous system *in vivo*.

In the second part of my thesis, I studied the role HSPGs play in VEGF164-driven vascular and neuronal patterning in the developing mouse brain. I first assessed the importance of HS fine structure on vascular patterning, and then whether the elimination of HSPGs in specific tissues affects vascular patterning. Finally, I investigated whether HSPGs are required in VEGF164-driven FBM neuronal migration.

2. MATERIALS AND METHODS

2.1 Materials

2.1.1 General laboratory materials

All reagents used were obtained from Sigma Aldrich, except where indicated. Plastic consumables were obtained from Corning or Nunc. Glassware was obtained from VWR International.

2.1.2 General laboratory solutions

Water used was purified using a MiliRo 15 Water Purification System (Milipore) and further purified where necessary using a Mili-Q reagent Grade Water Ultrafiltration System (Milipore). RNAse- and DNAse-free water was obtained from Sigma. Absolute ethanol, methanol and isopropanol were from Fischer Scientific.

1 x PBS: 137mM NaCl, 3mM KCl, 10mM Na_2HPO_4, 1.8mM KH_2PO_4, pH 7.2

1 x PBT: 1 x PBS + 0.1% TritonX100

1 x TE: 10mM Tris-HCl, 1mM EDTA, pH 8.0

1 x TAE: 40mM Tris-acetate, 1mM EDTA, pH 8.0

1 x TBS: 10mM Tris pH 8, 150mM NaCl (for immunolabelling)

1 x TBS: 25mM Tris pH 7.5, 150mM NaCl, 3mM KCl (for in situ hybridisation)

4% PFA: 4% formaldehyde, made freshly from paraformaldehyde, in PBS

2.2 Methods

2.2.1 Animal methods

2.2.1.1 Animal Maintenance and Husbandry

Mice were mated in the evening and the females checked for vaginal plugs in the morning. A plug found in the morning was taken as 0.5 embryonic days post coitum (E0.5). All mice were on mixed CD1 and C57Bl/6 genetic backgrounds.

2.2.1.2 Genetic mouse strains

Please see Table 2.1 for details of mouse strains used.

Gene/Mutation	Source	Reference
Nrp1 knockout	Dr Hajime Fujisawa	(Kitsukawa et al., 1997)
Nrp2 knockout	Dr Alex Kolodkin	(Giger et al., 2000)
$Nrp1^{sema}$ knockout	Dr David Ginty	(Gu et al., 2002)
Nrp1 "floxed"	Dr David Ginty	(Gu et al., 2003)
$Nrp1^{cyto}$	Drs. Quenten Schwarz, Christiana Ruhrberg	Unpublished
Wnt1Cre		(Chai et al., 2000)
Tie2Cre	Dr David Ginty	(Kisanuki et al., 2001)
$Vegf^{120/120}$ knockin	Drs. David Shima, Peter Carmeliet, Patricia D'Amore	(Ruhrberg et al., 2002)
Sema3A knockout	Dr Masahiko Taniguchi	(Taniguchi et al., 1997)
Sema3F knockout	Dr Alex Kolodkin	(Sahay et al., 2003)
Sema3G LacZ knockin	Dr Christer Betsholtz	(Kutschera et al., 2011)
Hs6st1 LacZ knockin	Dr Tom Pratt	(Leighton et al., 2001; Mitchell et al., 2001)
Hs6st2 LacZ knockin	Prof Mike Simons (Lexicon Ltd)	Unpublished
Hs2st LacZ knockin	Dr Valerie Wilson	(Bullock et al., 1998)
Ext "floxed"	Dr Yu Yamaguchi	(Inatani et al., 2003)
Nes8Cre	Dr Weimin Zhong	(Petersen et al., 2002)

Table 2.1: Genetic strains of mice used, with source and reference.

2.2.1.3 Compound mutant mice

To obtain compound *Nrp1^{sema}/Nrp2* mutants, mice heterozygous for the *Nrp2* mutation were crossed with mice heterozygous for the mutation in the SEMA-binding domain of *Nrp1*, and mice heterozygous for both mutations were crossed to each other. The resulting genotypes were mixtures of *Nrp1^{sema}* and *Nrp2* heterozygous and homozygous mutations and wildtypes, and the probability of getting a full wildtype or a full compound homozygous *Nrp1^{sema}/Nrp2* mutant was 1/16. The same method was carried out to obtain compound *Sema3a/Sema3f*, *Sema3a/Sema3g*, *Sema3f/Sema3g*, *Nrp1^{cyto}/Nrp2* and *Hs6st1/Hs6st2* mutants.

2.2.1.4 Tissue-specific genetic targeting

I utilised the CRE/LOX approach to achieve tissue-specific deletion of certain genes (reviewed by (Nagy, 2000)). This is based on the P1 phage CRE-recombinase, an enzyme that recognises a 34bp sequence called *LoxP*. Insertion of two *LoxP* sites flanking a region of DNA enables binding by CRE-recombinase and either inversion or excision of the sequence, depending on the orientation of the *LoxP* sites. Specificity of the deletion can be accomplished by inserting the CRE-recombinase under the control of a tissue-specific promoter. In a developmental context, this results in genetic deletion in the somatic cells and their entire progeny.

To inactivate genes in NCC-derived cells, mice expressing CRE under the control of the NCC specifying *Wnt1* promoter were used. These mice were crossed with mice that had its *Nrp1* gene flanked by *LoxP* sites, i.e. homozygous "floxed" *Nrp1* conditional mice (*Nrp1$^{fl/fl}$*). Genetic recombination results in *Nrp1* being deleted in cells in which the *Wnt1* promoter is active, i.e. in NCCs, in *Nrp1$^{fl/fl}$;Wnt1Cre+* mice. A similar approach was taken with mice expressing CRE under the control of the endothelial specific *Tie2* promoter and homozygous "floxed" *Nrp1* conditional mice to delete *Nrp1* in endothelial cells of blood vessels. To eliminate expression of *Ext* in neural progenitors and endothelial cells, mice expressing CRE under the control of the neural progenitor specific *Nes8* promoter or the *Tie2* promoter were crossed with homozygous "floxed" *Ext* conditional mice.

A recent report claimed that the *Tie2* promoter is able to drive the expression of CRE recombinase in the female germ line (de Lange et al., 2008). This would result in the "floxed" allele becoming null in the germ line and being transmitted through to offspring, thereby becoming a deletion in the whole embryo rather than in endothelial cells alone. Care was therefore taken to only transmit the CRE recombinase under the control of the *Tie2* promoter through males.

To obtain compound *Nrp1;Wnt1Cre/Nrp2* mutants, mice with heterozygous *Nrp2* mutations were crossed to *Wnt1Cre*-positive mice with a heterozygous *Nrp1* "floxed"

mutation (*Nrp1$^{fl/+}$ or Nrp1$^{fl/-}$*), and resulting compound heterozygous mutant mice were crossed to each other. The probability of obtaining a compound *Nrp1;Wnt1Cre/Nrp2* mutant was 1/32. To increase the frequency of mutants, the offspring were backcrossed for one more generation to obtain mice with heterozygous *Nrp2* mutation and homozygous *Nrp1* "floxed" mutation positive for *Wnt1Cre* (*Nrp2$^{+/-}$/Nrp1$^{fl/fl}$;Wnt1Cre^{+}).*

2.2.1.5 Genotyping

All genotyping was carried out by Kathryn Davidson and Laura Denti in the Ruhrberg lab. Tissue biopsies were taken from mice, either tail snips or yolk sacs from embryos or ear punches from pre-weening age mice. Genomic DNA was extracted from tissue biopsies by incubation in 500 μl lysis buffer (100mM Tris-HCl pH 8.5, 5mM EDTA, 0.2% SDS, 200mM NaCl, 100μg/ml proteinase K) at 55°C overnight with agitation for protein digestion. DNA was precipitated by adding 1 ml ethanol, and collected by centrifugation at 12000 rpm for 5 minutes. The pellet was washed with 70% ethanol, centrifuged as before, then air dried for 30 minutes and resuspended in 100 μl TBE buffer (0.2mM EDTA, 2mM Tris pH 8.0).

Polymerase Chain Reaction (PCR) amplification was performed using genomic DNA from mouse ear or tail biopsies on a MJ Research PTC-200 Peltier Thermal Cycler. 1 μl of genomic DNA was used with 10 μl Megamix Blue reaction mix (Microzone, containing Taq polymerase, dNTPs, buffer, loading dye) and 1 μg/μl of each oligonucleotide primer specific for the gene-targeted loci (see Table 2.2) using the relevant cycles (see Table 2.3). PCR products were visualised by electrophoresis on 2% agarose (BDH Electran) gels containing ethidium bromide.

Gene	Primer	Primer sequence
Nrp1	NPneo	5'-CGTGATATTGCTGAAGAGCTTGGC-3'
	NP-F	5'-CAATGACACTGACCAGGCTTATCATC-3'
	NP-R	5'-GATTTTTATGGTCCCGCCACATTTGTC-3'
Nrp2	Nrp2neo	5'-CAGTGACAACGTCGAGCACAG-3'
	Nrp2 -F	5'-TCAGGACACGAAGTGAGAAGC-3'
	Nrp2-R	5'-GCTCAATGTAGCTAAGTGGAGGG-3'
$Nrp1^{Sema}$	P1	5'-AGGCCAATCAAAGTCCTGAAAGACAGTCCC-3'
	P2	5'-AAACCCCCTCAATTGATGTTAACACAGCCC-3'
Sema3A	semF	5'-CATTGTCAGCGCGTCTAGTGAGTGTTGG-3'
	semWT2	5'-CTGCAGACGCTGGAGGTCCCTGAG-3'
	semR	5'-CTTGTAATGGTTCTGATAGGTGAGGCATGG-3'
Sema3F	3F-31	5'-GAATGCCCGGGTAAACACCA -3'
	3F-32	5'- TCGAAGCGTACCCTGGCTCT-3'
	3F-33	5'- AAGGAGCGCACAGAGGACCA-3'
Sema3G	WT-F	5'- ATGACGCAGGAAACTACACT-3'
	WT-R	5'- AGTTCTGGACTCCTCTTTCC-3'
	KOF	5'- TTGCCAAGTTCTAATTCCAT-3'
Wnt1Cre	Wnt1cre F	5'-TAAGAGGCCTATAAGAGGCGG -3'
	Wnt1cre 2	5'- GTGGCAGATGGCGCGGCAACACCATT-3'
Tie2Cre	Cre84	5'-TGCCACGACCAAGTGACAGCAATG-3'
	Cre85	5'-ACCAGAGACGGAAATCCATCGCTC-3'
$Vegfa^{120}$	120F2	5'-CAGTCTATTGCCTCCTGACCTTCAGGGTC-3'
	120R2	5'-CTTGCGTCCACACCGTCACATTAAGTCAC-3'
	120E2	5'-TTCAGAGCGGAGAAAGCATTTGTTTGTCCA-3'
$Nrp1^{cyto}$	Cyto F	5'-CCTTTTGATGGACATGTGACCTGTAGC-3'
	Cyto R	5'-CACCAGGTCTGATTGAAGAGAAGG-3'
	Cyto Neo	5'-ATGGTACCTTGAGCATCTGACTTCTG-3'
Hs6st1	6OST-F	5'-ATGGTGACTGTGACCCACAA-3'
	6OST-R	5'-GGGATATAGGGGACCTTGGA-3'
	hPLAP-F	5'-ACAGCTGCCAGGATCCTAAA-3'
	hPLAP-R	5'-ACAGCTGCCAGGATCCTAAA-3'
Hs6st2	HS6ST2-34	5'-GTTCGGCCAGGTTTGTACC-3'
	HS6ST2-35	5'- CAGCTGGTGAGCTCGGTC-3'

	HS6ST2-neo	5'-GCAGCGCATCGCCTTCTATC-3'
	HS6ST2-	5'-CTAAGATAGGCTCTAGTGTCTAC-3'
Hs2st	Hs2st-1	5'-ATCAATGAATAATTGCCTAGGTC-3'
	Hs2st-2	5'-GGGAAGAAATTCACCCCAACA-3'
	Hs2st-v	5'-TACTCAGTGCAGTGCAGTCA-3'
Ext	Burn1-11	5'- AAGGATTCTCGCTGTGACAG-3'
	Burn1-35	5'- CCAAAACTTGGATACGAGCC-3'
Nes8Cre	Cre1	5'- GCCTGCATTACCGGTCGATGCAACGA -3'
	Cre2	5'- GTGGCAGATGGCGCGGCAACACCATT-3'
SRY	SRY 1:	5'-TCATGAGACTGCCAACCACAG-3'
	SRY 2:	5'-CATGACCACCACCACCACCAA-3'

Table 2.2: Specific oligonucleotide primers used in genotyping, synthesised from ordered designs by Sigma.

Gene	Hot Start	Denaturing	Annealing	Extension	Cycles	End
Nrp1	94°C, 3min	94°C, 40s	66°C, 1min	72°C, 1.5min	35 x	72°C, 5min
Nrp2	94°C, 2min	94°C, 30s	66°C, 45s	72°C, 1.3min	35 x	72°C, 5min
Nrp1^{Sema}	93°C, 3min	95°C, 30s	66°C, 30s	72°C, 1min	35 x	72°C, 5min
Sema3A	94°C, 4min	94°C, 40s	62°C, 1min	72°C, 1.5min	35 x	72°C, 5min
Sema3F	95°C, 5min	95°C, 1min	60°C, 1min	72°C, 1min	30 x	72°C, 10min
Sema3G	95°C, 2min	94°C, 1min	57.5°C, 1min	72°C, 1min	32 x	72°C, 5 min
Wnt1Cre	94°C, 4min	94°C, 40s	62°C, 1min	72°C, 1.5min	35 x	72°C, 5min
Tie2Cre	94°C, 3 min	94°C, 1min	67°C, 1min	72°C, 1min	32 x	72°C, 3min
Vegf$^{120/120}$	94°C, 3min	94°C, 40s	52°C, 1min	72°C, 1.5min	5 x	
		94°C, 40s	60°C, 1min	72°C, 1.5min	28 x	72°C, 5min
Nrp1^{cyto}	94°C, 2min	94°C, 40s	60°C, 30s	72°C, 1min	35 x	72°C, 10min
Hs6st1	94°C, 4min	94°C, 20s	58°C, 30s	72°C, 30s	29 x	72°C, 1min
Hs6st2	94°C, 4min	94°C, 30s	65°C, 1min	72°C, 1min	32 x	72°C, 10min
Hs2st	94°C, 3min	94°C, 40s	60°C, 45s	72°C, 2min	36 x	72°C, 5min
Ext	94°C, 2min	94°C, 45s	56°C, 45s	72°C, 2min	32 x	72°C, 5min
Nes8Cre	94°C, 3min	94°C, 1min	67°C, 1min	72°C, 1min	32 x	72°C, 3min
SRY	95°C, 5min	95°C, 30s	71.5°C, 45s	72°C, 45s	32 x	72°C, 5min

Table 2.3: PCR cycling parameters used in genotyping.

2.2.1.6 Tissue fixation

Mice pregnant with embryos at the required day of gestation were culled in accordance with Home Office Schedule 1 regulations. Embryos were dissected from the uterus into 1 x PBS solution on ice. Embryos were either kept as wholemounts, or the internal organs and heads removed to reveal sympathetic chains, or the hindbrains or hearts dissected out in PBS. Samples were fixed in 4% PFA at 4°C for either 2 hours or overnight depending on method to be used (see Table 2.4). Mouse pups at postnatal day (P) 7 were sacrificed in accordance with Home Office Schedule 1 regulation, and their hearts and aortas were dissected and fixed overnight in 4% PFA at 4°C.

2.2.2 Sectioning

2.2.2.1 Cryosectioning

Wholemount embryos and P7 hearts for immunolabelling were cryosectioned after fixation. Embryos to be used for AP-binding assay were not fixed, but frozen fresh. Samples were washed twice in PBT, and incubated at 4°C for 2 hours (or until embryos sank in solution) in 20% sucrose in PBT. They were embedded in OCT (Sakura Tissue-Tek), frozen rapidly on dry ice, and stored overnight at -20°C. Samples were sectioned at a thickness of 20 μm using a histology cryostat (Leica CM1850) and collected on Superfrost Plus slides (VWR International).

2.2.2.2 Vibratome sectioning

Postnatal dorsal aortas or pre-stained hindbrains were washed in 1X PBT and mounted in molten but cooled 3% agarose in water, and allowed to set. Samples were sectioned immediately using the Vibratome 1000Plus Sectioning System. Pre-stained sections were collected on glass slides and mounted in 90% glycerol.

2.2.3 Immunolabelling

2.2.3.1 Immunolabelling of sections

Slides containing cryosections were air dried for 1 hour at room temperature (RT). Sections for immunolabelling with a horseradish peroxidase (HRP)-tagged secondary antibody were bleached to remove endogenous peroxidase activity in 1:100 H_2O_2 in PBT for 30 minutes at RT. Sections to be immunolabelled with MASH1 antibody (which is raised in mouse) were first incubated in a mouse-on-mouse IgG blocking reagent (Vector Labs) for 1 hour at RT. This improves specificity as it blocks endogenous IgG in the tissue that may be recognised by the secondary antibody and increase background staining. All

sections were incubated in blocking solution for 30 minutes at RT, then incubated in primary antibody at appropriate concentration in blocking solution, for 1.5 hours at RT or overnight at 4°C (see Table 2.4 for antibody dilutions and blocking solutions). Samples blocked with Dako serum-free were incubated in primary and secondary antibodies in PBS with one drop of Dako serum-free block added. Slides were washed 5 times for 5 minutes each at RT in PBS. Sections were incubated in secondary antibody in blocking solution for 1.5 hours at RT or overnight at 4°C, in the dark for immunofluorescence labelling. Slides were washed 5 times for 5 minutes each at RT in PBS. Sections labelled for immunofluorescence were post-fixed in 4% PFA for 5 minutes. Sections immunolabelled with HRP-tagged secondary antibodies were subjected to colour development: incubation with diaminobenzidine (DAB) and hydrogen peroxide (SigmaFast, Sigma) in water for 5 minutes at RT or until colour developed. Development was stopped with PBS and sections post-fixed with 4% PFA for 5 minutes. Sections were mounted in Mowiol (CalBiochem). Vibratome sections were immunolabelled in the same way, but in individual wells of a multidish 24-well plate. They were mounted on glass slides in 90% glycerol.

2.2.3.2 Wholemount Immunolabelling

Samples were washed twice in PBT to permeabilise cell membranes to allow antibodies to enter the cells. Wholemount embryos for TH immunolabelling or hindbrains for IB4 immunolabelling were usually dehydrated in 50% methanol/PBT for 5 minutes, then methanol for 5 minutes and stored in methanol at -20°C until use. Samples were rehydrated in ascending series of PBT/methanol (75% methanol, 50% methanol, 25% methanol, PBT) before use. Samples to be immunolabelled with HRP-tagged secondary antibodies were bleached using hydrogen peroxide (1:100 H_2O_2 in PBT) for 30 minutes at RT to remove endogenous peroxidase activity, then washed twice in PBT. All samples were incubated in blocking solution for 30 minutes at RT, then incubated in primary antibody at appropriate concentration in blocking solution overnight at 4°C (see Table 2.4). Samples were then washed in PBT five times for 1 hour each at RT, before incubating in secondary antibody at appropriate concentration in blocking solution overnight at 4°C. Samples were washed five times as above, and either post-fixed in 4% PFA for 10 minutes at RT or colour developing with DAB and hydrogen peroxide (SigmaFast; Sigma), followed by post-fixing.

Primary Antibody (Dilution, producer)	Secondary Antibody (Dilution)	Fixation	Blocking solution
Rabbit anti-tyrosine hydroxylase (1:750, Milipore)	Anti-rabbit IgG-HRP (1:100) or AlexaFluor 488 or 594 goat anti-rabbit IgG (1:200)	Overnight, 4% PFA	10% NGS/PBT
Cy3 conjugated anti-a-smooth muscle actin (1:500, Sigma)	N/A	Overnight, 4% PFA	10% NGS/PBT
Rat anti-Endomucin (1:50, Santa Cruz)	AlexaFluor 488 or 633 goat anti-rat IgG (1:200)	Overnight, 4% PFA	10% NGS/PBT
Rabbit anti-Tuj1 (1:250, Milipore)	AlexaFluor 633 goat anti-mouse IgG (1:200)	Dent's (1 DMSO:4 MeOH)	1 ml NGS, 250 μl DMSO, 12.5 μl thimerosal
Mouse anti-MASH1 (1:50, BD Pharmingen)	AlexaFluor 488 anti-mouse Fab fragment (1:200)	2 hours, 4% PFA	Dako serum-free (PBS + 1 drop Dako serum-free)
Rabbit anti-NRP1 (1:100, Epitomics)	488 donkey anti-rabbit Fab fragment (1:200)	2 hours, 4% PFA	Dako serum-free (PBS + 1 drop Dako serum-free)
Goat anti-NRP1 (1:100, R&D Systems)	594 rabbit anti-goat Fab fragment (1:200)	2 hours, 4% PFA	Dako serum-free (PBS + 1 drop Dako serum-free)
Goat anti-NRP2 (1:100, R&D Systems)	594 rabbit anti-goat Fab fragment (1:200)	2 hours, 4% PFA	Dako serum-free (PBS + 1 drop Dako serum-free)
Rabbit anti-activated Caspase3 (1:200, R&D Systems)	AlexaFluor 594 goat anti-rabbit IgG (1:200)	2 hours, 4% PFA	Dako serum-free (PBS + 1 drop Dako serum-free)
Rat anti-PECAM (CD31) (1:200, BD Pharmingen)	Anti-rat IgG-HRP (1:100)	30 minutes, 4% PFA	10% NRS/PBT
Biotinylated Isolectin B4 (IB4) (1:100, Sigma)	Streptavidin-HRP (1:100) or AlexaFluor 594 Streptavidin (1:200)	Overnight (or 2 hours), 4% PFA	10% NGS/PBT
Mouse anti-10E4 (IgM) (1:250, Seikagaku Biobusiness)	AlexaFluor 488 anti-mouse IgM (1:200)	2 hours, 4% PFA	10% NGS/PBT

Table 2.4: Primary antibodies with working dilutions, secondary antibodies and appropriate fix and blocking solutions used in immunolabelling protocols. NGS, normal goat serum; NRS, normal rabbit serum. AlexaFluor secondary antibodies were from Invitrogen. HRP-tagged secondary antibodies were from Dako.

2.2.4 *In situ* hybridisation

Digoxigenin-labelled *Mash1* and *Isl1* antisense RNA probes were synthesised for *in situ* hybridisation from cDNA plasmid preparations. *Mash1*-containing plasmid was provided by Francois Guillemot, National Institute for Medical Research, London, and *Isl1* containing plasmid was provided by Tom Jessel, Columbia University, USA. All solutions for this protocol were kept RNAse-free.

2.2.4.1 Bacterial culture of plasmid containing probe

Initially, transformation-competent cells were made. A single colony of DH5a–derived electrocompetent *Escherichia coli* bacterial cells were cultured overnight at 37°C without shaking in 10 ml L-broth medium (10 g/l Bacto-tryptone, 5 g/l yeast extract, 5 g/l NaCl). 100 ml L-broth medium was inoculated with the original 10 ml and grown at 37°C in a shaker until the $O.D._{600}$ (optical density) reached 0.4. Bacterial cells were pelleted by centrifugation at 4000 rpm for 15 minutes at 4°C, and resuspended gently in 500 ml water at 4°C. Cells were centrifuged at 4200 rpm for 15 minutes at 4°C, and resuspended gently in 250 ml 4°C water. Previous centrifugation was repeated, and cells were resuspended in 20 ml of 4°C 10% glycerol in water. Cells were centrifuged at 4000 rpm for 10 minutes at 4°C, and resuspended in 3 ml of 4°C cold 10% glycerol in water. Competent cells were put into 80 μl aliquots and stored at -80°C until use.

1 μl of plasmid containing cDNA for *Mash1* or *Isl1* was gently mixed into 40 μl of slowly thawed competent cells, which was then transferred into sterile, chilled electroporation cuvette and electroporated by briefly shocking them with an electric field of 10-20kV/cm. 1 ml L-broth was added to the cuvette and the solution was transferred to a 1.5 ml eppendorf and incubated at 37°C for 30 minutes. The culture was spread onto an LB agar plate (L-broth + 100 μg/ml ampicilin + 15 g/l agar added prior to autoclaving) and incubated overnight at 37°C. A single colony was picked and grown in 2 ml L-broth (+ 100 μg/ml ampicilin) overnight at 37°C.

2.2.4.2 RNA probe synthesis

Plasmid was isolated with the Qiagen QIAprep Spin Miniprep kit, according to manufacturer's instructions. Briefly, bacterial cells were pelleted by centrifugation at 12000 rpm for 5 minutes and resuspended in 250 μl cold Buffer P1 (containing RNAse A). 250 μl Buffer P2 (NaOH/SDS-containing lysis solution) was added and the solution mixed, then 350 μl Buffer N3 (high-salt neutralising solution) was added and mixed, then the solution centrifuged at 13000 rpm for 10 minutes. The supernatant was applied to QIAprep spin column, which was centrifuged for 30 seconds and washed with 750 μl Buffer PE followed by another 30 seconds centrifugation. DNA was eluted from the column

by applying 50 μl water, centrifuging for 1 minute and collecting flow-through in a fresh tube.

Restriction enzyme analysis was initially carried out to validate the plasmids. Then, the plasmid DNA was linearised by digestion with an appropriate restriction enzyme (New England Biolabs) for 2.5 hours at 37°C in a reaction mixture containing: 5 μl plasmid DNA, 4 μl buffer, 4 μl 10X BSA, 1 μl enzyme, 26 μl water. DNA was extracted by standard phenol/chloroform extraction and resuspended in 15 μl water. RNA was synthesised by reverse transcription, in a reaction mixture containing: 14.5 μl DNA and 2 μl 10X transcription buffer , 2 μ 10X DIG, 1 μl polymerase and 0.5 μl RNAse inhibitor (Roche) for 2.5 hours at 37°C. RNA was precipitated by adding 100 μl water, 8 μl 5M lithium chloride, 1 μl glycogen and 300 μl ethanol, leaving the tube at -80°C for 20 minutes followed by centrifugation at 13000 rpm at 4°C for 15 minutes, washing the pellet in 70% ethanol and resuspending the pellet in 40 μl water. For *Mash1* probe, XbaI restriction enzyme was used with buffer B2, and then SP6 polymerase. For *Isl1* probe, NcoI restriction enzyme was used with buffer B4, and then SP6 polymerase.

2.2.4.3 In situ hybridisation

Tissues were fixed overnight in 4% PFA at 4°C, dehydrated and stored as before. Wholemount samples were then bleached in 6% hydrogen peroxide in methanol for 1 hour at RT before rehydrating into PBT. Samples were incubated in hybridisation block (50% formamide, 5X SSC (sodium citrate, sodium chloride, citric acid) pH4.5, 50 μg/ml tRNA (Roche), 50 μg/ml heparin (Sigma), 1% SDS) for 30 minutes at 70°C and then incubated in RNA probe solution (3μl probe in 1ml hybridisation block) overnight at 65°C. Samples were then washed 3 times in solution 1 (50% formamide, 5X SSC pH4.5, 1% SDS) and 3 times in solution 3 (50% formamide, 2X SCC pH4.5) for 30 minutes each at 65°C, then twice briefly in TBST (1 X TBS, 0.1% Tween-20) at RT. Samples were blocked in 10% sheep serum in TBST for 30 minutes at RT, then incubated in anti-digoxigenin antibody (Roche) at 1:5000 in 1% sheep serum in TBST overnight at 4°C. Samples were washed in TBST 5 times for 1 hour at RT and once overnight at 4°C. Samples were washed 3 times in NTMT solution (0.1M NaCl, 0.1M Tris-HCl at pH9.5, 0.05M $MgCl_2$, 1% Tween20) for 10 minutes at RT, then incubated in developing solution (3.5 μl BCIP and 4.5 μl NBT (Roche) per ml NTMT) at RT until colour developed. The reaction was stopped by washing in TBST and fixing in 4% PFA for 10 minutes at RT.

2.2.5 Labelling techniques

2.2.5.1 X-gal assay

X-gal staining was used to visualise β-galactosidase activity in samples containing the gene for this enzyme (*lacZ*) inserted into the locus of a specific gene. Embryos were dissected and fixed in 4% PFA for 30 minutes at 4°C. Embryos washed in PBS/0.02% NP40 three times for 15 minutes at RT, then incubated in X-gal (stored at 1 mg/ml X-Gal in PBS/0.02% NP40) added 1:40 into staining solution (5 mM $K_3Fe(CN)_6$, 5 mM $K_4Fe(CN)_6xH_20$, 2 mM $MgCl_2$, 0.01% sodium deoxycholate) at 37°C for a few hours or until colour developed. The reaction was stopped by washing with PBS and post-fixing in 4% PFA.

2.2.5.2 Alkaline phosphatase (AP)-binding assay

Expression vectors encoding AP only, AP-SEMA3A and AP-SEMA3F were kindly provided by Drs Jonathan Epstein and Jonathan Raper, University of Pennsylvania, Philadelphia, USA. AP expression vectors were transformed into HEK-293T cells, the fusion proteins collected and their activity tested by Joaquim Vieira.

Cryosections of freshly frozen tissue were kept at -20°C until fixation in methanol cooled to -20°C for 5 minutes. Sections were then washed three times in AP wash buffer (1x PBS + 4mM $MgCl_2$) for 5 minutes at RT, blocked in 10% FBS in AP wash buffer for 30 minutes at RT, then incubated in AP-ligand overnight at 4°C in a wet chamber. After washing five times in PBS for 5 minutes each with gentle shaking, bound ligand was fixed using 4% PFA for 5 minutes at RT and sections were washed again three times in PBS for 5 minutes each. Sections were incubated for 3 hours in a wet chamber at 65°C in PBS to inactivate endogenous phosphatases. After washing briefly twice in PBS, sections were incubated in AP stain buffer (100mM Tris pH 9.5, 100mM NaCl, 5mM $MgCl_2$) for 5 minutes at RT, then in AP stain solution (3.375 μl NBT + 3.5 μl BCIP per 1 ml AP stain buffer) for 3 hours at 37°C then overnight at RT. Staining was stopped with PBS then 4% PFA for 5 minutes, and slides were mounted in glycerol.

2.2.6 Imaging

2.2.6.1 Imaging of cryosections and wholemount samples

Fluorescently labelled cryosections of embryos, postnatal hearts or dorsal aortas were imaged using the Zeiss LSM510 confocal microscope with Zeiss LSM510 operating software.

Cryosections of embryos immunolabelled with HRP for TH to visualise the sympathetic ganglia and cryosections of embryos labelled by *Mash1 in situ* hybridisation were imaged

using a stereo dissection microscope (Olympus SZX16) with Hamamatsu camera controller (C4742-95) and Simple PCI Version 6.6 software. Areas of ganglia and distances between ganglia were calculated using ImageJ Version 1.39u software.

Wholemount embryos immunolabelled with HRP for TH for visualisation of sympathetic chains were imaged using a stereo dissection microscope (Leica MZ16) and camera (Q Imaging Micropublisher 3.3 RTV) with Improvision OpenLab version 5.5.2 software.

Wholemount hearts were imaged using the Olympus stereo dissection microscope with an Olympus fluorescent lamp (U-RFL-T) with Hamamatsu camera and Simple PCI software, as above.

2.2.6.2 Quantification of blood vessel branching in hindbrains

Wholemount hindbrains immunolabelled with either PECAM antibodies or IB4 were flattened with glass coverslips onto 4% agarose gel plates and imaged using a stereo dissection microscope with camera and software, as above. Images were taken at a magnification of 11.5x in four areas, two in random areas on each side of the midline. The number of vessel branchpoints were quantified inside a rectangle template of dimensions 0.4mm x 0.5mm that was superimposed on the original image.

Wholemount hindbrains labelled with immunofluorescence were mounted on glass slides with mounts using Slowfade Antifade mounting kit (Invitrogen) and covered with glass coverslips. These were imaged using confocal microscopy on the Zeiss, and the number of vessel branches was quantified in a whole 20X image. Differences in numbers of vessel branchpoints were statistically analysed using paired student's t-tests.

2.2.7 Genetic studies

2.2.7.1 Microarray

RNA isolation was carried out by Alessandro Fantin from the Ruhrberg lab (see section 2.8.2 below). Affymetrix GeneChip Technology microarray and RNA quality control was carried out by the UCL Genomics department. Briefly, RNA samples from hindbrains of 6 E11.5 wildtype embryos were applied to Mouse Gene 1.0 ST Array microarray chips containing 27 small oligonucleotides spread over the full length of each gene in the mouse genome. The readout was the average fluorescent signal, normalised to a housekeeping gene, which was representative of relative expression of the gene.

2.2.7.2 q-PCR

RNA was isolated from two litters of E12.5 hindbrains. The tissue was homogenised in 1 ml Trizol in a 1.5 ml eppendorf by passing it through a 5/8" gauge needle and syringe. 250

μl chloroform was added per tube and the tube vortexed for 15 seconds, incubated at RT for 10 minutes, vortexed again for 15 seconds and centrifuged at 12000 rpm for 15 minutes at 4°C. The top layer of liquid was removed into a fresh tube and 500 μl isopropanol added. The tube was then mixed gently and incubated at RT for 10 minutes before centrifugation at 12000 rpm for 10 minutes at 4°C to pellet the RNA. The pellet was then washed in 70% ethanol, air dried for 30 minutes and resuspended in 20 μl RNAse-free water. RNA was quantified and quality assessed using a Nanodrop Spectrophotometer ND-1000 with Nanodrop 1000 Version 3.7.1 software (ThermoScientific).

Single stranded cDNA was synthesised from 1 μg RNA, firstly in a reaction mixture with 1 μl random primers and 2 μl dNTP mix made up to 12 μl with RNAse-free water, which was heated to 65°C for 5 minutes then quickly chilled on ice. Next, 4 μl of 5x First Strand buffer, 2 μl 0.1M DTT and 1 μl RNAse OUT were added and the tube mixed gently and incubated at 25°C for 5 minutes. Finally, 1 μl Superscript II polymerase enzyme was added and pipetted up and down to mix, before incubation at 25°C for 10 minutes, 42°C for 50 minutes, and the reaction inactivated at 70°C for 15 minutes. The cDNA was stored at -20°C until q-PCR was carried out (all reagents from Invitrogen).

Primers for *Hs6st1*, *Hs6st2*, *Hs6st3* and *18s* were made to order by Sigma (see Table 2.5). q-PCR was carried out in optical 96-well reaction plates using the PowerSybr system (Applied Biosystems). Each sample was analysed in triplicate for each primer set. *18s* amplification served as an internal control to normalise expression levels between samples. Reaction mixture per well for *Hs6st1*, *Hs6st2* and *Hs6st3* primers: 0.3 μl cDNA, 12.5 μl PowerSybr, 0.075 μl each primer, 12.05 μl water. For 18s housekeeping primers, a 1:10 dilution of all cDNA samples was used to account for the large amount of *18s* RNA in the samples, 0.15 μl each primer used and the volume of water added adjusted accordingly to make up to 25 μl total volume. Plates were centrifuged briefly to collect the liquid and run on a 7900HT Fast Real Time PCR System with 7900HT Version 2.2.2 Sequence Detection Systems software (Applied Biosystems). Raw fluorescence data was analysed using DART-PCR Version 1.0 software, which converts it to relative expression (Peirson et al., 2003). Relative expression was normalised to the internal control, *18s* RNA, and final data was presented as fold change from control samples, i.e. wildtype.

Gene	Primer	Primer sequence
Hs6st1	Hs6st1-F	5'-GTTCGCCCAGAAAGTTCTAC-3'
	Hs6st1-R	5'-GGATGAAAGATAGGTTGTAGCAG-3'
Hs6st2	Hs6st2-F	5'-GAGTGGGAAGAACTTCCATTAC-3'
	Hs6st2-R	5'-GTTGTAGCATCCCACTAGAG-3'
Hs6st3	Hs6st3-F	5'-AGCCACACCAGGAATTTCTA-3'
	Hs6st3-R	5'-GCTACAATCCATGAACTCCC-3'

Table 2.5: Primers designed for Hs6st gene amplification in q-PCR.

3. NEUROPILINS IN THE DEVELOPING SYMPATHETIC NERVOUS SYSTEM

3.1 Introduction

Mice lacking NRP1 have disorganised sympathetic chains and sympathetic axon misguidance, but NCC migration was previously reported to be normal (Kawasaki et al., 2002). In contrast, other work showed that NRP1/SEMA3A signalling repels trunk NCCs *in vitro* (Eickholt et al., 1999). A publication I co-authored in 2009 showed that NRP1/SEMA3A signalling does coordinate trunk NCC guidance, as mice lacking NRP1 have increased NCC migration along the intersomitic boundary and in the dermomyotome layer instead of the sclerotome (Schwarz et al., 2009b). I therefore wanted to investigate more thoroughly the implications of this misguided migration on the sympathetic nervous system. In mice lacking SEMA3F/NRP2 signalling, segmental NCC migration is disrupted (Gammill et al., 2006), but whether this affects the sympathetic nervous system has not been studied. SEMA3F repels sympathetic axons through NRP2 *in vitro* (Giger et al., 2000); however loss of NRP2 reportedly does not affect the sympathetic nervous system *in vivo* (Waimey et al., 2008). Therefore my first aim in this chapter was to investigate how NRP1 and NRP2 and their SEMA ligands control the early steps in the development of the sympathetic nervous system from sympathetic NCCs in the mouse.

SEMA3A patterns sympathetic innervation of the heart in postnatal mice by maintaining an epicardial-to-endocardial gradient of sympathetic fibres (Ieda et al., 2007). My second aim was to assess whether NRP1 patterns sympathetic axon extension in target organs by investigating postnatal heart innervation. The dorsal aorta is another target of sympathetic innervation, and I also investigated if this was affected by NRP1 signalling.

The recently discovered semaphorin, SEMA3G, binds NRP2 and repels sympathetic axons *in vitro*, and its embryonic expression is mainly restricted to arteries and sensory ganglia (Kutschera et al., 2011; Taniguchi et al., 2005). My third aim was to attempt to find an *in vivo* role for SEMA3G in helping pattern the sympathetic nervous system.

3.2 Results

3.2.1 Expression of the neuropilins in the sympathetic nervous system

3.2.1.1 NRP1 and NRP2 are differentially expressed by neural crest cells

Initially, I wanted to ascertain whether trunk NCCs express either or both of the neuropilin receptors. I cut transverse cryosections through wildtype embryos at E9.5 at forelimb level and immunolabelled these with antibodies against NRP1 and NRP2 (Fig. 3.1A-C). At this stage in mouse development, the first of the early wave NCCs destined to be

sympathetic neurons had aggregated at the dorsal aorta. NRP1 was expressed in recently delaminated NCCs migrating through the dorsal somite, as well as in sympathetic NCCs aggregated at the dorsal aorta (Fig. 3.1A,G). NRP1 was also strongly expressed in the endothelium of the dorsal aorta, as previously shown at this stage (Kitsukawa et al., 1995). The sympathetic NCCs at the dorsal aorta did not express NRP2 (Fig. 3.1B,C,H). A subset of migratory NCCs in the dorsal somite was NRP2-positive. NRP2 was also expressed in the sclerotome and the developing posterior cardinal vein. Venous expression of NRP2 had previously been shown in the cardinal veins of chick (Herzog et al., 2001). All migratory NCCs expressed NRP1 but only some co-expressed NRP1 and NRP2 (yellow in Fig. 3.1C), suggesting that all migratory NCCs are NRP1-positive, whereas only a subset is also NRP2-positive. The merged image confirmed that the sympathetic NCCs aggregated at the dorsal aorta were NRP1-positive and NRP2-negative (Fig. 3.1C,I).

3.2.1.2 NRP1 and NRP2 are expressed by mature sympathetic neurons

At later developmental stages, transverse cryosections through a wildtype mouse at E11.5 (Fig. 3.1D-F) showed that the dorsal aorta and cardinal veins continued to express NRP1 and NRP2, respectively. Several non-NC-derived neural structures, such as the dorsal funiculus and radial nerves, expressed NRP1 (Fig. 3.1D). NRP2 was expressed in parts of the sclerotome and myotome, and in the lower part of the neural tube (Fig. 3.1E). The neurons of the sympathetic ganglia were strongly NRP1-positive (Fig. 3.1J), and the sensory neurons of the DRG, another type of NC-derived structure, were also NRP1-positive (Fig. 3.1D,F). The sympathetic neurons in the ganglia were strongly NRP2-positive (Fig. 3.1E,F,K). This suggested that sympathetic neurons expressed NRP2 even though their NC precursors did not.

These findings were confirmed by co-labelling of sympathetic neurons with antibodies for sympathetic markers and neuropilins. Transverse cryosections through E9.5 and E11.5 wildtype embryos at forelimb level were immunolabelled with an antibody against the sympathetic NC marker MASH1 or the mature sympathetic marker tyrosine hydroxylase (TH) and NRP1 or NRP2 (Fig. 3.2). At E9.5, NRP1 and MASH1 staining co-localised in the sympathetic NCCs of the primary sympathetic ganglia at the dorsal aorta (yellow in Fig. 3.2A,C), but these MASH1-positive sympathetic NCCs were not NRP2-positive (Fig. 3.2B,D). The dorsal aorta was NRP1-positive, as were the migratory NCCs in the somite, as shown above (Fig. 3.2A). Some migratory NCCs were NRP2-positive, and NRP2 was also expressed in the sclerotome and the posterior cardinal vein, as shown above (Fig. 3.2B). At E11.5, mature sympathetic neurons in the ganglia co-expressed TH and NRP1 (Fig. 3.2E,G-I). TH-positive sympathetic neurons of the ganglia also expressed NRP2 (Fig. 3.2F,J-L). The dorsal aorta, DRGs and spinal nerves were NRP1-positive, and the posterior cardinal veins and the areas of sclerotome and myotome were NRP2-positive, as observed before (Fig.

3.1). Taken together, the results show that the early migratory wave of NCC destined to become sympathetic neurons express NRP1 but not NRP2, and once they have differentiated into mature sympathetic neurons, they express both NRP1 and NRP2. These observations suggest that the neuropilins may have different functions during sympathetic development.

3.2.1.3 SEMA3A binds NRP1 on sympathetic neurons

SEMA3A and SEMA3F act as axon guidance molecules in fasciculation and branching of the developing nervous system through NRP1 and NRP2, respectively, in plexin co-receptor complexes (Kitsukawa et al., 1997; Sahay et al., 2003; Taniguchi et al., 1997). An alkaline phosphatase (AP)-binding assay using protein constructs containing AP-tagged SEMA3A and SEMA3F or AP alone allowed visualisation of the localisation of SEMA-binding in wildtype embryos (Fig 3.3A,C,E). SEMA3A bound to the sympathetic ganglia and sympathetic axons (Fig. 3.3A, inset), as well as the radial nerves and dorsal funiculus (Fig. 3.3A), all of which were previously shown to express NRP1 (Figs. 3.1D and 3.2E). SEMA3A also bound the subepicardial layer of the heart and the lungs, in accordance with its functions in heart innervation and lung development (Ieda et al., 2007; Ito et al., 2000). SEMA3F bound to the sympathetic ganglia and axons (Fig. 3.3C, inset), which express NRP2 (Figs. 3.1E and 3.2F). SEMA3F also bound the ventral neural tube (Fig. 3.3C), which expressed NRP2 (Figs. 3.1E and 3.2D), the tissue surrounding developing rib bones (Fig. 3.3C), perhaps consistent with a role in patterning sympathetic innervation of the intercostal bones (Asmus et al., 2000), and weakly in lung tissue (Fig. 3.3C), consistent with its role in lung morphogenesis (Kagoshima and Ito, 2001). The control AP-only construct did not bind any tissues (Fig. 3.3E). Due to the endogenous AP activity of blood, tissues with blood accumulation, such as the dorsal aorta and heart ventricles, were positive in all reactions including the negative control (Fig. 3.3A,C,E).

To confirm that SEMA3A bound NRP1 in the sympathetic ganglia, I carried out the AP-binding assay with tissues from embryos with point mutations in the SEMA-binding domain of the *Nrp1* gene (termed $Nrp1^{Sema}$ mutation; (Gu et al., 2002))(Fig. 3.3B,D,F). SEMA3A did not bind the sympathetic ganglia, sympathetic axons (Fig. 3.3B, inset), axons of the dorsal funiculus or the subepicardium of the heart in $Nrp1^{Sema}$ mutants (Fig. 3.3B). Since these were all bound by SEMA3A in wildtype tissue, this indicates that SEMA3A requires NRP1 to bind these tissues. Surprisingly, lung tissue was still bound by SEMA3A, suggesting that SEMA3A can bind to another receptor in this tissue. There is precedence for this finding, as SEMA3A binds vomeronasal axons through either NRP1 or NRP2 (Cariboni et al., 2011). SEMA3F bound the sympathetic ganglia and axons (Fig. 3.3D, inset), ventral neural tube and the tissue surrounding the developing rib bones in $Nrp1^{Sema}$

mutants as in wildtype (Fig. 3.3D), confirming that SEMA3F requires NRP2 but not NRP1. Again, the AP control construct did not bind any tissue (Fig. 3.3F).

E9.5
E11.5
NRP1
NRP2
NRP1 / NRP2
A
B
C
D
E
F
G
H
I
J
K
L
nt
da
psg
sg
drg

Figure 3.1: Sympathetic NCCs express NRP1 and mature sympathetic neurons express both NRP1 and NRP2.

Transverse 20μm cryosections at forelimb level through wildtype embryos at E9.5 (A-C; box in C magnified in G-I) and E11.5 (D-F; box in F magnified in J-L) immunolabelled for NRP1 (green) and NRP2 (red). At E9.5, the first NCCs aggregated at the dorsal aorta (da) to seed the primary sympathetic ganglia (psg) expressed NRP1 (A) but not NRP2 (B); accordingly, they appeared green, not yellow, in the merged image (C,I). NCCs migrating through the somite were positive for both NRP1 and NRP2 (yellow in C). At E11.5, sympathetic neurons forming the sympathetic ganglia (sg) were positive for both NRP1 (D) and NRP2 (E), as ganglia appeared yellow in the merged image (F,L). nt, neural tube; drg, dorsal root ganglia. Scale bars: A-C – 50 μm; D-F – 200 μm.

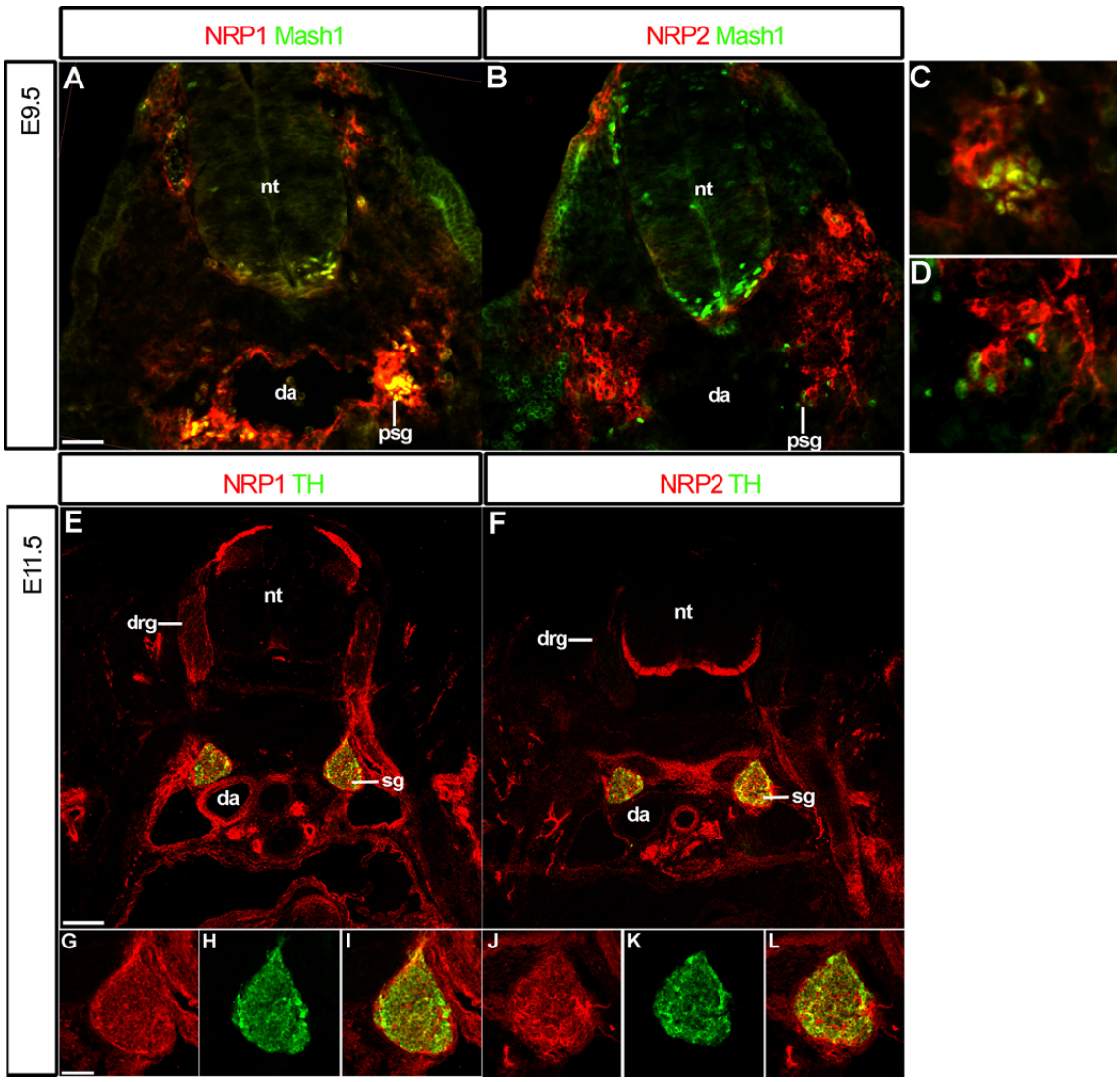

Figure 3.2: MASH1-positive NC sympathetic precursors express NRP1, and TH-positive sympathetic neurons express both NRP1 and NRP2.

Transverse 20μm cryosections at forelimb level through wildtype embryos at E9.5 (A-D) and E11.5 (E-L) immunolabelled for NRP1 or NRP2 (red) and TH or MASH1 (green). At E9.5, sympathetic precursors in the primary sympathetic ganglia (psg) expressed MASH1 and NRP1 (yellow, A; labelled psg magnified in C) but not NRP2 (B; labelled psg magnified in D). At E11.5, sympathetic neurons in the sympathetic ganglia (sg) expressed TH as well as NRP1 (E; labelled sg magnified in G-I) and NRP2 (F; labelled sg magnified in J-L). NRPs were localised to the cell surface, whereas TH was in the cytoplasm. nt, neural tube; drg, dorsal root ganglia. Scale bars: A-B – 50 μm; E-F – 500 μm.

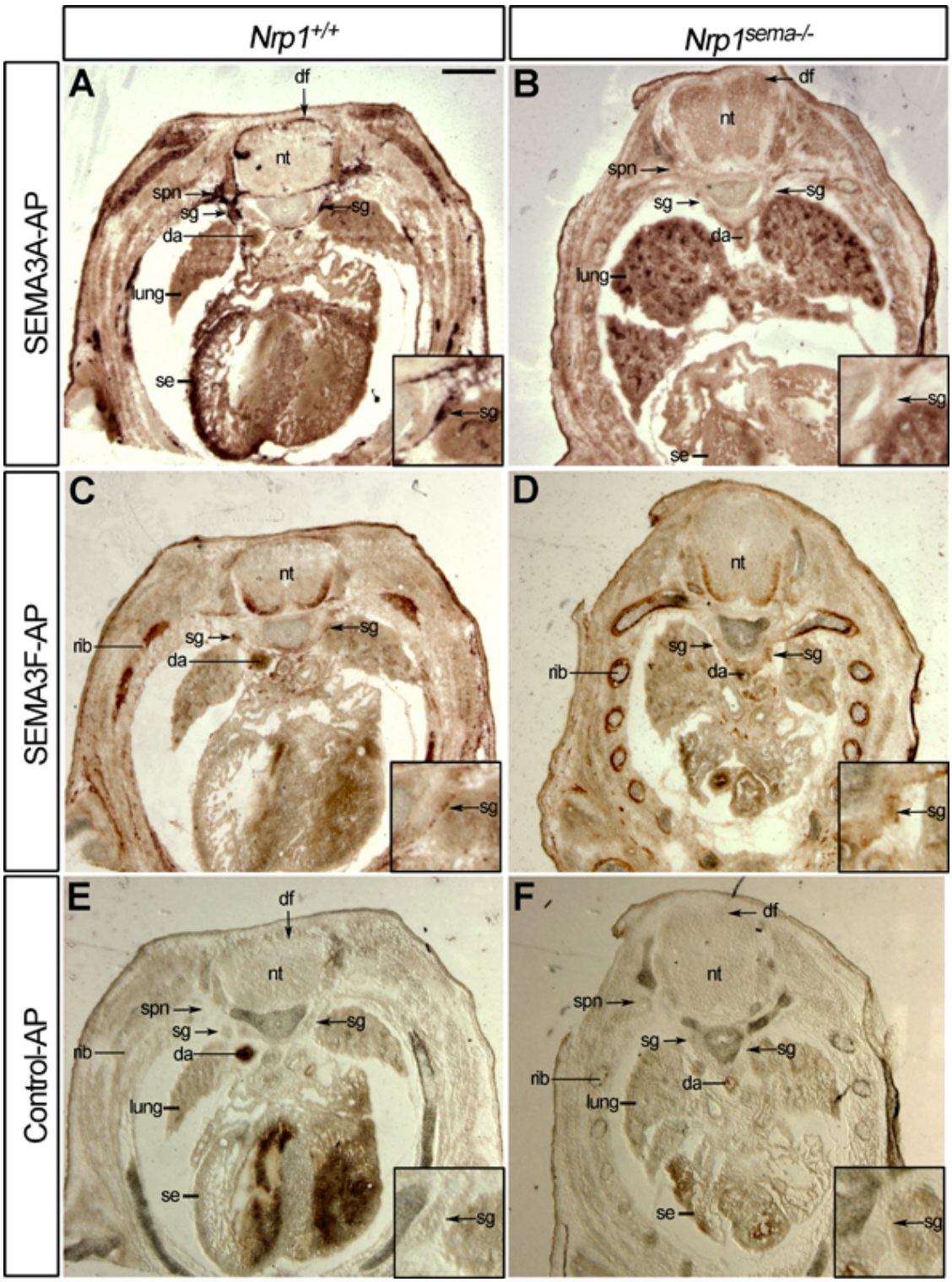
Nrp1+/+
Nrp1sema-/-
SEMA3A-AP
SEMA3F-AP
Control-AP
A
B
C
D
E
F
df
nt
spn
sg
da
lung
se
rib

Figure 3.3: SEMA3A and SEMA3F bind sympathetic neurons.

Transverse cryosections at forelimb level through E14.5 wildtype (A,C,E) and *Nrp1*$^{sema-/-}$ (B,D,F) embryos, with bound AP-tagged SEMA3A, SEMA3F or control AP-only construct. Higher magnification of the left sympathetic ganglia (sg) is shown in inset of each panel. In wildtype tissue, SEMA3A bound sympathetic ganglia and axons, as well as the dorsal funiculus (df), spinal nerves (spn), lung tissue (labelled) and subepicardium (se) of the heart (A). SEMA3A binding was abolished in *Nrp1*$^{sema-/-}$ embryos, except in lung tissue (B). SEMA3F bound sympathetic ganglia and axons, the ventral neural tube (nt) and tissue surrounding developing rib bones (C). Binding persisted in *Nrp1*$^{sema-/-}$ embryos (D). Control AP-construct did not bind tissue of wildtype or *Nrp1*$^{sema-/-}$ embryos (E,F). da, dorsal aorta. Scale bar: 500 μm.

3.2.2 Different roles for NRP1 and NRP2 in sympathetic nervous system development

3.2.2.1 NRP1 signalling controls sympathetic precursor placement

The findings so far suggest that NRP1 and NRP2 have different roles in the development of the sympathetic nervous system, most likely through signalling with their respective ligands SEMA3A and SEMA3F. Working on a project with Dr Quenten Schwarz, we provided evidence that NRP1 and NRP2 coordinate different aspects of trunk NCC migration (Schwarz et al., 2009a). To clarify the role of NRP1 in sympathetic nervous system development, I subjected E9.5 embryos lacking NRP1 and wildtype littermates to *in situ* hybridisation using an RNA probe for *Mash1*, the early sympathetic marker. I then immunolabelled transverse cryosections of these embryos with endomucin to mark the vasculature and smooth muscle actin to mark the dorsal aorta (Fig. 3.4). Two bilateral *Mash1*-positive primary sympathetic ganglia were visible adjacent to the dorsal aorta in wildtype embryos (Fig. 3.4A). Primary sympathetic ganglia were also present in 4/4 embryos lacking NRP1, however, they all had sympathetic precursors in ectopic locations, and 1/4 had small clusters of *Mash1*-positive sympathetic precursors lateral to the posterior cardinal veins (Fig. 3.4B).

Immunolabelling of cryosections from E11.5 wildtype embryos with endomucin, the sympathetic marker TH and the neuronal marker Tuj1 revealed TH- and Tuj1-positive sympathetic neurons in compact sympathetic ganglia between the dorsal aorta and posterior cardinal veins (Fig. 3.5A,C,E). In mutants, the sympathetic ganglia were dispersed (Fig. 3.5B), and some neurons were seen in ectopic locations lateral to the posterior cardinal veins (Fig. 3.5D,F), similar to the phenotype observed in earlier ages (Fig. 3.4B). The sympathetic neurons in all positions were TH- and Tuj1-positive, indicating that despite their aberrant location, sympathetic differentiation proceeded. Interestingly, ectopic neurons often seemed to be positioned in close proximity to blood vessels, perhaps because blood vessels are surrounded by a fibronectin-rich ECM favourable to migratory NCCs (Francis et al., 2002; Newgreen et al., 1982). DRGs were also misshapen in the *Nrp1*-null mutant, confirming previous observations that NRP1 regulates migration or differentiation of sensory NCC populations (Schwarz et al., 2009b).

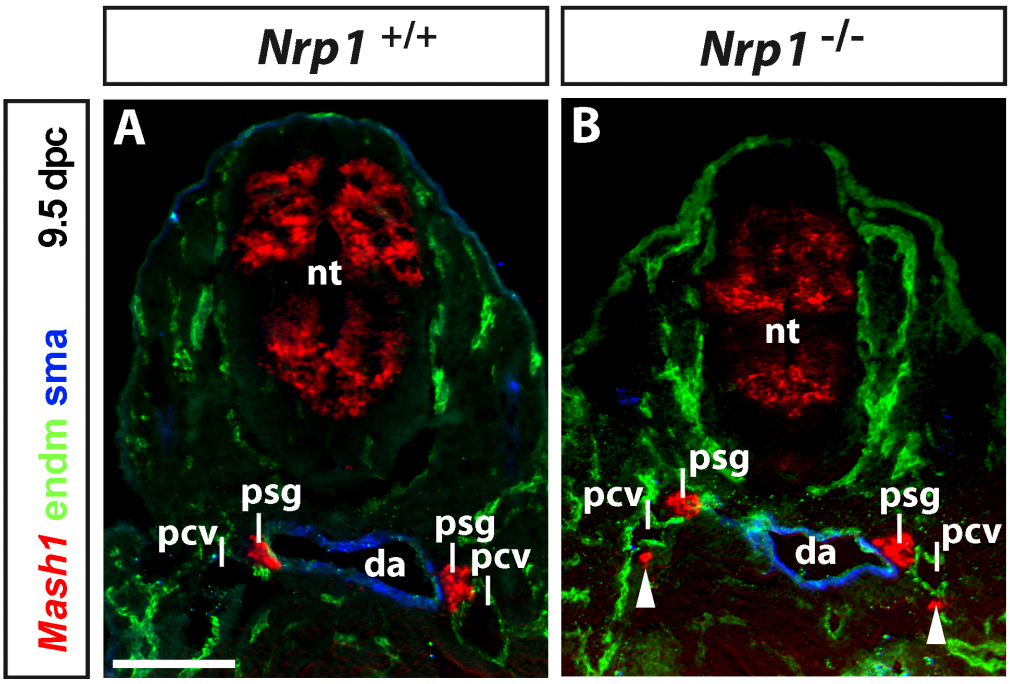

Figure 3.4: Ectopic sympathetic precursors in NRP1 mutants.

E9.5 wildtype and *Nrp1*-null mutant embryos labelled by wholemount *in situ* hybridisation with *Mash1* probe (alkaline phosphatase reaction product pseudocoloured in red), transverse sections at forelimb level were immunolabelled for endomucin (endm, green) and smooth muscle actin (sma, blue). In wildtype embryos (A; n=3), *Mash1*-positive sympathetic precursors aggregated into primary sympathetic ganglia (psg), in between the dorsal aorta (da) and the posterior cardinal veins (pcv). In *Nrp1*-null embryos (B; n=4), there were some *Mash1*-positive precursors in ectopic positions on the distal side of the pcv (white arrowheads). Scale bar: 100 μm.

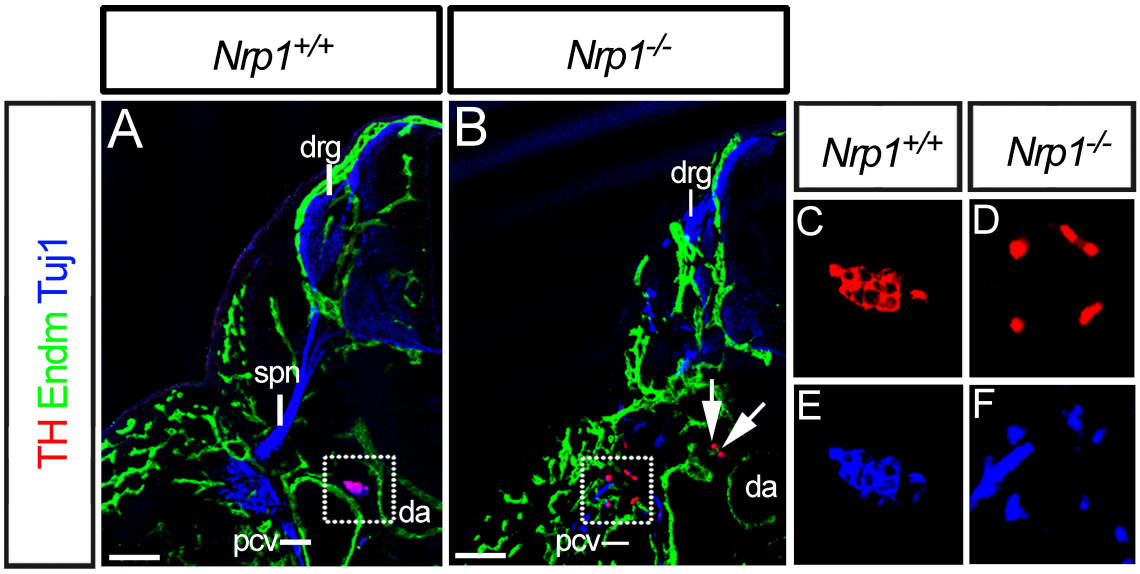

Figure 3.5: Ectopic sympathetic precursors in NRP1 mutants differentiate into neurons.

Transverse cryosections of E11.5 wildtype and *Nrp1*-null embryos immunolabelled for Tuj1 (blue), tyrosine hydroxylase (TH, red) and endomucin (Endm, green); half the section is shown. In wildtype (A), Tuj1-positive dorsal root ganglia (drg) formed properly in the same plane as a spinal nerve (spn). Tuj1- and TH-positive neurons were aggregated between the dorsal aorta (da) and the posterior cardinal vein (pcv), forming the primary sympathetic ganglia (box in A magnified in C,E; n=3). In *Nrp1*-null mutants (B), DRGs were misshapen and there were fewer sympathetic neurons in the primary sympathetic ganglia (arrows in B), with TH- and Tuj1-positive ectopic neurons lateral to the pcv (box in B magnified in D,F; n=3). Scale bars: 100 μm.

3.2.2.2 NRP1/SEMA3A and NRP2/SEMA3F signalling control sympathetic chain organisation

To visualise sympathetic chains in wholemounts, the head and internal organs including liver, stomach, heart and lungs were dissected away from E13.5 embryos and the remaining trunk immunolabelled with TH antibody and an HRP-conjugated secondary antibody (Fig. 3.6). Sympathetic chains in wildtype embryos lay either side of the dorsal aorta, and stretched from the anterior superior cervical ganglia towards the posterior end of the embryo (Fig. 3.6A, long bracket). Individual ganglia were visible as grouped clusters of TH-positive neurons in a string formation (Fig. 3.6A, short bracket), with axons stretching the length of the string of ganglia, completing the chain structure. In *Nrp1*-null embryos, the sympathetic chains were disorganised. The neuronal cell bodies were dispersed in loose clusters instead of tight ganglia (Fig. 3.6B,F). Many sympathetic axons did not remain in the chain, but prematurely extended inwards towards the dorsal aorta. Sympathetic neurons were seen in ectopic locations distal to the dorsal aorta (Fig. 3.6G), consistent with observations from earlier developmental stages (Figs. 3.4B and 3.5B), and particularly at forelimb level. This agrees with the high expression of SEMA3A in the forelimb (Schwarz et al., 2009b), as without NRP1/SEMA3A signalling the sympathetic NCC could stray into these areas. These characteristics were phenocopied in embryos lacking SEMA3A (Fig. 3.6, compare B with C, and G with H), and were consistent with previous findings (Kawasaki et al., 2002).

The sympathetic nervous system was affected mildly in embryos lacking NRP2, as some sympathetic axons extended from the chain prematurely and reached towards and around the dorsal aorta (Fig. 3.6D,I). Similarly, in mice lacking SEMA3F, some axons were lying on top of and around the dorsal aorta (Fig. 3.6E,J). However, in contrast to *Nrp1*- or *Sema3a*-null embryos, the sympathetic ganglia appeared well condensed. To verify that the sympathetic neurons were as condensed in mutants as in wildtypes, I quantified the area of ganglia and the distance between the ganglia in cryosections through the trunk of E14.5 wildtype and *Nrp2*-null mice immunolabelled with TH (Fig. 3.7A-D). There were large changes in ganglia area and distance at different anteroposterior levels in each embryo. Therefore I took measurements from two different levels: the anterior SCG level and further posteriorly in the trunk where the sympathetic chains are thinner, termed sympathetic chain level. There were no significant differences between wildtypes and *Nrp2*-null mutants in ganglia area (Fig. 3.7E; mean SCG area: wildtypes $0.034mm^2 \pm 0.002mm^2$ versus NRP2 mutants $0.034mm^2 \pm 0.004mm2$, $P = 0.974$ in a paired t-test); mean chain area: wildtypes $0.01mm^2 \pm 0.002mm^2$ versus mutants $0.012mm^2 \pm 0.002mm^2$, $P = 0.465$ in a paired t-test) or in distance between ganglia (Fig. 3.7F; mean inter-SCG distance wildtypes 0.53mm ± 0.006mm versus mutants 0.57mm ± 0.034mm, $P = 0.310$ in a paired t-test; mean chain inter-ganglia distance wildtypes 0.44mm ± 0.02mm versus

mutants 0.46mm ± 0.03mm, P = 0.507 in a paired t-test). Together, these observations suggested that NRP2 is not essential for neuron cell body organisation in the sympathetic ganglia, but functions in sympathetic axon guidance.

3.2.2.3 Signalling mechanism in NRP1 controlled sympathetic nervous system development

Mice lacking NRP1 have severe cardiovascular defects, and my earlier work suggested that ectopic neurons are often placed proximal to blood vessels (Fig. 3.5B). I therefore asked if the sympathetic phenotype in *Nrp1*-null mutants was secondary to a defective vasculature or due to a cell-autonomous defect in the sympathetic NCC lineage. I used transgenic mouse lines expressing CRE recombinase under the control of the endothelial-specific *Tie2* promoter (Kisanuki et al., 2001) or the NC promoter *Wnt1* (Chai et al., 2000) crossed to a conditional *Nrp1* "floxed" line to target NRP1 in these specific cell lineages. Mice lacking endothelial NRP1 had no defects in sympathetic chain organisation (Fig. 3.8B), whereas mice lacking NRP1 in the NC lineage had defects that phenocopied the *Nrp1*-null mice (Fig. 3.8D); ganglia were dispersed, axons extended from the chain and neurons were scattered in ectopic locations. Consistent with the lack of phenotype in endothelial NRP1 mutants, mice lacking the vascular NRP1 ligand VEGF164, which also have a disrupted vasculature (Ruhrberg et al., 2002), had no defects in the sympathetic chain organisation (Fig. 3.8C).

Taken together, these results suggest that SEMA3A signals through NRP1 on NC-derived sympathetic precursors to regulate sympathetic NCC migration and placement, and subsequent development of the sympathetic nervous system, independently of blood vessels.

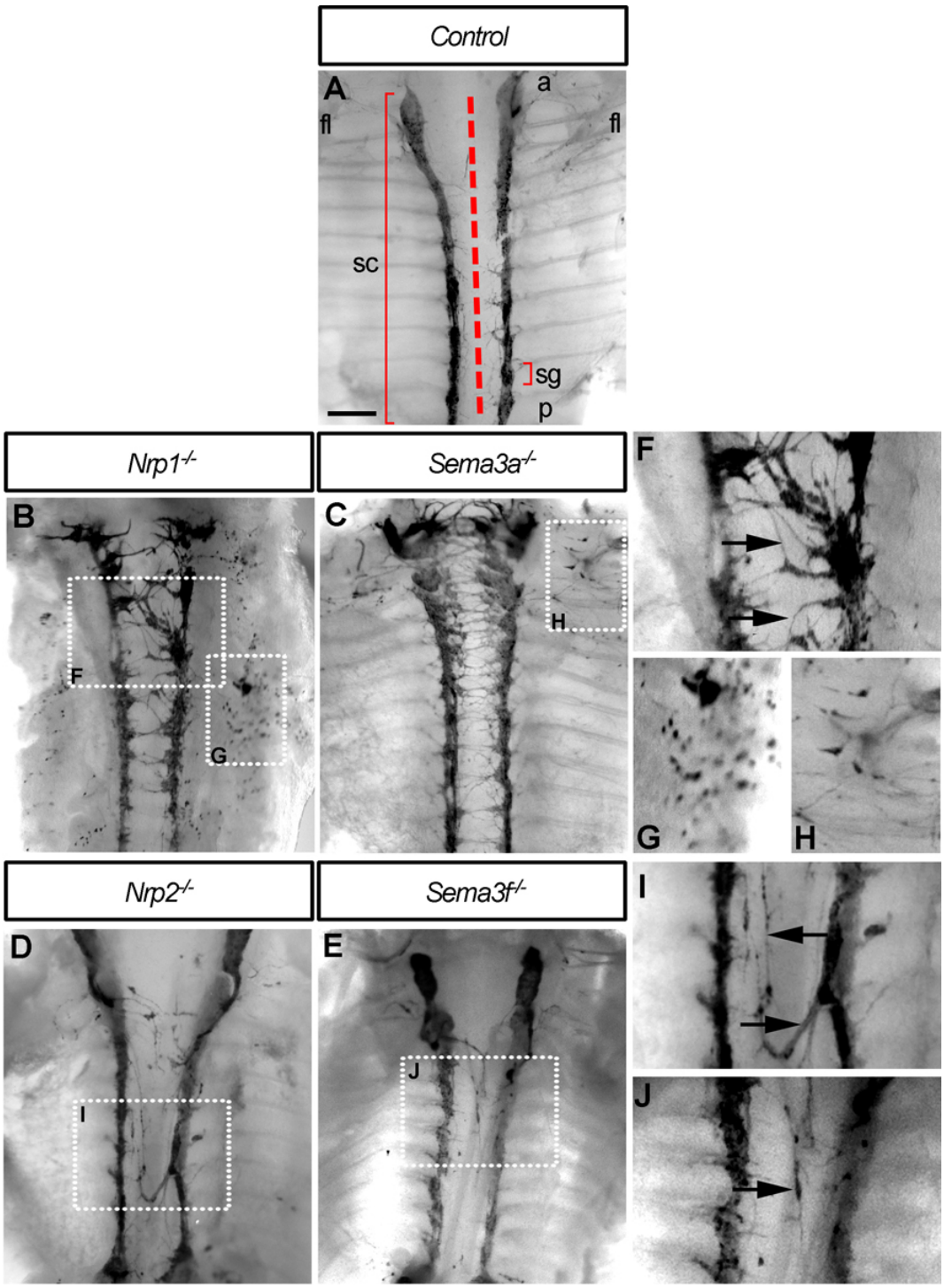

Figure 3.6: Sympathetic chain is disorganised in mutants deficient in semaphorin or neuropilin signalling.

E13.5 embryos with internal organs removed immunolabelled for TH and presented in ventral view to visualise the sympathetic chains. In wildtype (A), sympathetic chains (sc, long bracket) extend anteroposteriorly either side of the spinal cord, with individual sympathetic ganglia visible (sg, short bracket) and all axons remaining within the chain (n=10). Position of dorsal aorta (hashed red line), level of forelimb (fl) and anterior (a) and posterior (p) directions are indicated. In all *Nrp1*-null mutants (B; boxes in B magnified in F and G), axons extended prematurely across the midline (arrows in F) and ectopic neurons were visible (G; n=3). *Sema3a*-null

mutants (C; box in C magnified in H) phenocopied these defects, with misguided sympathetic axons and ectopic neurons, particularly at forelimb level (H; n=4). *Nrp2*-null mutants (D, box in D magnified in I) exhibited mild axon guidance defects, with sympathetic axons reaching towards and around the dorsal aorta (arrows in I; n=4). *Sema3f*-null mutants (E, box in E magnified in J) also had mild defects in sympathetic axon guidance (arrow in J; n=5). Scale bar: 200 μm.

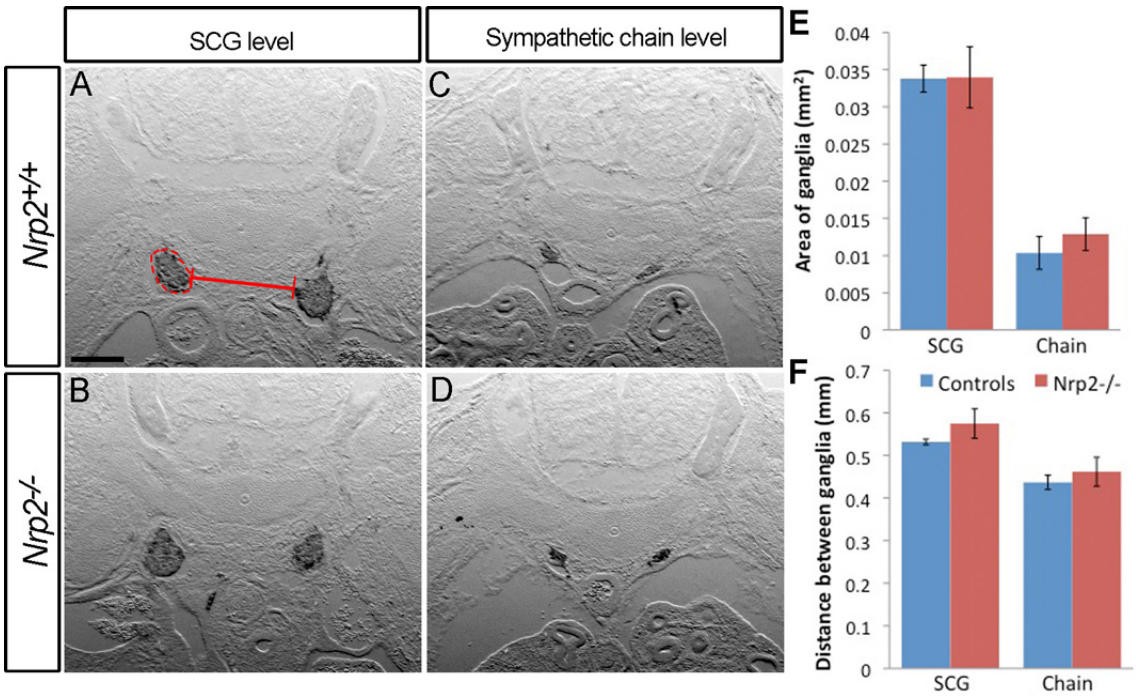

Figure 3.7: Sympathetic ganglia in embryos lacking NRP2 are not dispersed.

Transverse sections through E14.5 wildtype (A,C) and *Nrp2*-null (B,D) embryo trunks were immunolabelled for TH to measure the cross section area of the paired ganglia (red dotted line in A) and distance between ganglia (red straight line in A) at anterior superior cervical ganglion level (SCG; A,B) and further posterior at the sympathetic chain level (C,D). There were no significant differences in area of ganglia at SCG or chain level (E) or distance between the two ganglia at SCG or chain level (F) between wildtypes and *Nrp2* mutants (paired t-test, n=4 each). Scale bar: 200 μm.

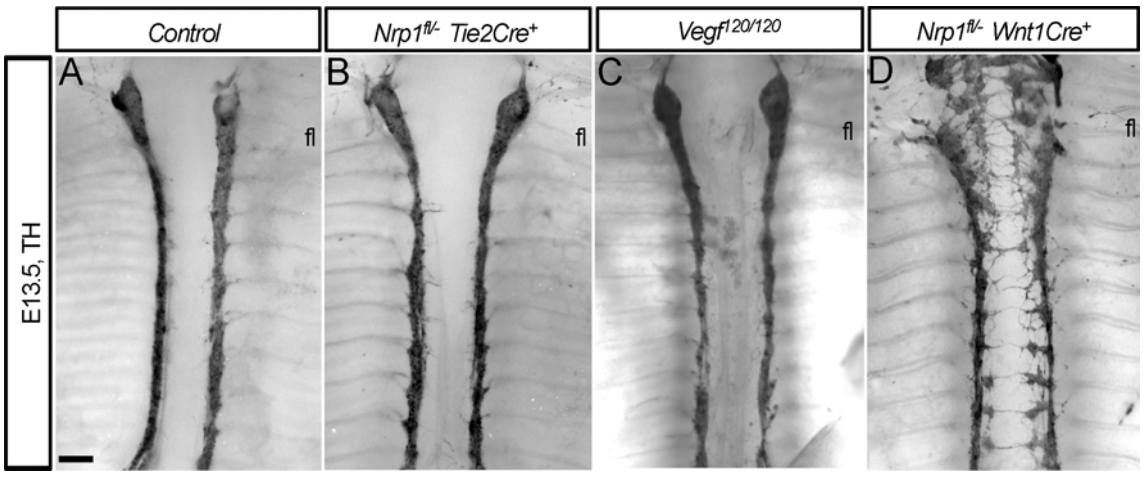

Figure 3.8: Defect in sympathetic chain from loss of NRP1 is cell autonomous and independent of vascular defects.

E13.5 embryos with internal organs removed immunolabelled for TH presented in ventral view to visualise the sympathetic chains. The sympathetic chains were normal in embryos lacking endothelial NRP1 (B; n=4) or the VEGF164 isoform (C; n=3), as in wildtype (A; n=14). Embryos lacking NRP1 in NC-derived tissues (D) had disorganised sympathetic chains with ectopically placed sympathetic neurons distal to the chains at the forelimb (fl) and sympathetic axons extending out of the chain (n=5). Scale bar: 250μm.

3.2.2.4 Ectopic sympathetic precursors in the absence of NRP1 differentiate into sympathetic neurons

Even though abnormal blood vessel patterning does not account for sympathetic NCC displacement, the proximity of ectopic sympathetic neurons to blood vessels (Fig. 3.5B) suggests they respond to blood vessel-derived cues. The dorsal aorta releases BMPs, which have been implicated in induction of sympathetic differentiation or in survival of sympathetic NCCs (Morikawa et al., 2009; Shah et al., 1996). Many ectopic neurons in mutants with disrupted NRP1 signalling are positioned far from the dorsal aorta (Figs. 3.6B and 3.8D), so would be unlikely to be affected by dorsal aorta-derived BMP signals. To assess whether any misplaced NCCs die due to the lack of dorsal aorta-derived signals, I immunolabelled sections through E10.5 wildtype and *Nrp1*;*Wnt1Cre* mutant embryos with antibodies for MASH1 and activated Caspase3 (aCasp3), a marker for apoptosis (Fig. 3.9A-D). Consistent with previous findings in *Nrp1*-null embryos (Figs. 3.4B and 3.5B), mutant embryos had dispersed primary sympathetic ganglia compared to wildtypes (Fig. 3.9B) and ectopic MASH1-positive sympathetic precursors (Fig. 3.9B,D). No MASH1-positive ectopic sympathetic precursors appeared to undergo apoptosis, as there was no MASH1/aCasp3 colocalisation in sympathetic precursors (Fig. 3.9B,D). Note that autofluorescent blood cells appeared yellow and were visible within the blood vessels of these sections; they should not be confused with apoptotic cells. At E11.5, MASH1 immunolabelling of the sympathetic ganglia was reduced in intensity as most sympathetic precursors had differentiated into sympathetic neurons in wildtype embryos (Fig. 3.10A,C). Similarly in *Nrp1*;*Wnt1Cre* mutant embryos, few sympathetic precursors in the ganglia expressed MASH1 (Fig. 3.10B,D), and few ectopically located sympathetic precursors remained MASH1-positive at this stage (Fig. 3.10B,D). None of the ectopic MASH1-positive cells were co-labelled with aCasp3 (Fig. 3.10D) so were not apoptotic. To confirm that ectopic sympathetic precursors differentiated properly, I immunolabelled cryosections through E10.5 embryos for MASH1 and TH (Fig. 3.9E-H). MASH1-positive sympathetic precursors were beginning to differentiate and express TH in wildtype embryos (Fig. 3.9E,G). In *Nrp1;Wnt1cre* mutants, some MASH1-positive sympathetic precursors at the ganglia and in ectopic locations were also beginning to produce TH (Fig. 3.9F,H). MASH1 is a transcription factor and localises to the cell nucleus, whereas the TH enzyme localises to the cytoplasm, therefore cells co-expressing the markers had red TH-positive cytoplasm surrounding green MASH1-positive nucleus. Blood cells were also autofluorescent in these sections. At E11.5, no MASH1-positive sympathetic precursors in wildtype and very few in *Nrp1;Wnt1cre* mutant cryosections were apparent (Fig. 3.10E-H). Sympathetic neurons in the wildtype ganglia strongly expressed TH, and exhibited a tight ganglionic structure (Fig. 3.10E,G). In mutants, sympathetic neurons in the ganglia

expressed TH, however the neurons were more dispersed and ganglia not as condensed as in wildtype (Fig. 3.10F,H). The ectopic sympathetic precursors had also differentiated into TH-expressing sympathetic neurons (Fig. 3.10F,H). These results suggest that ectopic sympathetic NCC precursors do not undergo apoptosis, but have the ability to differentiate into sympathetic neurons despite their errant location.

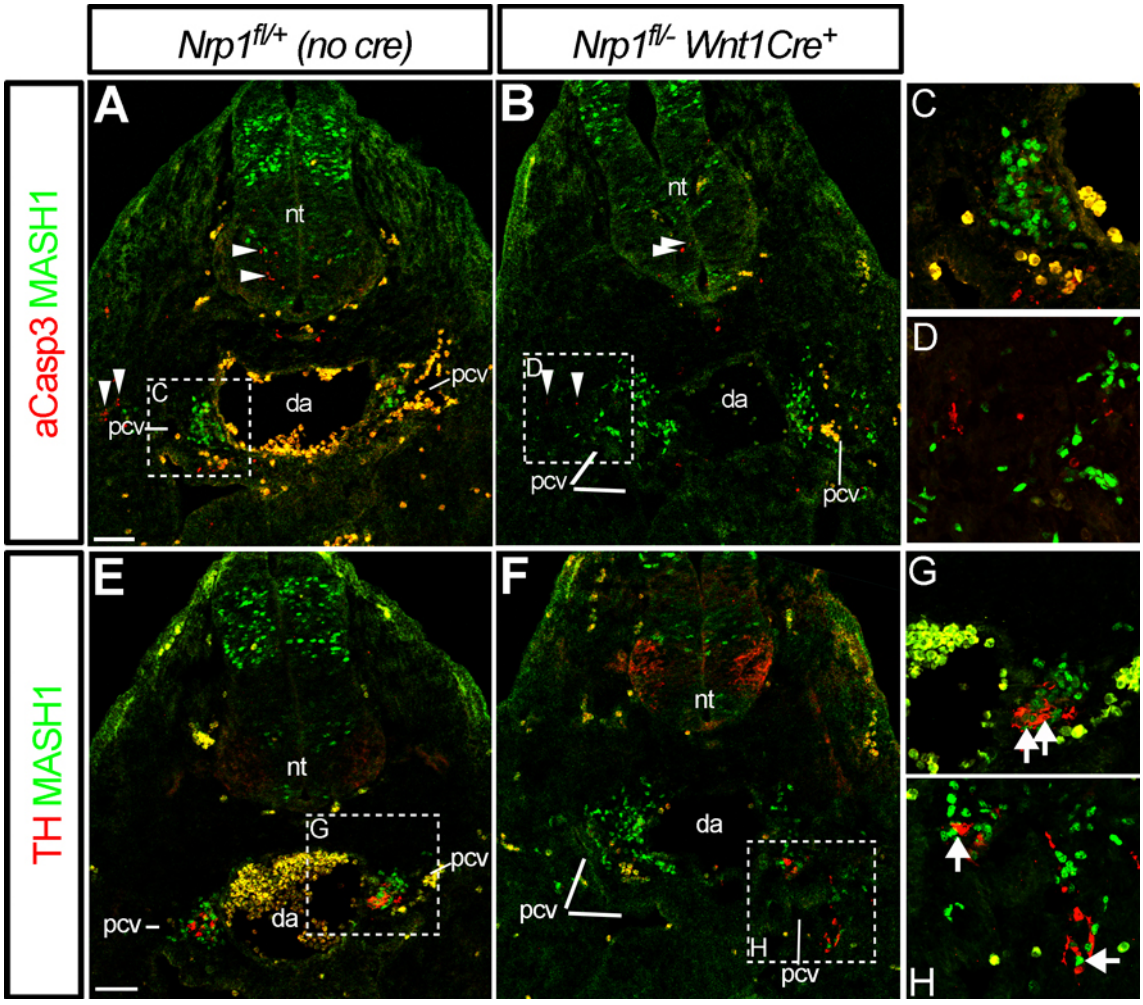

Figure 3.9: Ectopic sympathetic NCCs are not apoptotic but begin to differentiate at E10.5.

Transverse cryosections at forelimb level through E10.5 wildtype and *Nrp1;Wnt1Cre* mutant embryos. Immunolabelling with activated Caspase3 (aCasp3; red, A-D) and MASH1 (green, A-D) revealed MASH1-positive cells aggregated into primary sympathetic ganglia located between the dorsal aorta (da) and the left and right posterior cardinal veins (pcv) in wildtype embryos (A,C; n=1); aCasp3 was localised to a few cells in the neural tube (nt) and limb (arrowheads, A). In *Nrp1;Wnt1Cre* mutants (B,D), MASH1-positive sympathetic anlagen were in dispersed primary sympathetic ganglia and misplaced distal to the posterior cardinal veins, and none of them were aCasp3-positive (n=1); aCasp3 was present in a few cells in the neural tube and limb (arrowheads, B). Immunolabelling for MASH1 (green, E-H) and TH (red, E-H) revealed some of the MASH1-positive sympathetic anlagen at the dorsal aorta in wildtypes expressed TH (E,G; n=1). In *Nrp1;Wnt1Cre* mutants (F,H), some MASH1-positive sympathetic anlagen at the primary ganglia expressed TH, and some MASH1-positive ectopically located sympathetic anlagen also expressed TH (n=1). MASH1 was localised to the nucleus, whereas TH was in the cytoplasm. Autofluorescence was seen in blood cells in the da and pcv. Scale bars: 200μm.

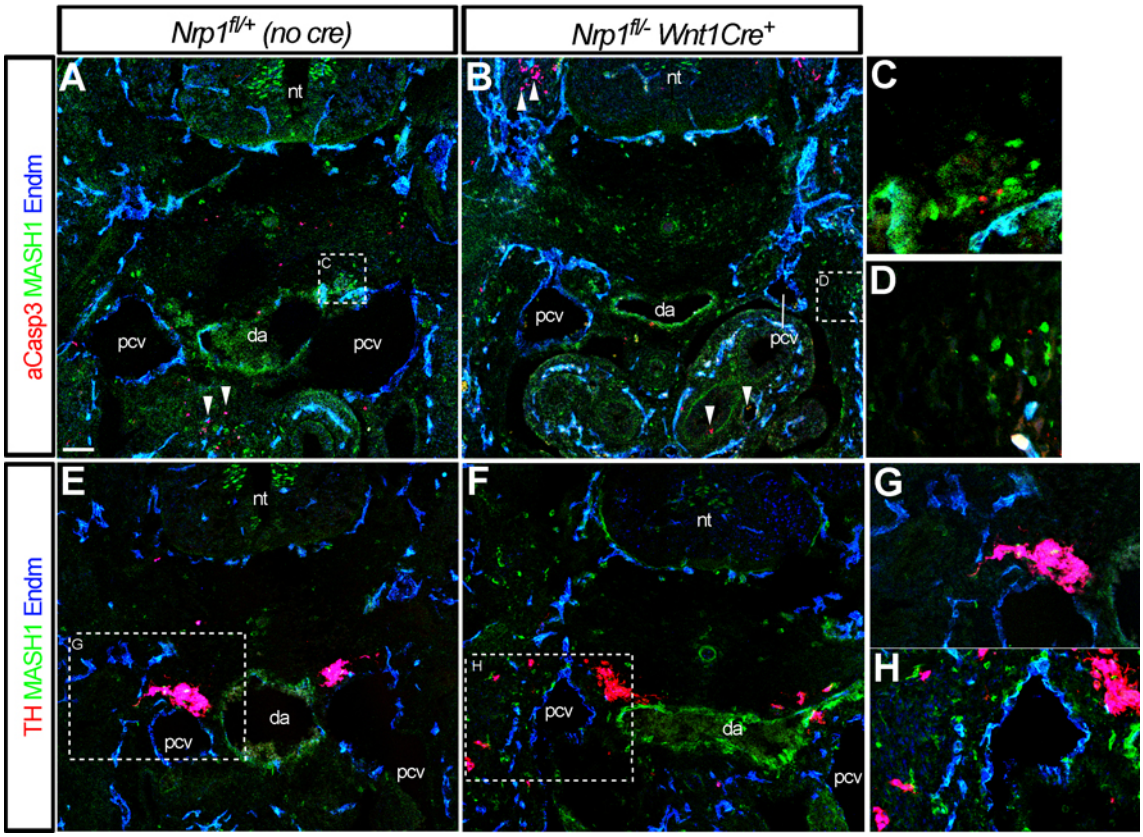

Figure 3.10: Ectopic sympathetic NCCs are not apoptotic but can differentiate into sympathetic neurons at E11.5.

Transverse cryosections at forelimb level through E11.5 wildtype and *Nrp1;Wnt1Cre* mutant embryos. Immunolabelling for activated Caspase3 (aCasp3, red), MASH1 (green) and endomucin (Endm, blue; A-D) reveals few MASH1-positive sympathetic anlagen between the dorsal aorta (da) and the left and right posterior cardinal veins (pcv) in wildtype (A,C; n=1). aCasp3 was localised to cells in the gut (arrowheads, A). *Nrp1;Wnt1Cre* mutant (B,D) had few MASH1-positive sympathetic anlagen at the dorsal aorta and some anlagen misplaced distal to the posterior cardinal veins (D), none of which were aCasp3-positive (n=1). aCasp3 was localised to cells in the gut and many cells in the DRG (arrowheads, B). Immunolabelling for TH (red), MASH1 (green) and endomucin (blue; E-H) revealed TH-positive sympathetic ganglia at the dorsal aorta with no MASH1-positive anlagen in wildtypes (E,G; n=1). In *Nrp1;Wnt1Cre* mutants (F,H), loose TH-positive sympathetic ganglia were formed between the dorsal aorta and the posterior cardinal veins and TH-positive neurons were misplaced in ectopic locations distal to the posterior cardinal veins. There were also a few MASH1-positive sympathetic precursors in the mutant (H; n=1). nt, neural tube. Scale bar: 200μm.

3.2.2.5 Sympathetic NCC placement is severely affected when NRP1 and NRP2 are lost

I have shown that NRP2 is expressed in the sympathetic nervous system (Figs. 3.1 and 3.2) and functions in sympathetic axon guidance (Fig. 3.6D). NRP2 also guides early NCC segmental migration (Gammill et al., 2006), and I therefore wanted to assess whether it has a role in sympathetic NCC migration and sympathetic precursor placement. I also wanted to further investigate any interaction between NRP2 and NRP1 in early sympathetic development. Abolishing both *Nrp1* and *Nrp2* results in early embryonic lethality due to severe cardiovascular defects, presumably due to defective VEGF164 signalling (Takashima et al., 2002). Hence, I utilised mice with a null allele for *Nrp2* as well as a mutated SEMA-binding domain in *Nrp1*, which preserves VEGF-binding domain of NRP1 to allow development to birth (Gu et al., 2003).

Assembling primary sympathetic chains were visualised by *in situ* hybridisation with a *Mash1* RNA probe on wholemount E9.5 mouse embryos (Fig. 3.11). Viewed laterally, the *Mash1*-positive primary sympathetic ganglia in wildtype animals formed loosely arranged strands along the anteroposterior axis, either side of the notochord, below the neural tube (Fig. 3.11A). Transverse cryosections at forelimb level through these embryos allowed visualisation of clustering of NC sympathetic precursors into primary sympathetic ganglia either side of the dorsal aorta, in between the dorsal aorta and posterior cardinal veins (Fig. 3.11E). *Mash1*-positive primary sympathetic ganglia in $Nrp1^{Sema}$ mutant embryos formed in the same location as in wildtype, but appeared less condensed (Fig. 3.11B). Cryosections showed that the primary sympathetic ganglia were indeed more dispersed, and some sympathetic precursors were located further laterally to the posterior cardinal veins from the dorsal aorta (Fig. 3.11F), consistent with previous observations in *Nrp1*-null embryos (Figs. 3.4B and 3.5B). In embryos lacking NRP2, all sympathetic precursors were placed correctly adjacent to the dorsal aorta and well condensed as in wildtype (Fig. 3.11C,G). Compound *Nrp2*/$Nrp1^{sema}$ homozygous mutants had more severely dispersed primary sympathetic ganglia than $Nrp1^{sema}$-null mutants that could barely be identified in the lateral wholemount view (Fig. 3.11D). Transverse cryosections showed that individual *Mash1*-positive sympathetic precursors were so scattered that the primary sympathetic ganglia were barely visible (Fig. 3.11H). Few sympathetic precursors could be seen at the dorsal aorta; instead many were spread in ectopic locations distal to the posterior cardinal vein (Fig. 3.11H, arrowheads). Since the phenotype in the compound *Nrp2*/$Nrp1^{sema}$ mutant was more severe than in the $Nrp1^{sema}$-null mutant (Fig. 3.11B,F), and the *Nrp2*-null mutant had no phenotype at all, this suggests a genetic interaction between NRP1 and NRP2 in sympathetic development.

There appeared to be increased numbers of *Mash1*-positive NCCs in the gut of $Nrp1^{sema}$-null and compound *Nrp2*/$Nrp1^{sema}$ mutants (Fig. 3.11F,H) compared to control or *Nrp2*-

null embryos (Fig. 3.11E,G). MASH1 is expressed by enteric neuron precursors in the gut of embryonic rats (Lo et al., 1991), and this observation suggests that NRP1 could be acting to prevent vagal NCCs entering the gut, similar to Slit/Robo signalling as previously described (De Bellard et al., 2003). However, this needs to be repeated for confirmation.

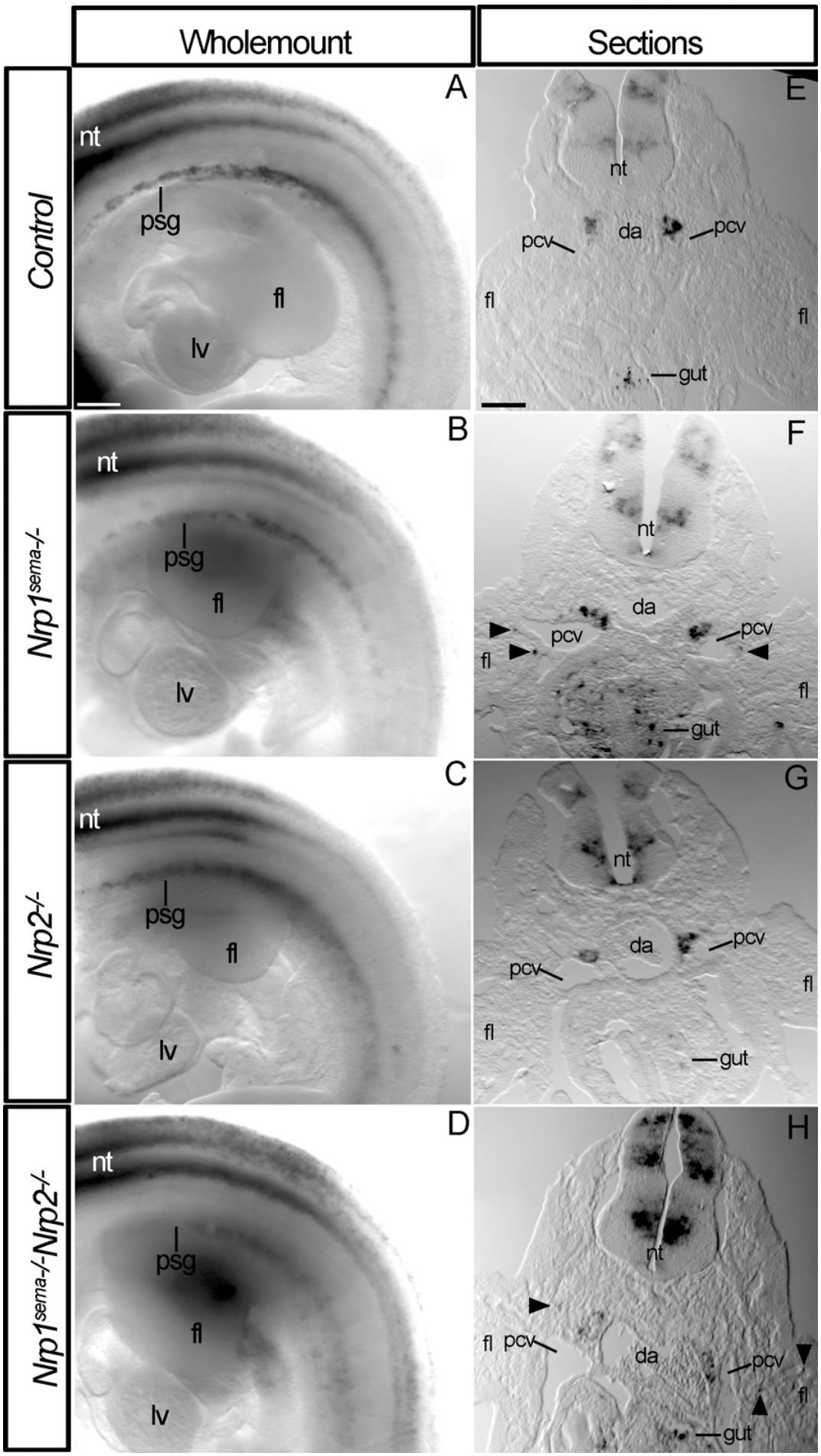
Wholemount
Sections
Control
Nrp1sema-/-
Nrp2-/-
Nrp1sema-/-Nrp2-/-
A
B
C
D
E
F
G
H
nt
psg
fl
lv
da
pcv
gut

Figure 3.11: Compound NRP1/NRP2 mutants have disrupted primary sympathetic ganglia.

In situ hybridisation with a *Mash1* probe on E9.5 embryos to visualise sympathetic NCCs in the developing primary sympathetic ganglia (psg); wholemount embryos were viewed laterally, anterior to the left, with the position of the developing heart indicated (lv – left ventricle) (A-D) and transverse cryosections at forelimb (fl) level were taken (E-H). In wholemount wildtype embryos (A), *Mash1*-positive NCCs formed loosely arranged chains of psg ventrally to the neural tube (nt) in an anteroposterior orientation; *Mash1* was also expressed in the neural tube. In transverse sections (E), *Mash1*-positive psg were positioned in between the dorsal aorta (da) and the posterior cardinal veins (pcv; n=1). *Mash1* was expressed in two areas of the neural tube and the gut (E). In wholemount $Nrp1^{sema}$ -null embryos, psg appeared less well condensed (B); in transverse sections, psg were dispersed and some *Mash1*-positive NCCs were misplaced distal to the pcv (arrowheads, F; n=2). There were increased numbers of Mash1-positive cells in the gut (F). In wholemount *Nrp2*-null embryos, psg formed normally with no ectopically placed sympathetic NCCs (C,G; n=1). Compound $Nrp1^{sema}$/*Nrp2*-null mutant had psg that were severely dispersed in wholemounts (D) and in transverse sections (H); more *Mash1*-positive sympathetic NCCs were ectopically placed distal to the pcv, and also in the gut, than in $Nrp1^{sema}$ -null embryos (arrowheads, H; n=1). Scale bars: A-D – 200μm; E-F – 100μm.

3.2.2.6 A 'back-up' role for NRP2 in sympathetic precursor placement

To assess the effects of the *Nrp2* and *Nrp1*^{sema} mutations later in development, I immunolabelled transverse cryosections through E11.5 embryos with TH, SMA and endomucin to visualise the location of differentiated sympathetic neurons relative to the SMA-positive dorsal aorta and endomucin-positive posterior cardinal veins (Fig. 3.12). Control embryos with heterozygous mutations in both *Nrp2* and *Nrp1*^{Sema} exhibited tightly aggregated TH-positive sympathetic ganglia, positioned in between the dorsal aorta and the posterior cardinal veins, as in wildtypes (Fig. 3.12A,E). *Nrp2*-null embryos with a *Nrp1*^{Sema} heterozygous mutation had well formed and condensed sympathetic ganglia, but a few TH-positive neurons were placed ectopically, distal to the dorsal aorta towards the limb (Fig. 3.12B,F). Sympathetic ganglia in *Nrp1*^{Sema}-null embryos with a heterozygous *Nrp2* mutation were less well condensed and had more TH-positive sympathetic neurons mispositioned distal to the posterior cardinal vein, towards the limb (Fig. 3.12C,G). This was similar to observations in *Nrp1*-null embryos (Figs. 3.4B and 3.5B). TH-positive sympathetic ganglia at the dorsal aorta in compound *Nrp2*/*Nrp1*^{Sema}-null mutants were scattered, and even more sympathetic neurons were placed ectopically toward the limbs distal to the posterior cardinal vein (Fig. 3.12D,H). The finding that abolishing both the NRP1 and NRP2 signalling pathway had a worse effect on sympathetic neuron placement than the effect of abolishing either NRP1 or NRP2 signalling was consistent with the results from E9.5 *Mash1 in situ* hybridisations (Fig. 3.11). This suggests that NRP1 and NRP2 signalling interact genetically. Since *Nrp2*-null mutants did not have a phenotype, I suggest that NRP2 provides a 'back-up' function for NRP1 in sympathetic NC guidance.

I next assessed the sympathetic phenotype in E13.5 mice lacking both NRP1 and NRP2 signalling pathways in sympathetic neurons (Fig. 3.13). I utilised the *Nrp1;Wnt1Cre* mutant mice to abolish NRP1 in the NC lineage instead of using the *Nrp1*^{sema} mutation to confirm the phenotype was due to a cell autonomous effect on sympathetic neurons. Compound *Nrp1;Wnt1Cre/Nrp2*-null mutants had more ectopic neurons (arrowheads, Fig. 3.13 compare F and H) and more severely disrupted sympathetic chains than in the *Nrp1;Wnt1Cre* mutant (Fig. 3.13 compare B,E with C,G). This is in support of the theory that NRP2 compensates for the loss of NRP1, since *Nrp2*-null mutants do not have defects in the sympathetic ganglia (Fig. 3.7). There were also misguided axons and axons lying on top of the dorsal aorta (arrows Fig. 3.13G), similar to the axon guidance defects in *Nrp2*-null mutants (Fig. 3.6D).

I next investigated ligand mutants to explore whether embryos lacking SEMA3A and SEMA3F phenocopy embryos lacking NRP1 and NRP2, given that SEMA3A is thought to signal through NRP1 and SEMA3F through NRP2. As expected, compound *Sema3a/Sema3f*-null mutants (Fig. 3.14C,F) also had more severely disrupted sympathetic

chains than either single *Sema3a*-null or *Sema3f*-null embryos (Fig. 3.14A,B,D,E). *Sema3f*-null embryos with a heterozygous mutation in *Sema3a* had a few misguided sympathetic axons (Fig. 3.14A,D), similar to, and not worse than, embryos lacking NRP2 or SEMA3F alone (Fig. 3.6D,E). Vice versa, *Sema3a*-null embryos on a *Sema3f* heterozygous background had disorganised sympathetic chains with ectopic sympathetic neurons and misguided sympathetic axons (Fig. 3.14B,E), similar to the phenotype in embryos lacking NRP1 or SEMA3A alone (Fig. 3.6B,C). The phenotype did not seem worse than that of embryos lacking SEMA3A or NRP1, despite having a heterozygous *Sema3f* mutation. These findings suggest that homozygous mutants for lone ligands (i.e. SEMA3A or SEMA3F) may not be compromised further by an additional heterozygous mutation in the other ligand, contrasting with the findings from earlier receptor mutants (Fig. 3.12).

The phenotype in the compound *Sema3a/Sema3f*-null mutants was similar to that observed in the *Nrp1;Wnt1cre/Nrp2*-null mutants, indicating that SEMA3A and SEMA3F are the ligands required to control sympathetic nervous system patterning through NRP1 and NRP2.

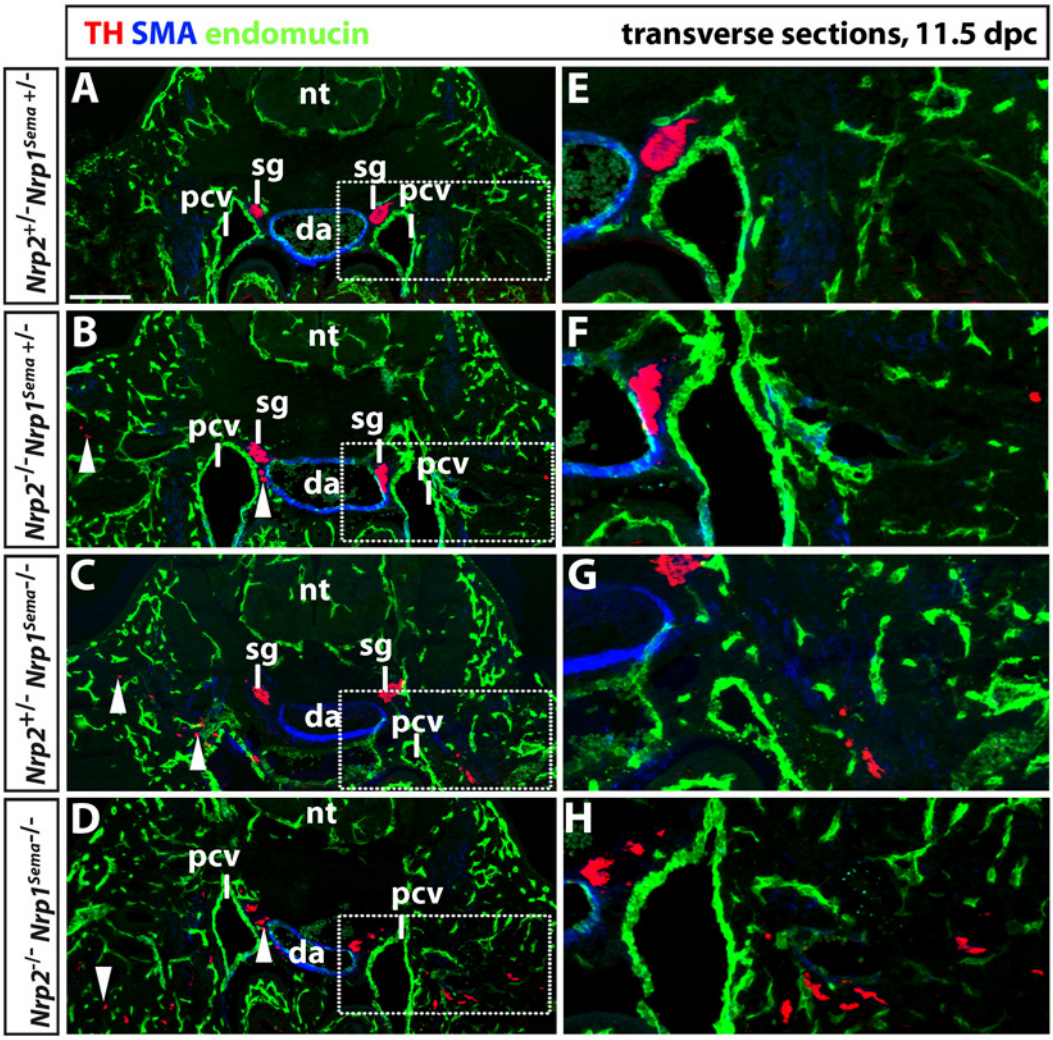

Figure 3.12: Compound NRP mutants have severely disrupted sympathetic ganglia.

Transverse cryosections through E11.5 control, *Nrp1*^{sema}-null, *Nrp2*-null and compound *Nrp1*^{sema}/*Nrp2*-null mutant embryos immunolabelled for TH (red), smooth muscle actin (SMA, blue) and endomucin (endm, green). Sympathetic ganglia (sg) in control embryos (A,E) were tightly packed bundles of TH-positive neurons, located between the dorsal aorta (da) and the posterior cardinal veins (pcv; n=1). A *Nrp1*^{sema} heterozygous mutation on a homozygous *Nrp2*-null background (B,F) resulted in a mild phenotype; TH-positive sympathetic ganglia were positioned at the correct location, with a few neurons in ectopic locations (arrowheads in B; n=1). Introducing a heterozygous *Nrp2* mutation onto an *Nrp1*^{sema} -null background (C,G) worsened this phenotype; more ectopic neurons were positioned lateral to the pcv (arrowheads in C; n=1). Double *Nrp2/Nrp1*^{sema} knockout mutants (D,H), had dispersed ganglia and many TH-positive sympathetic neurons were placed distally in the forelimb (arrowheads in D; n=1). nt, neural tube. Boxes in A-D magnified in E-H. Scale bar: 200μm.

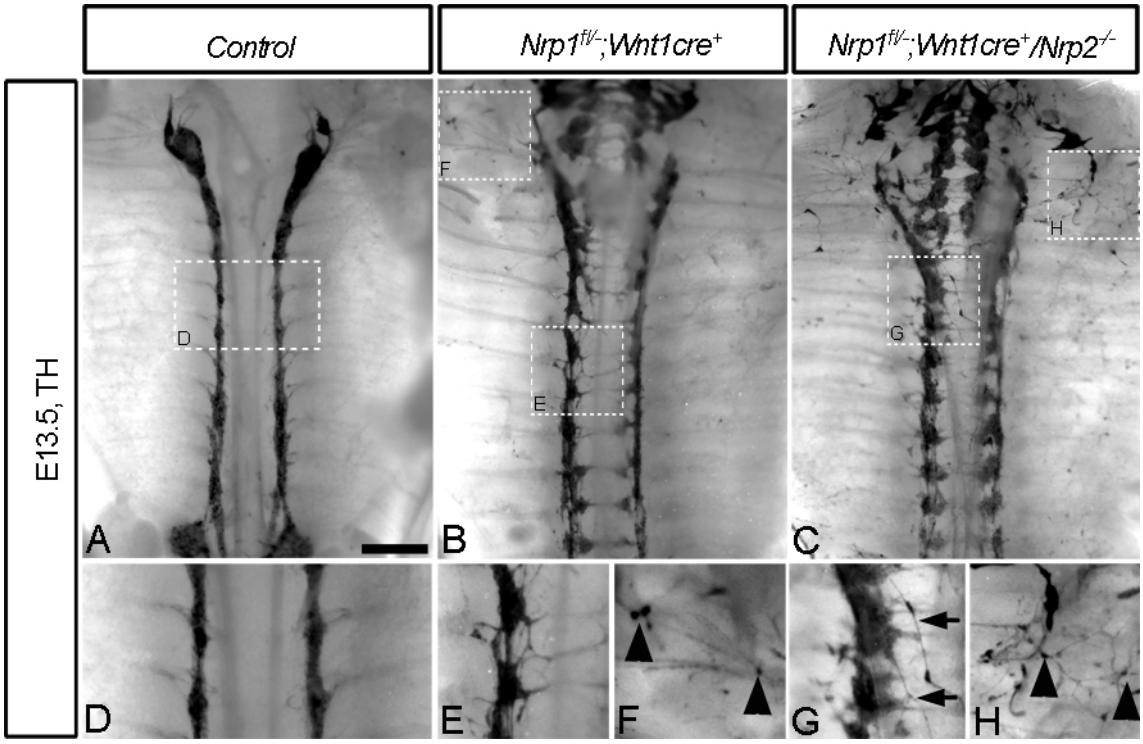

Figure 3.13: Sympathetic chains are disorganised in mutants lacking NRP1 and NRP2.

E13.5 embryos with internal organs removed were subjected to immunolabelling with TH to visualise the sympathetic chains, as in wildtype (A; box magnified in D). In *Nrp1;Wnt1Cre* mutants (B, boxes magnified in E,F), ganglia were dispersed, with misguided axons under the dorsal aorta (E) and ectopic sympathetic neurons distal to the chains (arrowheads in F). In compound *Nrp1;Wnt1Cre/Nrp2*-null mutants (C, boxes magnified in G,H; n=3), ganglia were more dispersed (G) with misguided axons on top of the dorsal aorta (arrows in G) and many sympathetic neurons in ectopic locations (arrowheads in H). Scale bar: 500μm.

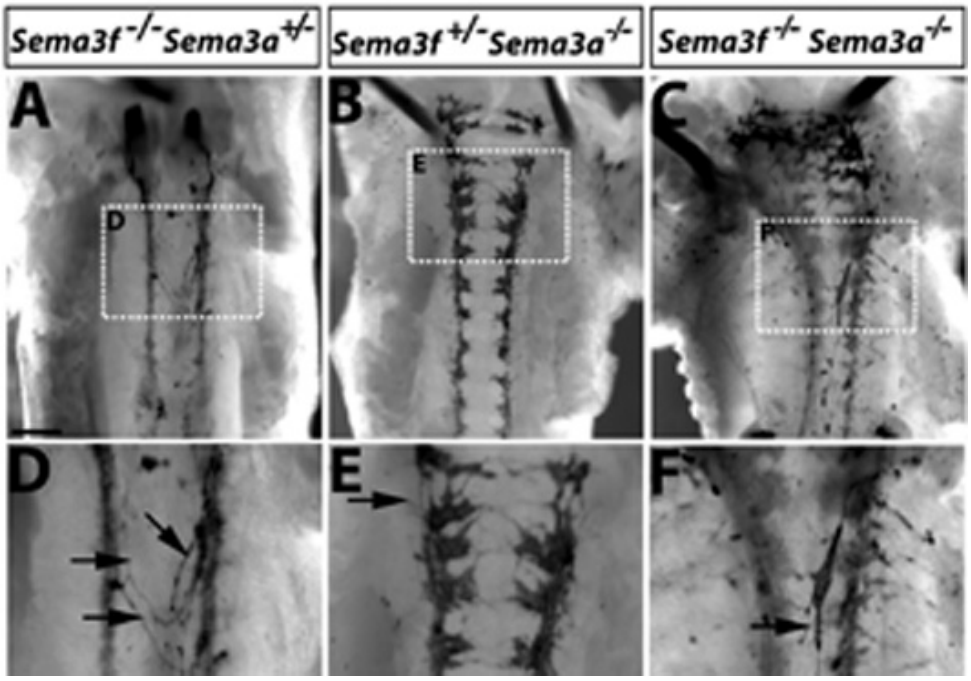

Figure 3.14: Sympathetic chains are disorganised in mutants lacking SEMA3A and SEMA3F.

E13.5 embryos with internal organs removed and immunolabelled for TH. *Sema3f*-null mutants with a *Sema3a* heterozygous mutation (A, box magnified in D) had some sympathetic axons extending towards and around the dorsal aorta (arrows in D). *Sema3a*-null embryos with a heterozygous *Sema3f* mutation (B, box magnified in E) had dispersed sympathetic ganglia, axons extending across the midline (arrow in E) and ectopic neurons distal to the sympathetic chain. Compound *Sema3a*/*Sema3f*-null embryos (C, box magnified in F) had more severely disrupted sympathetic chains, with sympathetic ganglia less well condensed, axons extending in anteroposterior directions in ectopic locations, for example on top of the dorsal aorta (arrow in F), and more sympathetic neurons in ectopic distal locations (n=1). Scale bar: 200μm.

3.2.3 NRP1 controls postnatal sympathetic innervation of target organs

Sympathetic axons from the stellate ganglia innervate the heart to modulate heart rate in response to stress. I next asked if the disorganisation observed in the sympathetic nervous system of embryos with disrupted NRP signalling persists into adulthood and affects target organ innervation. For the following analysis, I used *Sema3a*-null mutants that have ablated signalling through NRP1, and *Nrp1;Wnt1Cre* mutants that have ablated NRP1 in the NC lineage, since NRP1 signalling on NCCs was shown to be critical for sympathetic development (Fig. 3.8D). Additionally, these mice are viable into adulthood in contrast to *Nrp1*-null and *Nrp1*^{sema}-null mutants.

Immunolabelling wholemount hearts from embryos at E17.5 allowed visualisation of sympathetic axons lying on the epicardial surface. Consistent with previous observations (Ieda et al., 2007), SEMA3A-deficient embryonic hearts had fewer axons on the epicardial surface of the heart compared to wildtype hearts (Fig. 3.15A,B). This was also observed in embryonic hearts lacking NRP1 in the NC lineage (Fig. 3.15C,D). Previous observations showed that SEMA3A acts as a repulsive guidance molecule to maintain the epicardial-to-endocardial gradient of sympathetic fibres through the cardiac wall (Ieda et al., 2007). Because AP-tagged SEMA3A bound NRP1 in the subepicardial layer of the heart at E14.5 (Fig. 3.3A), these results suggest that the reduction in sympathetic fibres on the epicardial surface of hearts lacking SEMA3A or NRP1 is because NRP1-deficient fibres are more able to invade the endocardium.

To test whether more sympathetic fibres invade the endocardium in hearts lacking NRP1 in the NC lineage, I examined the pattern of sympathetic innervation in the cardiac wall in longitudinal cryosections through postnatal day (P) 7 wildtype and *Nrp1;Wnt1Cre* mutant mouse hearts immunolabelled for TH and endomucin (Fig. 3.16,A-D). Quantification of the number of sympathetic fibres per field in the outer epicardium and inner endocardium of wildtype and *Nrp1;Wnt1Cre* mutant mice revealed that the epicardial-to-endocardial gradient was less steep in mice lacking NRP1 in the NC lineage compared to wildtype (compare red line to blue line in Fig. 3.16E). There were fewer sympathetic fibres at the surface epicardium in *Nrp1;Wnt1Cre* mutant hearts than wildtype hearts (Fig. 3.16A,C,E; wildtype mean number of fibres 85 ± 14 versus mutant mean 80 ± 5), and more fibres in the endocardium of *Nrp1;Wnt1Cre* hearts compared to wildtype hearts (Fig. 3.16B,D,E; wildtype mean number of fibres 20 ± 1 versus mutant mean 38 ± 4). This resulted in a 4.4-fold difference in sympathetic fibres between epicardium and endocardium in wildtype hearts, compared to a 2.1-fold difference in *Nrp1;Wnt1Cre* mutant hearts, and represented a significant decrease in fold change (P = 0.019 in a two-sample student's t-test, Fig. 20F). Thus, the overall numbers of sympathetic fibres within the heart are unaltered, but many more sympathetic axons reached the endocardium in mice lacking NC-derived NRP1 than

in wildtype due to the loss of SEMA3A/NRP1-mediated repulsive sympathetic axon guidance.

I next wanted to assess whether innervation of another sympathetic target organ was affected by the loss of NRP1 in the NC lineage. The dorsal aorta is innervated by axons from the sympathetic chain to help control blood pressure (Gerova et al., 1973). I took 30 consecutive 100μm vibratome sections of the dorsal aorta, stretching 3 mm, from P7 wildtype and *Nrp1;Wnt1Cre* mutant mice and immunolabelled them with TH and SMA (Fig. 3.17A,B). I found that significantly fewer sympathetic axons had contacted the dorsal aorta in *Nrp1;Wnt1Cre* mutant compared to wildtype mice (Fig. 3.17C; wildtype mean number of fibres 7 ± 1 versus mutant mean 3.5 ± 0.5, $P = 0.011$ in a two-sample student's t-test). This result suggests that in the absence of SEMA3A signalling through NRP1 in the NC lineage, sympathetic axons en route to the dorsal aorta are misguided and fewer axons reach their target organ. This is in contrast to sympathetic innervation of the heart, in which most axons destined for the heart seem to reach their target but are mis-patterned within it.

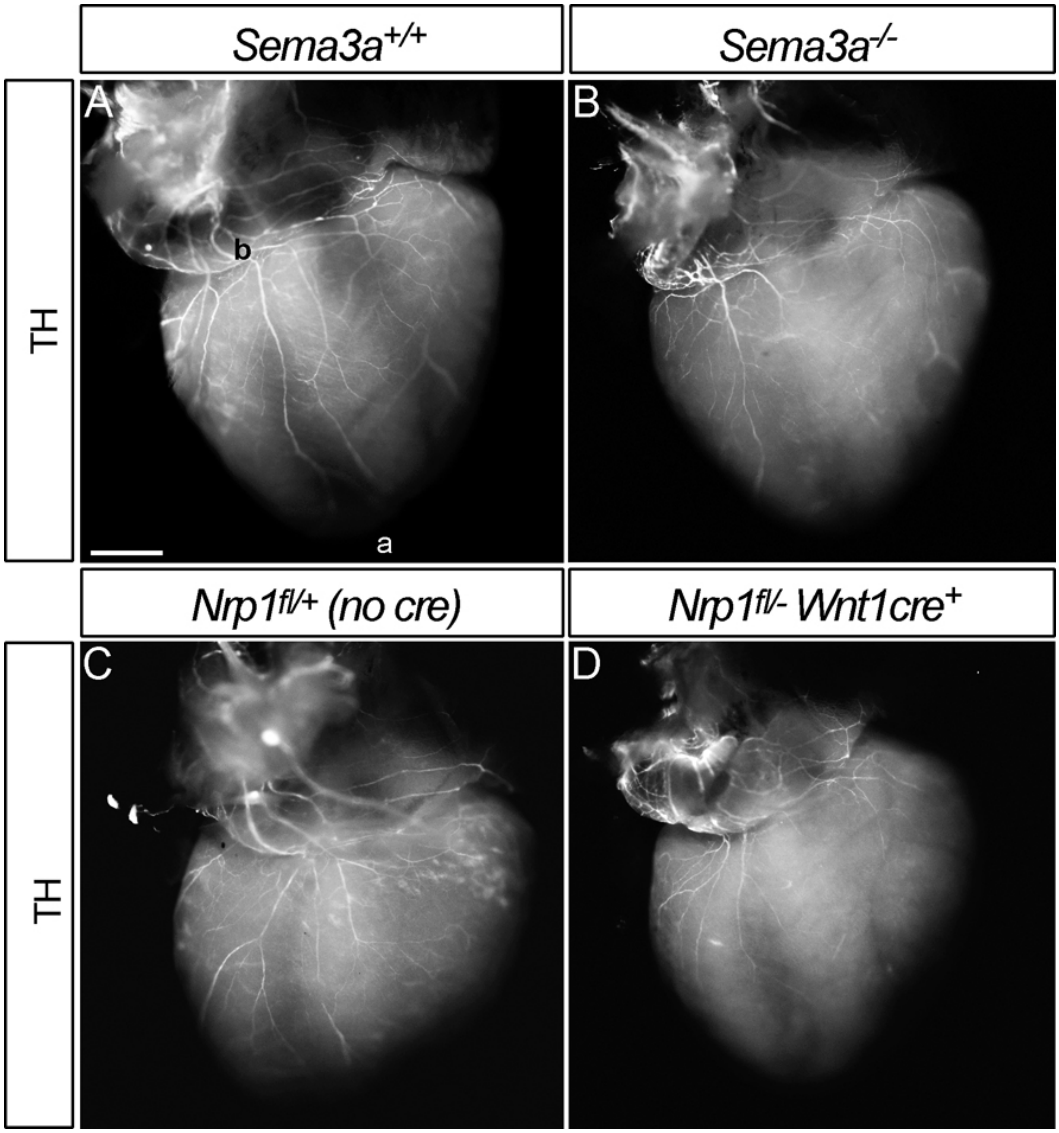

Figure 3.15: Fewer sympathetic nerve fibres on the epicardial surface in embryonic hearts lacking SEMA3A or NRP1 in the NC lineage.

E17.5 wildtype, *Sema3a*-null or *Nrp1;Wnt1Cre* mutant hearts subjected to immunolabelling with TH, visualised from the base of the heart with the apex towards the bottom. Sympathetic nerve bundles were abundant on the epicardial surface of control hearts (A,C), with three to five bundles reaching towards the apex of each heart (n=6). *Sema3a*-null mutants (B) had fewer sympathetic nerve bundles on the epicardial surface, and only one bundle was seen reaching towards the apex (n=3). *Nrp1;Wnt1Cre* mutants (D) also had fewer sympathetic nerve bundles on the epicardial surface; none were seen reaching towards the apex (n=3). b, base; a, apex. Scale bar: 500μm.

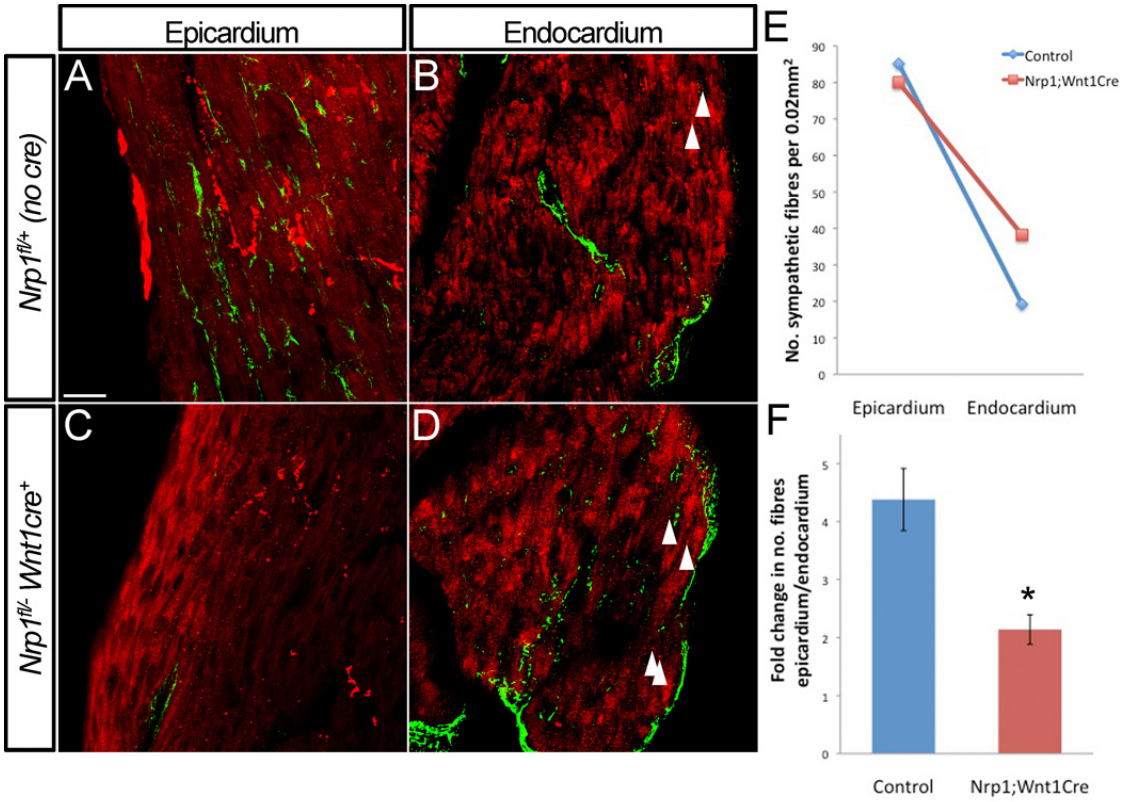

Figure 3.16: Loss of NRP1 in NC alters the epicardial-to-endocardial distribution of sympathetic nerve fibres in postnatal hearts.

Longitudinal sections of P7 hearts from wildtype and *Nrp1;Wnt1Cre* mutants were immunolabelled for TH (red) and endomucin (green). *Nrp1;Wnt1Cre* mutants had fewer sympathetic fibres on the heart epicardial surface than wildtype (A), and nerves in mutants were defasciculated. The number of sympathetic fibres per 0.02mm^2 field in epicardial (A,C) and endocardial (arrowheads, B,D) tissue of the left ventricular wall were quantified (E,F); compared to wildtypes, mutant hearts had a reduced epicardial-to-endocardial sympathetic fibre gradient (E) and a significantly lower fold difference of sympathetic fibres between epicardium and endocardium (F; n=3 each). * $P < 0.05$ in a two-sample student's t-test. Scale bars: 50μm.

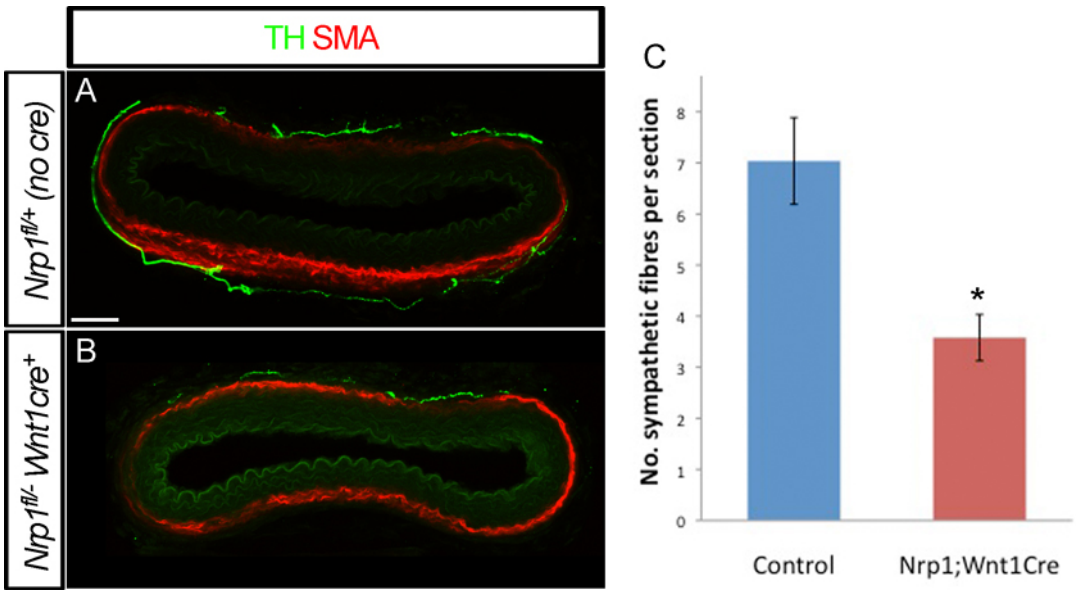

Figure 3.17: Loss of NRP1 in NC reduces the number of sympathetic nerve fibres innervating the aorta.

50μm vibratome sections of P7 aortas from wildtypes (A) and *Nrp1;Wnt1Cre* mutants (B) immunolabelled with TH (green) and SMA (red). Quantification of sympathetic fibres in contact with the dorsal aorta in each section (C) reveals significantly fewer sympathetic fibres on the dorsal aorta in mutants compared to wildtypes (n=3 each). * $P < 0.05$ in a two-sample student's t-test. Scale bars: 100 μm.

3.2.4 Investigating a function for SEMA3G in the sympathetic nervous system

Preliminary studies showed that, despite the predominantly vascular embryonic expression of SEMA3G, *Sema3g*-null mice have no defects in vascular patterning or smooth muscle actin coating (personal communication, Minoru Takemoto and Prof Christer Betsholtz). Similarly, no gross patterning defects were found in the PNS (personal communication, Minoru Takemoto and Prof Christer Betsholtz). A recent study claimed that SEMA3G has an autocrine destabilising effect on endothelial cells and a paracrine effect on smooth muscle cell outgrowth *in vitro* (Kutschera et al., 2011). However no *in vivo* function for SEMA3G was declared from analysis of the *Sema3g*-null mice.

Major arteries are innervated by the sympathetic nervous system before birth, and these arteries express SEMA3G in the embryo (personal communication, Minoru Takemoto and Prof Christer Betsholtz). Taking into account *in vitro* work showing that SEMA3G repels sympathetic neurons (Taniguchi et al., 2005), these results make SEMA3G a likely candidate for a chemorepellant sympathetic axon guidance molecule.

3.2.4.1 SEMA3G expression studies

To confirm the expression pattern of *Sema3g*, I used a mouse with the lacZ reporter allele inserted into the *Sema3g* locus and carried out X-gal assays. As recently shown by others at E10 (Kutschera et al., 2011), *Sema3g* is expressed at E11.5 in the major arteries in the limb, the carotid arteries of the head and the dorsal aorta at E11.5 but not in the capillaries (Fig. 3.18A,B,E). Arterial expression was maintained through E12.5 to E13.5 (Fig. 3.19A,C,D,F). *Sema3g* expression is reported to remain in major arteries through E14.5 until about E17.5 (Kutschera et al., 2011). After E17.5, *Sema3g* expression switches to smaller arteries, and after P20 it is no longer expressed in arteries (Kutschera et al., 2011). At E11.5 *Sema3g* was also expressed in the sensory DRG and trigeminal ganglia (Fig. 3.18B-E), which was maintained through E12.5 to E13.5 (Fig. 3.19A-F). *Sema3g* is also expressed in postnatal rats in the brain, heart, lung, kidney and pancreas (Taniguchi et al., 2005). Combined with the lack of vascular patterning defects, these observations support a possible role for SEMA3G in regulating sympathetic innervation.

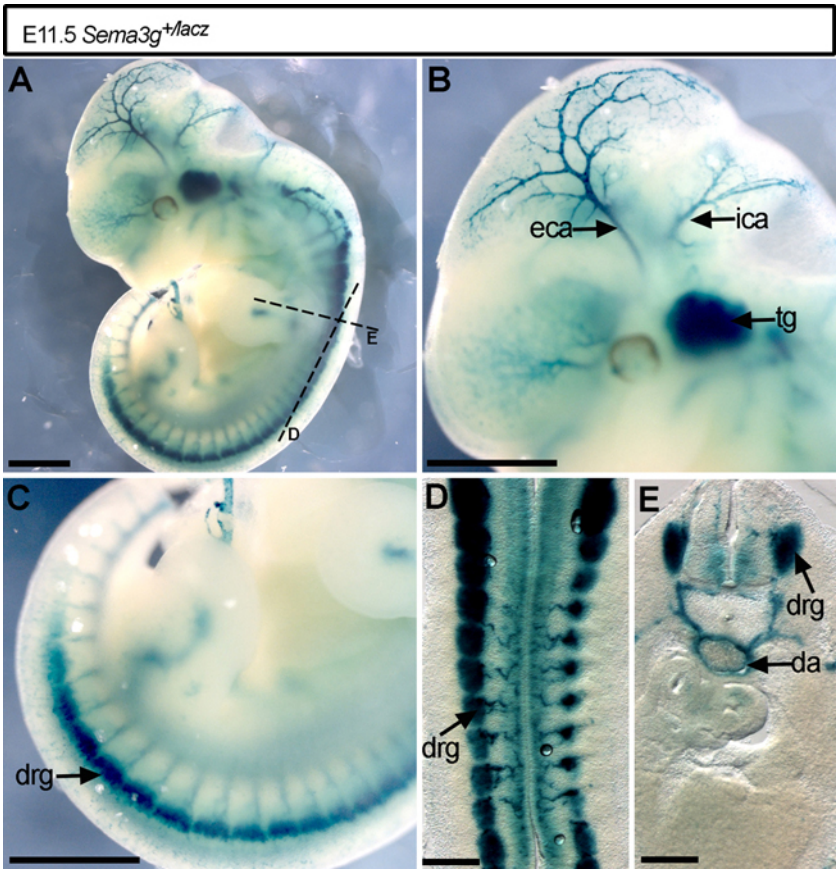

Figure 3.18: *Sema3g* is expressed in arteries and sensory ganglia at E11.5.

Visualisation of *Sema3g* expression using lacZ reporter in E11.5 *Sema3g* heterozygous mutants (A). *Sema3g* is expressed by major arteries, including the internal and external carotid arteries (ica, eca; B) and the dorsal aorta (da; E), and in the trigeminal ganglia (tg; B) and dorsal root ganglia (drg, C-E). Vibratome sections in D and E were taken at positions indicated in A. Scale bars: A-C – 1mm; D-E – 250μm.

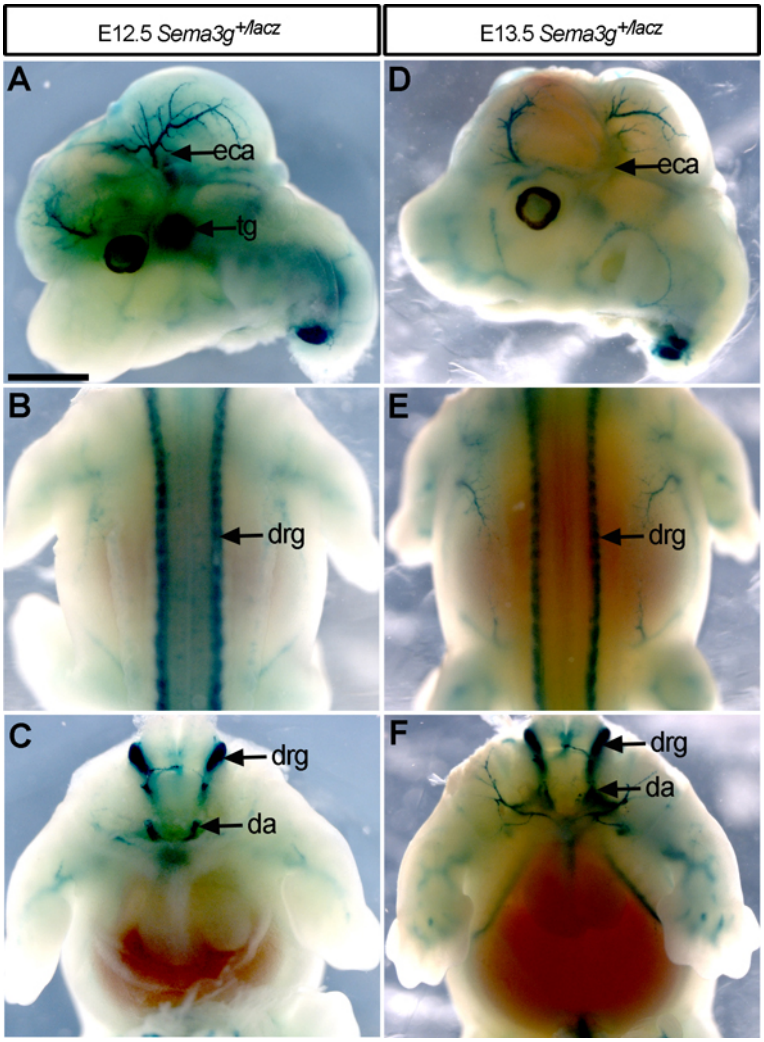

Figure 3.19: *Sema3g* expression in arteries and sensory ganglia is maintained at E12.5 and E13.5.

Visualisation of *Sema3g* expression using lacZ reporter in *Sema3g* heterozygous mutants at E12.5 (A-C) and E13.5 (D-F). At E12.5 *Sema3g* is expressed in major arteries, including the external carotid arteries (eca; A) dorsal aorta (da; C), and trigeminal ganglia (tg; A) and DRG (B,C). At E13.5, expression in external carotid arteries (D), dorsal aorta (F) and DRGs (E,F) is maintained. Scale bars: 1mm.

3.2.4.2 No function for SEMA3G in sympathetic nervous system development

To address whether SEMA3G is essential for sympathetic nervous system development, I immunolabelled E13.5 *Sema3g*-null mouse embryos with TH to visualise the developing sympathetic chains. However, the sympathetic chains were correctly positioned with no premature axon extensions (Fig. 3.20A,B).

Semaphorins have been suggested to functionally compensate for each other (Kutschera et al., 2011). Since SEMA3G and SEMA3F both bind and signal through NRP2, I next asked whether SEMA3F compensates for the absence of SEMA3G by analysing sympathetic chain development in compound *Sema3g/Sema3f*-null mutant embryos by immunolabelling with TH. As previously observed, loss of SEMA3F resulted in some axons prematurely extending from the sympathetic chain (Fig. 3.6E), but the phenotype was not aggravated with a concurrent loss of SEMA3G (Fig. 3.21E). I then asked whether SEMA3A could compensate for the loss of SEMA3G. Loss of SEMA3A resulted in the same phenotype as previously found (Fig. 3.6C, Fig. 3.21C) and there was no aggravation of this phenotype in embryos lacking both SEMA3G and SEMA3A (Fig. 3.21D).

I next asked whether SEMA3G might instead play a role in later sympathetic innervation patterning in the postnatal heart and aorta. I quantified the number of sympathetic fibres in the epicardium and endocardium of cryosectioned wildtype and *Sema3g*-null P7 hearts immunolabelled with TH and endomucin (Fig. 3.22A-D), and found no difference in number of sympathetic fibres in the epicardium or endocardium. The fold difference between number of sympathetic fibres in epicardium and endocardium was therefore the same in mutant and wildtype (Fig. 3.22E; wildtype mean fold change 5.8 ± 0.003 (n=2) versus mutant mean fold change 6.1 ± 1.7 (n=2)). Immunolabelling of dorsal aorta vibratome sections with TH and SMA (Fig. 3.22F-G) revealed that there was also no difference between wildtypes and *Sema3g*-null mutants in number of sympathetic fibres contacting the aorta (Fig. 3.22H; wildtype 6.6 ± 0.9 versus mutant 7.0 ± 0.6). These observations suggest that SEMA3G does not guide sympathetic innervation in the postnatal heart and aorta. The physiological function of SEMA3G therefore remains elusive.

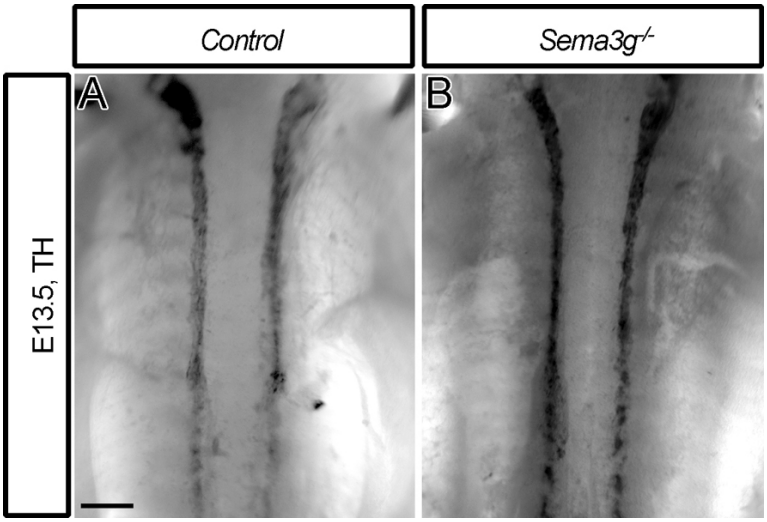

Figure 3.20: Loss of SEMA3G does not affect development of the sympathetic nervous system.

E13.5 wildtype (A; n=5) and *Sema3g*-null mutants (B; n=4) with internal organs removed immunolabelled with TH revealed that the sympathetic chains developed normally, with no defects in axon guidance, in the absence of SEMA3G. Scale bar: 200μm.

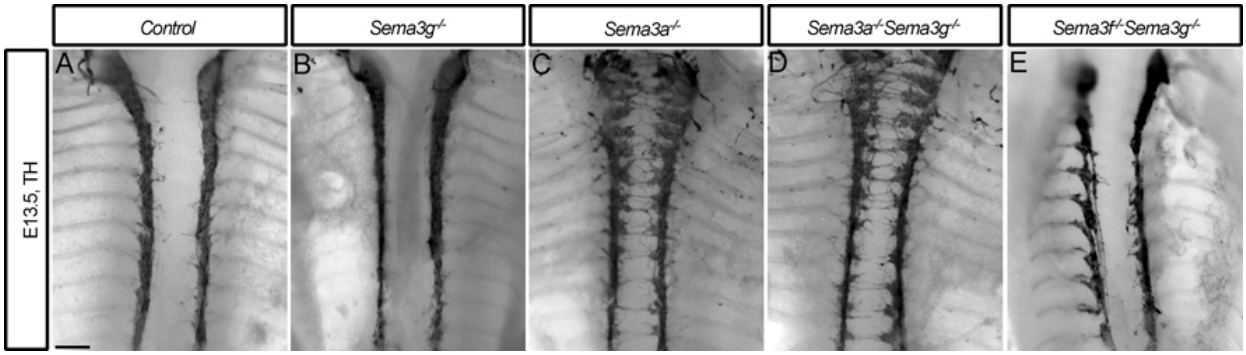

Figure 3.21: Loss of SEMA3G in absence of SEMA3A or SEMA3F does not exacerbate sympathetic nervous system defects.

E13.5 control (A), *Sema3g*-null (B), *Sema3a*-null (C), compound *Sema3a/Sema3g*-null (D) and compound *Sema3f/Sema3g*-null (E) mutant embryos subjected to TH immunolabelling, viewed ventrally with internal organs removed. The phenotypes previously observed when SEMA3A is lost, including misplaced sympathetic neurons and disorganised ganglia (C), or the axon guidance defect observed when SEMA3F was lost, were not worsened by the concurrent loss of SEMA3G (D,E, respectively). Scale bar: 200μm.

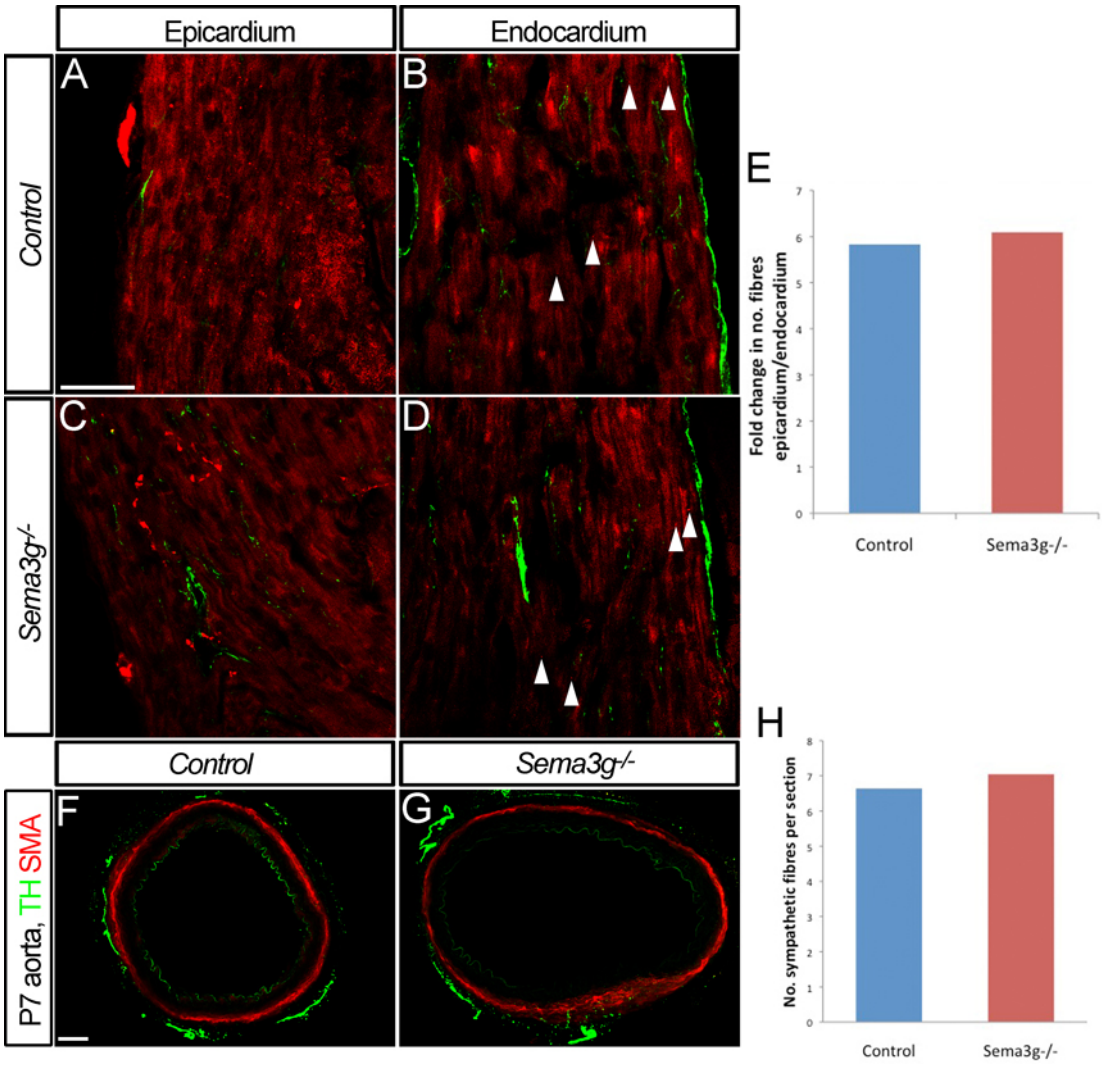

Figure 3.22: Loss of SEMA3G does not affect postnatal sympathetic innervation patterning of the heart or dorsal aorta.

Longitudinal cryosections from P7 wildtype (A,B) and *Sema3g*-null (C,D) hearts were immunolabelled for TH (red) and endomucin (green), and the number of sympathetic fibres per 0.02mm^2 field in epicardial (A,C) and endocardial (arrowheads, B,D) tissue of the left ventricular wall was quantified. No difference in number of sympathetic fibres in epicardium or endocardium was found, resulting in no change in fold difference in sympathetic fibres between epicardium and endocardium (E; n=2 each). Vibratome sections of P7 dorsal aortas were cut from wildtypes (F) and *Sema3g*-null mutants (G), immunolabelled with TH (green) and SMA (red), and the number of sympathetic fibres on each section quantified. There was no difference between the numbers of sympathetic fibres on the aorta of mutant mice compared to wildtype (H; n=2 each). Scale bars: A-D – 50μm; F,G – 100 μm.

3.3 Discussion

The aim of the work described earlier in Chapter 3 was to investigate the roles of NRP1 and NRP2 and their SEMA3 ligands in the development of the sympathetic nervous system. As discussed in Chapter 1.1, a previous study in mice showed that loss of SEMA3A or NRP1 disrupts sympathetic nervous system patterning, and it was suggested that these defects are caused once NCCs have differentiated into sympathetic neuronal progenitors (Kawasaki et al., 2002). I here show that the defects originate during sympathetic NCC migration (Figs. 3.4 and 3.11) (Schwarz et al., 2009b). In agreement with the previously proposed idea that SEMA3A acts on sympathetic neurons through NRP1 to guide axons in the sympathetic nervous system (Kawasaki et al., 2002), NRP1 was expressed on sympathetic neurons (Figs. 3.1 and 3.2) where it bound SEMA3A (Figs. 3.3). I further show that the sympathetic nervous system defects observed in mice lacking NRP1 are cell autonomous and are independent of vascular problems (Figs. 3.6 and 3.8).

Due to defective NCC migration, mice lacking NRP1 have increased numbers of NCC entering the intersomitic furrow and the dermomyotome pathway (Schwarz et al., 2009b). I contributed to this study by showing that, due to this defective migration, sympathetic-fated NCCs end up in ectopic locations (Figs. 3.4 and 3.5) (Schwarz et al., 2009b). This finding is supported by previous work implicating NRP1/SEMA3A signalling in the migration of trunk NCCs *in vitro* (Eickholt et al., 1999), and in cranial NCC migration *in vivo* (McLennan and Kulesa, 2007; Osborne et al., 2005). The technique used in the study that reported normal NCC migration in *Nrp1*-null mice (Kawasaki et al., 2002) involved an antibody that also labelled blood vessels (Kubota et al., 1996), meaning that ectopic sympathetic NCCs might not have been identified because they migrate close to blood vessels. I now show that ectopically placed sympathetic NCCs in NRP1-deficient mice survive to differentiate into sympathetic neurons (Figs. 3.9 and 3.10), resulting in the previously described disorganisation of the sympathetic nervous system (Figs. 3.6 and 3.8).

Work using mice lacking the BMP receptor ALK3 on NCCs previously showed that without BMPs derived from the dorsal aorta, sympathetic NCCs die at E10 (Morikawa et al., 2009). In my work, most ectopic sympathetic NCCs in mice lacking NRP1 were in close proximity to the posterior cardinal vein or other, smaller blood vessels (Fig. 3.5). This observation raised the possibility that ectopically positioned NCCs may receive survival factors from blood vessels other than the dorsal aorta. A previous study showed that endothelial cells in bone express BMP4 to stimulate bone formation (Goldman et al., 2009a), therefore endothelial cells other than those in the dorsal aorta might also express BMPs. BMP4 is also required for limb development (Goldman et al., 2009b) and is expressed in the

forelimb at E9.5, E10.5 and E12 (Selever et al., 2004). Consistent with the possibility that limb-derived BMP4 provides a survival factor for ectopic sympathetic neurons, they were particularly prevalent at the forelimb level compared to other anteroposterior positions (Fig. 3.6).

My work showing that ectopic NCCs can differentiate into sympathetic neurons supports the idea of NCC fate predetermination. Past experiments have led to the hypothesis that NCC fate is predetermined by time of delamination from the neural tube. For example, single cell tracing in zebrafish showed that the first NCCs to delaminate become neuroglial structures and NCCs delaminating later become melanocytes (Schilling and Kimmel, 1994). More recently, timing of delamination was linked to previous dorsoventral location of NCCs in the mouse neural tube and correlated with expression of specific markers (Wilson et al., 2004). My observations show that sympathetic fate is not altered by mislocation of sympathetic NCCs, endorsing the hypothesis that NCC fate is predetermined at the time of delamination from the neural tube. To further substantiate the idea that sympathetic fate in NCCs is predetermined, sympathetic NCCs could be derived from chick embryo neural tube explants and inserted into the melanocyte-fated stream of an older chick embryo, as in previous experiments with neural progenitor NCCs (Krispin et al., 2010). I would predict that the sympathetic NCCs would reach their sympathetic fate even in the melanocyte stream.

Consistent with NRP2 expression in differentiated sympathetic neurons (Figs. 3.1 and 3.2) (Chen et al., 1997) and SEMA3F binding to sympathetic neurons (Fig. 3.3), I demonstrated here using mouse mutants that SEMA3F/NRP2 signalling plays a role in sympathetic axon guidance (Figs. 3.6). This agrees with *in vitro* work showing that the normally repulsive effect of SEMA3F is lost in sympathetic axons from NRP2-deficient mice (Giger et al., 2000). However, a previous study found no obvious defect in sympathetic patterning of mice lacking NRP2 (Waimey et al., 2008). The authors of this previous study did not explicitly look at sympathetic axon guidance, and images showed the superior cervical and stellate ganglia at E13.5 rather than the sympathetic chain. Perhaps it is warranted to look at axon extension from these ganglia later in development in mice lacking NRP2, since sympathetic innervation of the heart, which originates in the stellate ganglia, was not apparent at E13.5 in my investigations (not shown). Alternatively, the axons innervating the carotid arteries extend anteriorly from the superior cervical ganglia into the cranium, and removal of the head to expose the ganglia may have resulted in accidental removal of misguided sympathetic axons in the previous study. Examination of other sympathetically innervated organs in mice lacking NRP2, such as the carotid arteries or the heart at later stages, would further establish the presence of the sympathetic axon guidance defect.

As well as the sympathetic axon guidance function, I have also described a novel function for NRP2 in early sympathetic nervous system development. NRP2 can partially compensate for the loss of NRP1 in sympathetic NC migration and placement, because when both NRP1 and NRP2 are lost, the sympathetic NCC migration defect is worse than when NRP1 alone is lost (Fig. 3.11 and 3.12). However, I could not find NRP2 expression in sympathetic NC precursors (Figs 3.1 and 3.2). To address whether NRP2 is switched on in sympathetic NCCs when NRP1 expression is lost, *Nrp1*-null embryos at E9.5 could be immunolabelled with NRP2 and the NC marker p75. Alternatively, a subset of sympathetic NCCs might express NRP2, but went undetected since I did not look at contiguous sections. It has been previously shown that NRP2-positive NCCs migrate through the anterior somite (Gammill et al., 2006; Schwarz et al., 2009a). Therefore, NRP2-positive sympathetic NCCs might exist in the primary sympathetic ganglia at the axial level of the anterior somite. To investigate whether there are NRP2-positive sympathetic NCCs, contiguous sections through two complete somites should be double immunolabelled for NRP2 and the NCC marker p75 and examined for potential NRP2-positive NCCs en route to the dorsal aorta.

Recent work provides evidence for the unconventional ability of SEMA3A to signal through NRP2 in specific cases of axon guidance (Cariboni et al., 2011). In agreement, the AP-binding assay I carried out showed that SEMA3A bound lung tissue even in the absence of SEMA-binding NRP1 (Fig. 3.3). Together, these observations raise the possibility that SEMA3A might signal through NRP2 in the absence of NRP1 to help guide sympathetic NCCs, which might provide an alternative explanation for why the loss of NRP2 worsens the NCC migration phenotype in the absence of NRP1. This could be investigated by reacting AP-tagged SEMA3A with sections from E9.5 embryos lacking NRP1. Once confirmed, perhaps by testing if AP-tagged SEMA3A binding in lung tissue is abolished in embryos lacking NRP2 and SEMA-binding NRP1, this may further substantiate evidence of SEMA3A binding NRP2.

By analysing postnatal mice lacking NRP1 in the NC lineage, I confirmed and extended the finding that SEMA3A contributes to sympathetic patterning in the postnatal heart (Ieda et al., 2007) by showing that SEMA3A signals through NRP1 on sympathetic neurons to regulate innervation of the cardiac wall (Fig. 3.16). Mice lacking NRP1 in the NC lineage are viable so the defects observed in sympathetic patterning do not affect survival.

In collaboration with John Gomes and Prof Andrew Tinker at University College London, we have now begun heart function studies on mice lacking NRP1 in the NC lineage at 6 months of age. Telemetry on live mice and ECG on mice under anaesthesia were used to follow resting heart rates and analyse them by measurement of the time lapse between the R points of two adjacent ECG curves, known as RR values. It was found that heart rates

of mutants were on average decreased compared to control heart rates (personal communication, data not shown). Since the sympathetic nervous system is thought to increase heart rate (Cao et al., 2000a), the reduced heart rate in the *Nrp1;Wnt1Cre* mutant mice may be due to a reduction in functional cardiac sympathetic innervation. Defective sympathetic activity causes arrhythmias in dogs (Yanowitz et al., 1966), and interestingly, the most consistent defects observed in *Nrp1;Wnt1Cre* mutant mice were arrhythmias (personal communication, data not shown). Further examination is required to substantiate thesis findings, for example telemetry studies on live mice during exercise, to see if their heart rates respond abnormally to physiological stimuli.

In addition, I found that the sympathetic innervation of the dorsal aorta is misguided in *Nrp1;Wnt1Cre* mutant mice, resulting in fewer axons in contact with the dorsal aorta (Fig. 3.17). Stimulation of sympathetic ganglia that innervate the dorsal aorta in the dog alters blood pressure (Gerova et al., 1973), suggesting that the defects in *Nrp1;Wnt1Cre* mutant mice may cause problems in modulation of blood pressure. This could be tested experimentally by taking measurements of blood pressure in the mice before and after exercise to assess whether the mutant mice can sufficiently alter blood pressure.

The defects in sympathetic heart innervation in mice lacking NRP1 in the NC lineage appeared mild compared to other published reports of mutant mice with defects in sympathetic innervation. For example, in mice with defective NGF signalling, sympathetic innervation of the heart is almost entirely lacking (Glebova and Ginty, 2004). Defects in sympathetic innervation were also present in the salivary glands and eyes of NGF mutant mice; however, the trachea maintained normal sympathetic innervation (Glebova and Ginty, 2004). This raises the possibility that a range of different guidance molecules specific to the target structure may cooperate to pattern the sympathetic nervous system. It would be interesting to compare innervation of other vascular sympathetic targets in *Nrp1;Wnt1Cre* or *Sema3a*-null mutant mice, such as the carotid arteries, to assess their sympathetic innervation defects. Comparison with sympathetic innervation of organs such as the trachea and salivary glands would also be interesting to assess whether non-vascular structures are also affected by the loss of NRP1 signalling.

A recent study suggested that SEMA3G is a vascular-acting molecule that increases migration of smooth muscle cells (Kutschera et al., 2011). However, the vascular system is normal in embryos lacking SEMA3G (personal communication, Prof Christer Betsholtz & Minoru Takemoto). The arterial expression of SEMA3G in development and its *in vitro* ability to bind NRP2 and repel sympathetic axons (Taniguchi et al., 2005) led me to hypothesise that SEMA3G might guide sympathetic axons to their arterial targets. However, I found no function for SEMA3G in regulating sympathetic chain organisation or later sympathetic innervation of the heart or aorta (Figs. 3.20 and 3.22). Partially

overlapping expression patterns of SEMA3G and SEMA3F in the postnatal mouse brain have been suggested to indicate functional compensation between these two signalling molecules (Matsuda et al., 2010). Since neither SEMA3F nor SEMA3A compensate for the loss of SEMA3G in embryonic sympathetic patterning (Fig. 3.21), I searched the mouse genome with BLAST to find genes similar to SEMA3G that might encode a compensating class 3 semaphorin. This proved unsuccessful, however, as the nearest homologues to SEMA3G that I found were all previously identified semaphorins. Whether SEMA3A compensates for the loss of SEMA3G in sympathetic innervation of the postnatal heart remains to be investigated using compound *Sema3a*/*Sema3g*-null mice.

Decreased expression in adulthood (Taniguchi et al., 2005) suggests that the function of SEMA3G is likely to be developmental. Even though patterning of the PNS is grossly normal in mice lacking SEMA3G (personal communication, Prof Christer Betsholtz & Minoru Takemoto), the developmental expression of SEMA3G in the sensory ganglia might be significant to its adult function. Using an AP-tagged SEMA3G construct to visualise the localisation of bound SEMA3G might shed more light on potential sites of action of SEMA3G outside the vascular and nervous systems to identify an essential role in an as yet unidentified organ system.

4. HSPGS IN VEGF-A SIGNALLING IN THE DEVELOPING BRAIN

4.1 Introduction

In the second part of this thesis, I studied the role HSPGs play in VEGF164-driven vascular and neuronal patterning in the developing mouse brain. Early *in vitro* work into the binding affinities of VEGF-A isoforms to their receptors suggested that heparin promotes VEGF165 binding to VEGFR1 and VEGFR2 (Gitay-Goren et al., 1992; Tessler et al., 1994), as well as to NRP1 (Soker et al., 1998). Consistent with this, cell surface HS produced by pericytes can activate VEGFR2 in *trans* to mediate VEGF165-stimulated angiogenesis *in vitro* (Jakobsson et al., 2006). 2-*O*- and 6-*O*-sulphated HS in particular have been implicated in VEGF165 mitogenic activity and endothelial tube formation *in vitro* (Ashikari-Hada et al., 2005; Chen et al., 2005; Robinson et al., 2006). I here aimed to investigate whether HSPGs have a role in presenting VEGF165 to its receptors, as suggested by these studies. I also tested whether HSPGs are required to retain VEGF164 in the ECM to maintain the VEGF-A gradients required for blood vessel branching, as loss of heparin-binding VEGF164 results in vascular branching defects in the mouse brain due to the loss of VEGF-A gradients (Gerhardt et al., 2003; Ruhrberg et al., 2002).

The migration path followed by the cell bodies of FBM neurons is guided by VEGF164 signalling through NRP1 (Schwarz et al., 2004). A co-receptor for this signalling pathway has not yet been found. Since VEGF164 and NRP1 both bind HS, I investigated whether HSPGs are required in FBM neuronal migration.

4.2 Results

4.2.1 HSPGs in VEGF-A driven vascular patterning in the brain

4.2.1.1 Expression of HSPGs in the hindbrain

Initially, I confirmed the expression of HSPGs in the developing hindbrain using an antibody specific for HSPGs, 10E4 (David et al., 1992), as previously described (Stenzel et al., 2009). At E11.5, HSPGs were expressed in the developing subventricular vascular plexus (Fig. 4.1A,D), indicated by co-expression with isolectin B4 (IB4), a marker of blood vessels and macrophages (Fig. 4.1C,F). Macrophages were not positive for 10E4. HSPGs were present on neural progenitor cells (Fig. 4.1A-F).

To identify the expression of genes for HSPG biosynthetic enzymes or for the core protein of HSPG, an Affymetrix GeneChip microarray was carried out on RNA from E11.5 mouse hindbrains, which is the age at which sprouting angiogenesis is occurring. The results

were normalised to *gapdh*, a housekeeping gene due to its stable and constitutive expression in most cells, and presented as relative intensity of fluorescent signal, which was indicative of gene expression (Fig. 4.2). The signal obtained for expression of the *Pu1* gene was used as a negative control to identify the level of background noise; three of the six hindbrains used were *Pu1*-null, but showed an 'expression' of 5, so expression of less than 5 was considered background noise. Most of the HSPG biosynthetic enzymes were expressed in the hindbrain. Both *Ext1* and *Ext2* enzymes were expressed at a high level, along with *Ndst1*, whereas *Hsepi*, the gene encoding C5-epimerase, and *Ndst2* were slightly lower. Of the sulphotransferase enzymes, *Hs2st* and *Hs6st1* were both highly expressed, and *Hs6st2* and *Hs6st3* were expressed at a lower level. The former had a large error bar, suggesting variability in expression. *Hs3st1* expression was not detected in the hindbrain. HS3ST1 functions in blood coagulation (Atha et al., 1985) and there are no reports of its expression any earlier than E16 (Yabe et al., 2005). It is therefore unlikely that this enzyme functions in VEGF164 signalling. I also looked at genes for HSPG core proteins. *Syndecan-1* and *-3* were highly expressed and *syndecan-2* and *-4* were expressed at a lower level. Expression of *glypican-1, -2, -3* and *-6* was high, whereas *glypican-4* expression was lower, and *glypican-5* expression was not detected. Of the ECM HSPGs, *perlecan* expression was low and *agrin* expression was very high.

Previously, expression studies were carried out on three of the sulphotransferase enzymes by Joaquim Vieira. He carried out a β-galactosidase assay on E10.5 embryos containing a *lacZ* reporter allele in the *Hs2st* and *Hs6st1* loci, and an *in situ* hybridisation with an *Hs6st2* probe on E10.5 wildtype embryos. *Hs6st1* and *Hs6st2* were expressed in the rhombomere boundaries and some neural progenitors in the hindbrains. *Hs2st* was expressed in r4, the region where the FBM neurons are born, and in the hindbrain/midbrain boundary (J. Vieira & C. Ruhrberg, unpublished data, not shown).

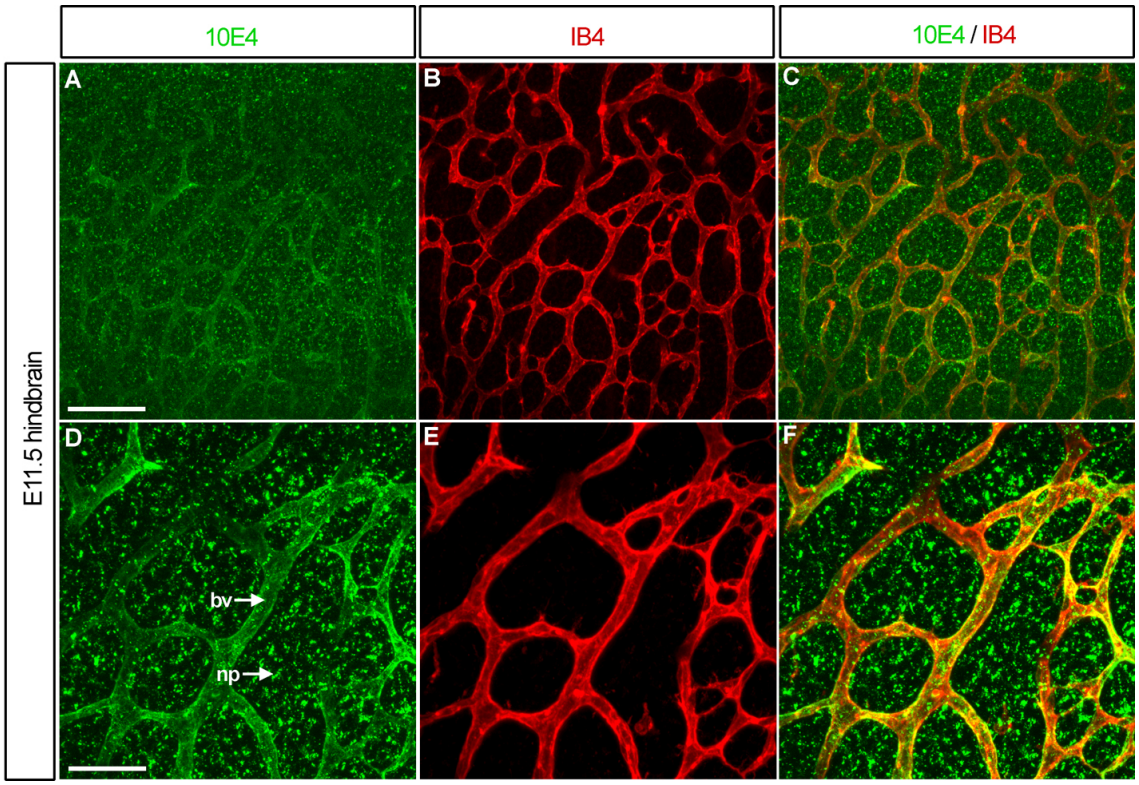

Figure 4.1: HSPGs are expressed in blood vessels and neural progenitors of the hindbrain at E11.5.

Immunolabelling of E11.5 hindbrains with HSPG marker 10E4 (green in A, higher magnification in D) and endothelial marker isolectin4 (IB4; red in B, higher magnification in E) to visualise HSPG expression (merged image in C, higher magnification in F). HSPGs were expressed in blood vessels (bv) and in the neural progenitors (np). Scale bar: A-C – 100μm; D-F – 50μm.

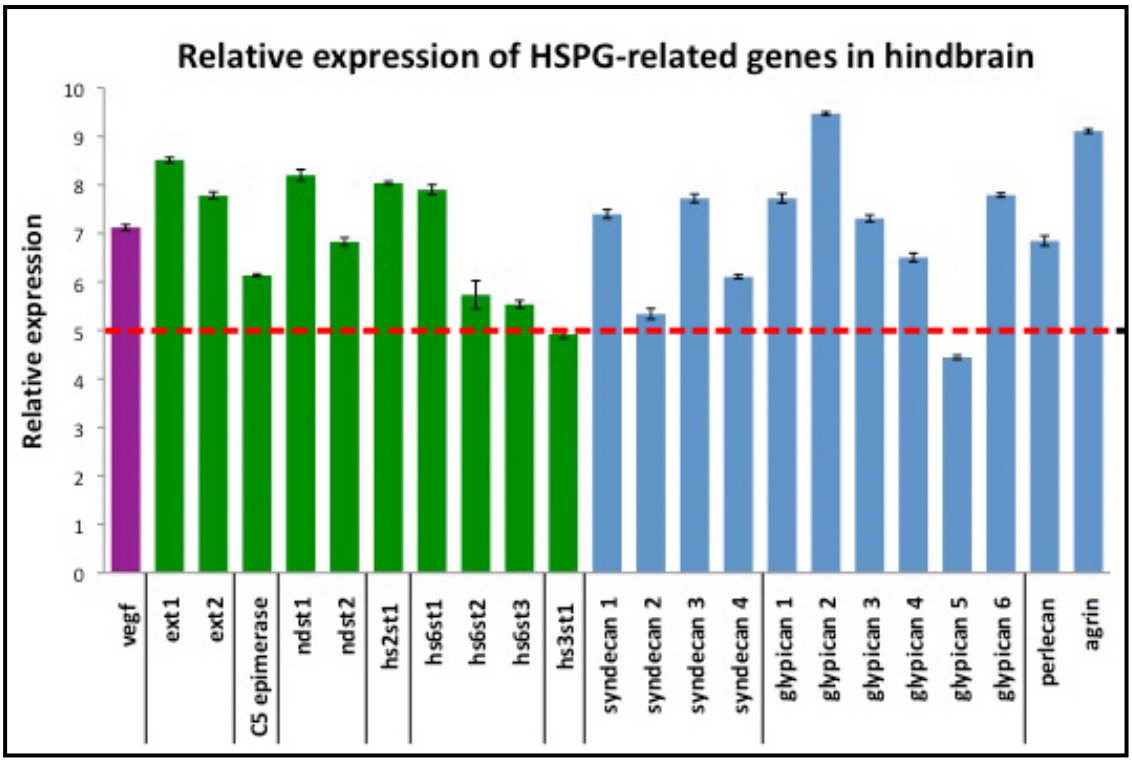

Figure 4.2: HSPG-related genes are expressed in the E11.5 mouse hindbrain.

Graph of expression of HSPG-related genes in E11.5 hindbrains from GeneChip microarray, normalised to *gapdh*. Hashed red line indicates background noise. Most HSPG biosynthetic enzymes were expressed at a high level, including *Ext1*, *Ext2*, *Ndst1*, *Ndst2*, *Hs2st*, *and Hs6st1*. The others were also expressed, including *C5-epimerase*, *Hs6st2* and *Hs6st3*. *Hs3st* was not expressed above background noise. Most HSPG proteins were also highly expressed, including *syndecan1* and *3*, *glypican1, 2, 3* and *6*, and *agrin*. *Glypican5* was not expressed above background noise.

4.2.1.2 Previous investigations into vessel branching of mice lacking sulphotransferase enzymes

Previous analysis of blood vessel patterning in the hindbrain subventricular plexus of embryos lacking these enzymes revealed that removal of HS2ST or HS6ST1 or both did not perturb vessel branching (J. Vieira & C. Ruhrberg, unpublished data). Embryos lacking HS6ST2 had a 15% decrease in branching of the subventricular vascular plexus (J. Vieira & C. Ruhrberg, unpublished data). These samples were sent from Dr Koji Kimata at the Aichi Medical University in Japan as fixed, severed heads of embryos, from which the hindbrains were then dissected. To obtain clear immunolabelling with PECAM, hindbrains need to be dissected prior to fixing. The quality of the immunolabelling was variable between hindbrains and it was difficult to accurately quantify the number of vessel branchpoints in the hindbrain. The laboratory supplying these mice then closed down, so to obtain further embryos, we obtained a mouse lacking HS6ST2 from Lexicon Pharmaceuticals Inc.

4.2.1.3 Genetic analysis of the Hs6st2 mutant mouse

Like the *Hs2st* and *Hs6st1* knockout mice, the Lexicon Pharmaceuticals *Hs6st2* mouse had a lacZ/Neo cassette inserted into exon 1 of the gene. To confirm the efficacy of the *Hs6st2* gene knockout, I carried out quantitative (q)-PCR on RNA extracted from the hindbrains of E12.5 embryos null for *Hs6st1* or *Hs6st2* (Fig. 4.3A,B). Expression was normalised to *18s*, a housekeeping gene encoding a ribosomal RNA subunit present in every cell, and presented as fold change in expression from wildtype. Consistent with previous findings (Pratt et al., 2006), the *Hs6st1*-null mutant had a 0.05-fold decrease from wildtype (Fig. 4.3A), and was therefore an efficient knockout. The *Hs6st2* mutation was not as effective as the *Hs6st1* mutation. Homozygous *Hs6st2* mutants had a 0.24- or 0.29-fold change in expression from wildtype in the presence or absence of HS6ST1, respectively (Fig. 4.3B), meaning the primers still detected HS6ST2 RNA. The reasons for this are not yet clear and warrant further investigation. The presence of HS6ST2 protein could be tested for by immunoblotting with HS6ST2 antibody, or simply immunolabelling of knockout embryos with the antibody. To test for the presence of a functional enzyme, HS could be purified from fibroblasts from *Hs6st2*-null embryos and their structure assessed to check for any 6-*O*-sulphation, as described previously for the *Hs2st* mutant mouse (Merry et al., 2001).

I used the q-PCR to address whether there was compensatory upregulation of the other 6-*O*-sulphation enzymes in the absence of HS6ST2 by quantifying the expression of *Hs6st3* as well as *Hs6st1* in embryos lacking HS6ST1 or HS6ST2 or both. Expression of *Hs6st1* was not affected by the loss of *Hs6st2*, as there was no difference in fold change of *Hs6st1* expression in the presence or absence of HS6ST2 (Fig. 4.3A). *Hs6st3* expression levels were highly variable, but no significant difference was found in the fold change of *Hs6st3*

expression in the presence or absence of HS6ST1 or HS6ST2 (Fig. 4.3C). Therefore, other *Hs6st* genes are not upregulated in embryos lacking HS6ST2.

The raw data from the qPCR in wildtype hindbrain samples suggested that the expression of *Hs6st1* relative to *18s* is 5-fold higher than *Hs6st2*, which in turn is 10-fold higher than *Hs6st3*. These data cannot generally be used as actual levels of expression due to possible variation in reaction efficiency. However, they agreed with the microarray expression data (Fig. 4.2) that showed that *Hs6st1* is expressed at the highest level of the three *Hs6st* genes, followed by *Hs6st2* then *Hs6st3*.

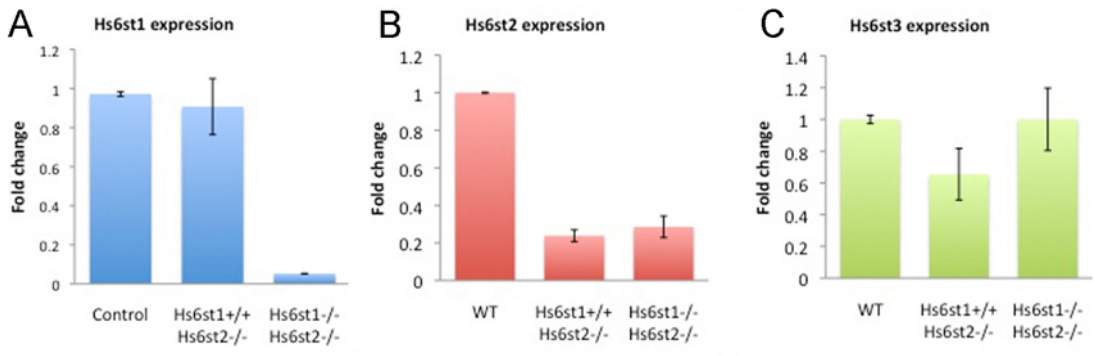

Figure 4.3: q-PCR reveals *Hs6st2* mRNA is produced in homozygous *Hs6st2* mutant.

Quantification of *Hs6st1* (A), *Hs6st2* (B) and *Hs6st3* (C) mRNA levels by q-PCR in E12.5 compound *Hs6st1* and *Hs6st2* mutant hindbrains, normalised to *18s* and shown as fold change from wildtype. *Hs6st1* expression did not change from wildtype when *Hs6st2* was lost. In compound *Hs6st1/Hs6st2*-null hindbrains, *Hs6st1* expression was negligible. *Hs6st2* was expressed in homozygous *Hs6st2* mutant hindbrains in the presence and absence of *Hs6st1*. *Hs6st3* expression was not affected by loss of *Hs6st2* or *Hs6st1* or both, and was highly variable. For controls, n=3; *Hs6st1+/+Hs6st2-/-,* n=4; *Hs6st1-/-Hs6st2-/-,* n=4. Error bars represent standard error of the mean. Raw data: wildtype relative expression of *Hs6st1* is 5.25, *Hs6st2* is 0.98 and *Hs6st3* is 0.08.

4.2.1.4 Knockdown of 6-O-sulphated HSPGs does not affect vascular patterning

I immunolabelled hindbrains from E12.5 wildtype and *Hs6st2*-null embryos with the endothelial marker PECAM (Fig. 4.4A-D), and quantified the number of vessel branchpoints in a 0.2mm^2 field of the subventricular vascular plexus (Fig. 4.4E). Hindbrains from mice lacking HS6ST2 exhibited a small but non-significant reduction in average number of vessel branchpoints compared to control hindbrains, which included wildtypes and heterozygous *Hs6st2* mutants (Fig. 4.4E; wildtypes 60 branchpoints ± 4.3 versus mutant 53 ± 4.2). There was high variability in branchpoints in HS6ST2-deficient hindbrains, ranging between 46 and 62 vessel branchpoints per field. Since the *Hs6st2* gene is X-linked, I separated male and female embryos by genotyping for the presence of the *Sex-determining Region Y* (*SRY*) gene and analysed embryos for vessel branching to address whether it was affected by gender (Fig. 4.4A-D). Small differences between the controls and mutants were seen in both males and females (Fig. 4.4F; male controls 69 ± 0 versus male mutants 60 ± 2.4; female controls 57 ± 2.4 versus female mutants 46 ± 0.4). The difference in males was slightly less than the difference in females, suggesting that in the absence of HS6ST2 the vasculature was more severely affected in females than in males. These samples were from a single litter and statistical analysis of vessel branching in male and female hindbrains could not be carried out because the *n* numbers were too low.

HSPG biosynthetic enzymes may compensate for each other in knockout mutant animals, for example mice lacking HS2ST have increased *N*- and 6-*O*-sulphation of HS chains (Merry et al., 2001). Therefore, HS6ST1 or HS6ST3 might compensate for the loss when *Hs6st2* is knocked out. Compensation by HS6ST3 is unlikely since it was expressed at a very low level in wildtype hindbrains (Fig. 4.2) and was not upregulated in the absence of HS6ST2 (Fig. 4.3C). *Hs6st1* was highly expressed in the hindbrain (Fig. 4.2) and although it was not upregulated in the absence of HS6ST2 (Fig. 4.3A), might functionally compensate for it. To address this, I analysed the subventricular vascular plexus in embryos lacking both HS6ST1 and HS6ST2. To simplify the analysis, wildtypes and heterozygous mutants (e.g. pooled *Hs6st1*$^{+/+}$*Hs6st2*$^{+/+}$ with *Hs6st1*$^{+/-}$*Hs6st2*$^{+/+}$) were pooled into the 'control' group. Similarly, embryos homozygous for *Hs6st1* and wildtype or heterozygous for *Hs6st2* were pooled (*Hs6st1*$^{-/-}$*Hs6st2*$^{+/+}$ with *Hs6st1*$^{-/-}$*Hs6st2*$^{+/-}$), and vice versa. An initial investigation using final samples sent from Japan immunolabelled with IB4 suggested that the subventricular plexus of embryos lacking both HS6ST1 and HS6ST2 (Fig. 4.5C; *Hs6st1/Hs6st2* mutant 40 branchpoints ± 3.3; n=1) had fewer vessel branches than embryos lacking either HS6ST1 or HS6ST2 (Fig. 4.5A,B; Hs6st1 mutant 49 branchpoints ± 2.0 and Hs6st2 mutants 48 branchpoints ± 2.5; n=1 and n=2, respectively). However, these

hindbrains were from a single litter with no control heterozygous or wildtype embryos so comparison to controls could not be carried out.

Using the new *Hs6st2*-null mouse line crossed with the *Hs6st1*-null mouse already used in the lab, I found that at E12.5 (Fig. 4.6), vessel branching in the subventricular plexus of male *Hs6st2*-null or compound *Hs6st1/Hs6st2*-null mutants was not reduced compared to controls (Fig. 4.6E; male controls 55 ± 7.8, male *Hs6st2* mutants 55 ± 1.9, male *Hs6st1/Hs6st2* mutants 52 ± 0). Surprisingly, and in contrast to previous suggestions (Fig. 4.4), there was a small but non-significant increase in vessel branching in female *Hs6st1*-null, *Hs6st2*-null and compound *Hs6st1/Hs6st2*-null mutants compared to controls (Fig. 4.6E; female controls 46 ± 1.8, female *Hs6st1* mutants 50 ± 3.0, female *Hs6st2* mutants 54 ± 5.3, female *Hs6st1/Hs6st2* mutant 59 ± 0). These results confirmed that there were no significant differences in hindbrain vessel branching between males and females and no dependence of changes in vascular branching on gender, therefore I pooled males and females to increase *n* numbers. The resultant graph and statistical analysis confirmed there was no decrease in vascular branching in the absence of HS6ST1 and HS6ST2 compared to control (Fig. 4.6F; controls 49 ± 3.4, *Hs6st1* mutants 50 ± 3.1, *Hs6st2* mutants 56 ± 2.1, *Hs6st1/Hs6st2* mutants 55 ± 3.4).

The visual inspection of the E12.5 hindbrains suggested a developmental delay in animals lacking both HS6ST1 and HS6ST2. Vibratome sections through E12.75 compound *Hs6st1/Hs6st2*-null hindbrains revealed that they were thinner than controls and resembled E12.5 hindbrains (Fig. 4.7A,B). This 0.25-day developmental delay was also apparent when analysing FBM somata migration, as fewer neurons had migrated at E12.75 in compound *Hs6st1/Hs6st2*-null hindbrains compared to littermate controls, as discussed later in the chapter (Fig. 4.13). At E12.75, compound *Hs6st1/Hs6st2*-null mutants had no significant difference in vessel branching compared to control (Fig. 4.7C,F,G; controls 69 branchpoints ± 4.1 versus *Hs6st1/Hs6st2* mutants 72 ± 1.2). There was a small, but non-significant increase in subventricular vessel branching in *Hs6st1*-null and *Hs6st2*-null mutants compared to control (Fig. 4.7C-E,G; *Hs6st1* mutants 82 ± 5.3, *Hs6st2* mutants 78 ± 3.0). Since HS6ST3 is not expressed at a high level, and HS6ST1 and HS6ST2 are not required for normal hindbrain vascularisation, it appears that 6-*O*-sulphated HSPGs are not required for VEGF164-driven sprouting angiogenesis during brain development.

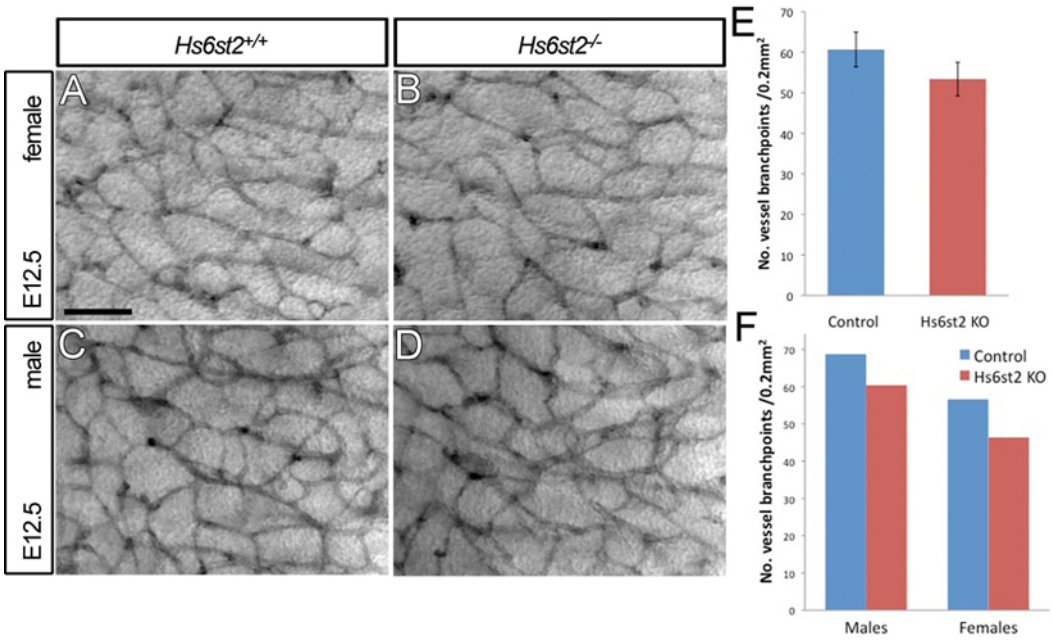

Figure 4.4: Loss of HS6ST2 results in no significant decrease in subventricular vessel plexus branching.

Immunolabelling of E12.5 wildtype (A,C) and *Hs6st2*-null (B,D) hindbrains with endothelial marker PECAM and quantification of blood vessel branches per 0.2mm^2 field revealed a small but non-significant decrease in vessel branching in mutants compared to controls (E; controls n=3, mutants n=4). Separation of female controls (A) and mutants (B) from male controls (C) and mutants (D) revealed female control hindbrains had fewer branchpoints than male controls (F). Both females and males had small but non-significant reductions in vessel branching in mutants compared to controls (F, male control n=1, female controls n=2, male mutants n=2, female mutants n=2). 'Control' groups included wildtype and heterozygous *Hs6st2* mutants. Scale bar: A-D – 100μm.

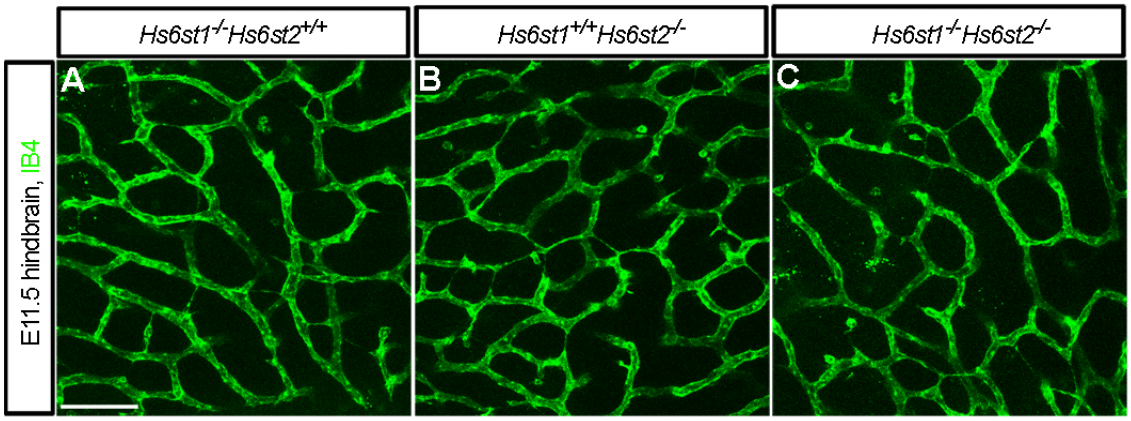

Figure 4.5: Hindbrain vasculature appears altered in absence of both HS6ST1 and HS6ST2.

Hindbrains from *Hs6st1*-null (A; n=1), *Hs6st2*-null (B; n=2) or compound *Hs6st1/Hs6st2*-null (C; n=1) E11.5 embryos subjected to immunolabelling with IB4 to visualise the vasculature, revealing slight decrease in vascular complexity in the compound mutant compared to either single mutant. Scale bar: 100 μm.

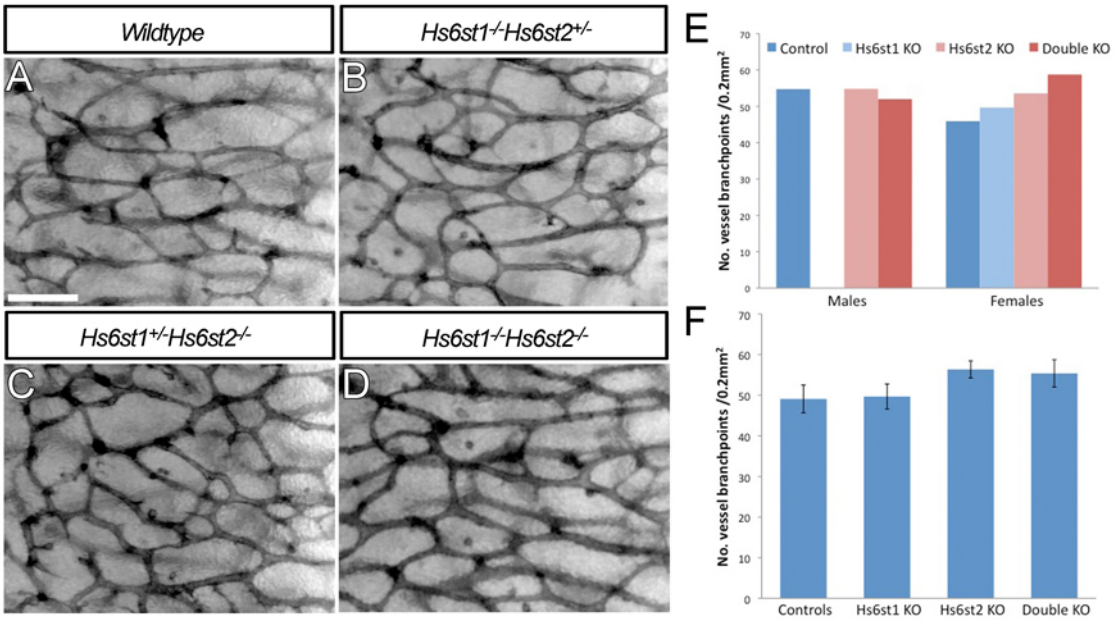

Figure 4.6: Loss of 6-*O*-sulphation does not affect subventricular vascular branching.

Immunolabelling of hindbrains from E12.5 wildtype (A), *Hs6st1*-null (B), *Hs6st2*-null (C) and compound *Hs6st1/Hs6st2*-null embryos (D) with endothelial marker IB4 for quantification of vessel branchpoints in 0.2mm^2 field. In males, the number of vessel branchpoints in control, *Hs6st2*-null and *Hs6st1/Hs6st2*-null hindbrains remained similar (E; n=2, n=7 and n=1, respectively). In females, the number of vessel branchpoints in control, *Hs6st1*-null, *Hs6st2*-null and *Hs6st1/Hs6st2*-null hindbrains increased slightly in this order (E, n=3, n=3, n=4 and n=1, respectively). When males and females were pooled (F), *Hs6st2*-null or compound *Hs6st1/Hs6st2*-null mutants had slightly higher numbers of branchpoints (n=11 and n=2, respectively) than controls or *Hs6st1*-null hindbrains (n=5 and n=3, respectively). The difference was not significant. Images in A-D are female hindbrains. Scale bar: 100μm.

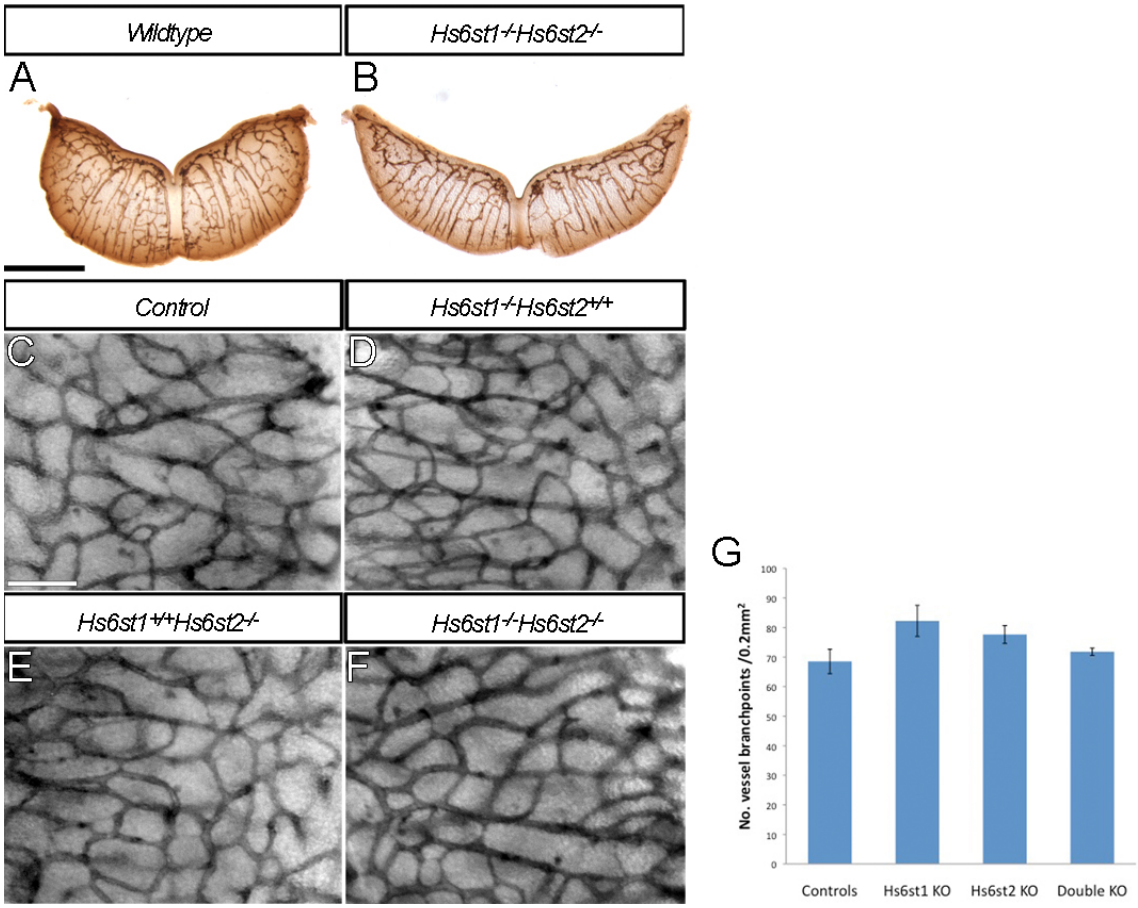

Figure 4.7: Loss of 6-*O*-sulphation does not affect vascular patterning but causes a developmental delay.

Immunolabelling E12.75 hindbrains with IB4 revealed a developmental delay, shown in transverse sections of wildtype (A) and compound *Hs6st1/Hs6st2*-null mutant (B) hindbrains. Hindbrain was thinner in mutant than in wildtype, as if it was 0.25 days younger. High magnification images of control (C), *Hs6st1*-null (D), *Hs6st2*-null (E) and compound *Hs6st1/Hs6st2*-null hindbrains (F) allow quantification of vessel branchpoints (G). No decrease in vessel branching was observed in any of the mutants compared to controls. A slight non-significant increase was observed in *Hs6st1*-null mutants compared to controls. (Controls, n=4; *Hs6st1* mutants, n=2; *Hs6st2* mutants, n=5; compound mutants, n=3). Scale bars: A,B – 500μm; C-F – 100μm.

4.2.1.5 A potential lymphatic defect in mice lacking HS6ST1 and HS6ST2

Even though no blood vessel defects were found, mice lacking HS6ST1 and HS6ST2 had severe oedema at E14.5, in the form of swelling under the skin in the trunk and head (Fig. 4.8A,B), which was not seen in embryos lacking only HS6ST1 or HS6ST2 (not shown). There were also blood spots on the skin, suggesting haemorrhaging induced by the pressure from the oedema (Fig. 4.8B, arrowheads). These characteristics were similar to mice lacking VEGF-C (Karkkainen et al., 2004), suggesting a defect in lymphatic development, and also to mice lacking HSPGs in pericytes (Stenzel et al., 2009). The authors of the latter study suggest that the oedema in these mice is indicative of a problem with vessel stability. The compound *Hs6st1/Hs6st2*-null mice also exhibited a developmental delay at E14.5 (Fig. 4.8B), consistent with findings at earlier ages (Fig. 4.7A,B). The delay was apparent in the limbs, which were less developed as the digits were not completely separated from each other as they were in wildtype (Fig. 4.8A,B).

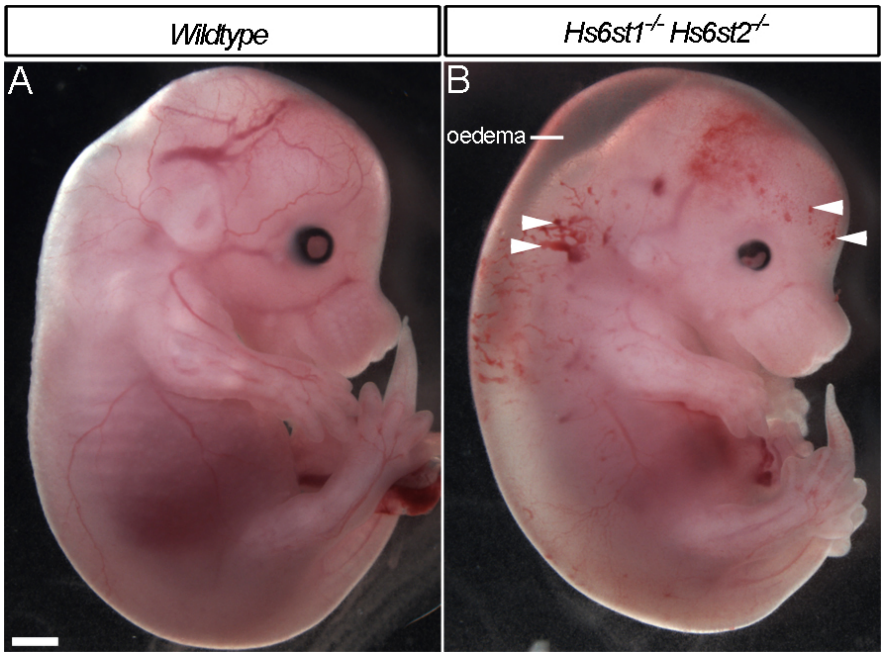

Figure 4.8: E14.5 embryos lacking HS6ST1 and HS6ST2 are oedematous.

Wholemount wildtype (A) and compound *Hs6st1/Hs6st2*-null (B) embryos shown laterally to visualise differences in gross development. Mutant mice exhibit oedema of the trunk and head and blood spots on the skin (arrowheads, B). They were developmentally delayed in comparison to wildtype, indicated by less well-developed digits and smaller eyes (n=2). Scale bar: 1 mm.

4.2.1.6 Endothelial cell HSPGs are not required for blood vessel branching

I next investigated vascular patterning in embryonic brains deficient in HSPG synthesis in specific cell types. I first deleted the conditional null *Ext* "floxed" gene with CRE under the control of the endothelial cell specific *Tie2* promoter (hereafter referred to as *Ext;Tie2Cre* mutant) to abolish HSPG production in endothelial cells. To assess whether the knockout was successful, I immunolabelled E11.5 hindbrains with the HSPG antibody 10E4. In wildtype hindbrains, HSPGs were visible on the vasculature and in the neural progenitor cell layer (Fig. 4.9A), consistent with earlier observations (Fig. 4.1). In contrast, HSPGs were no longer visible on the vasculature in *Ext;Tie2Cre* mutant hindbrains, but were still present in neural progenitor cells (Fig. 4.9B), indicating that the endothelium-specific knockout was efficient. I quantified the blood vessel branchpoints in hindbrains immunolabelled with PECAM (Fig. 4.9C,D), and found no decrease in subventricular vessel branching when HSPG production was abolished in endothelial cells compared to wildtypes (Fig. 4.9E; controls 57 branchpoints ± 2.7 versus mutants 63 ± 2.9). The findings were consistent with previous work (J. Vieira & C. Ruhrberg, unpublished data) and suggest that HSPGs produced by endothelial cells are not essential for blood vessel branching. Perhaps HSPGs produced by neural cells or pericytes could act in *trans* in VEGF164-driven blood vessel branching, as pericyte-derived HSPGs can potentiate VEGF165/VEGFR2 signals *in vitro* (Jakobsson et al., 2006).

4.2.1.7 Neural progenitor cell HSPGs are not required for blood vessel branching

To address whether neural cells produce HSPGs required for blood vessel branching, I ablated the conditional null *Ext* "floxed" gene with CRE under control of the neural-specific *Nestin8* promoter (hereafter referred to as *Ext;Nes8Cre* mutant). *Ext;Nes8Cre* mutant mice had severe head malformations: forebrains protruded from the skull (Fig. 4.10B), midbrain-hindbrain patterning was disrupted and hindbrains were truncated (Fig. 4.10D). These characteristics were consistent with previous observations in a similar mutant, and are indicative of problems in FGF8 signalling (Inatani et al., 2003). In addition, the tails had not grown sufficiently and the forelimbs exhibited syndactyly (Fig. 4.10B), which is also seen in mouse mutants with disrupted BMP signalling (Wang et al., 2004). Immunolabelling for PECAM revealed that the hindbrain vasculature in *Ext;Nes8Cre* mutants was morphologically different, as vessels were elongated and stretched laterally away from the midline (Fig. 4.10E,F). Despite this, quantification of vessel branchpoints in the hindbrains indicated that there was no difference in branching of mutants compared to wildtypes (Fig. 4.10E,F,I; controls 66 branchpoints ± 3.4 versus mutants 67 ± 9.8), suggesting that the altered morphology of the vasculature was most likely secondary to the altered brain morphology. To examine the vasculature in an area with unaffected brain

morphology, I also quantified vessel branchpoints at the cervical spinal cord, adjacent to the border of the hindbrain (Fig. 4.10G,H,J). Again, no significant decrease in branching was found between mutants and wildtypes (Fig. 4.10J; controls 58 branchpoints ± 3.2 versus mutants 49 ± 5.5). These results suggested that HSPGs produced by neural cells are not required for sprouting angiogenesis in the hindbrain. The possibility remains that HSPGs produced by pericytes could be rescuing the blood vessel branching phenotype when endothelial or neural HSPGs are lost.

4.2.1.8 Mice lacking HSPGs in endothelial cells and neural progenitors exhibit embryonic lethality

Neighbouring cells might rescue the defects in VEGF164-driven vessel sprouting due to deficiencies in HSPG production in endothelial or neural cells (Jakobsson et al., 2006). To address this, I crossed a conditional heterozygous *Ext* "floxed" *Tie2Cre* positive mouse to a conditional heterozygous *Ext* "floxed" *Nes8Cre* positive mouse. The Mendelian probability of obtaining a *Tie2Cre* and *Nes8Cre* positive conditional null *Ext* "floxed" embryo was 1/16. The first E12.5 litter contained 15 live embryos and 4 dead resorbed embryos, and no live compound mutants. In two E11.5 litters containing 6 and 8 live embryos, there were 4 and 2 resorptions and no live compound mutants. Wildtype litters occasionally contain one resorption, therefore this was above the normal rate of embryonic lethality. This suggests that abolishing HSPG production in both endothelial and neural cells does not produce enough HSPGs to support development. However, CRE recombinase under the *Nes8* promoter is only expressed from E8.5 onwards (Petersen et al., 2002), and neural defects do not normally cause embryonic lethality. Further examination into embryos at earlier stages of development is required to help elucidate the cause of lethality, and ectopic CRE activity should be addressed.

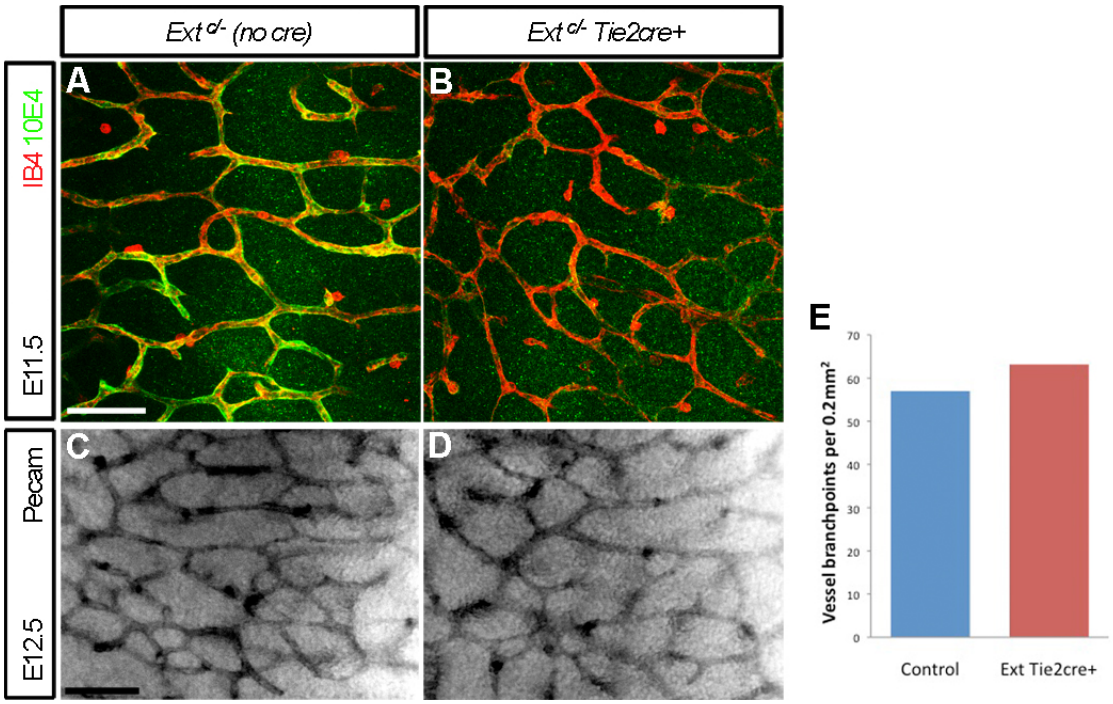

Figure 4.9: Vessel branching is not affected in the absence of HSPGs in the endothelium.

Immunolabelling E11.5 hindbrains with 10E4 and IB4 allowed visualisation of the vasculature and localisation of HSPGs. In wildtype hindbrains (A), HSPGs are present on the endothelium and in the neural progenitor cell layer. HSPGs were not present on the endothelium of *Ext;Tie2Cre* mutant hindbrains, but were still present in the neural progenitor cell layer (B). Immunolabelling E12.5 hindbrains with PECAM allowed quantification of vessel branchpoints in wildtype (C) and *Ext;Tie2Cre* mutants (D). No difference in number of branchpoints was observed in mutants (n=3) compared to wildtype (E; n=4). Scale bars: A,B – 100μm; C,D – 100μm.

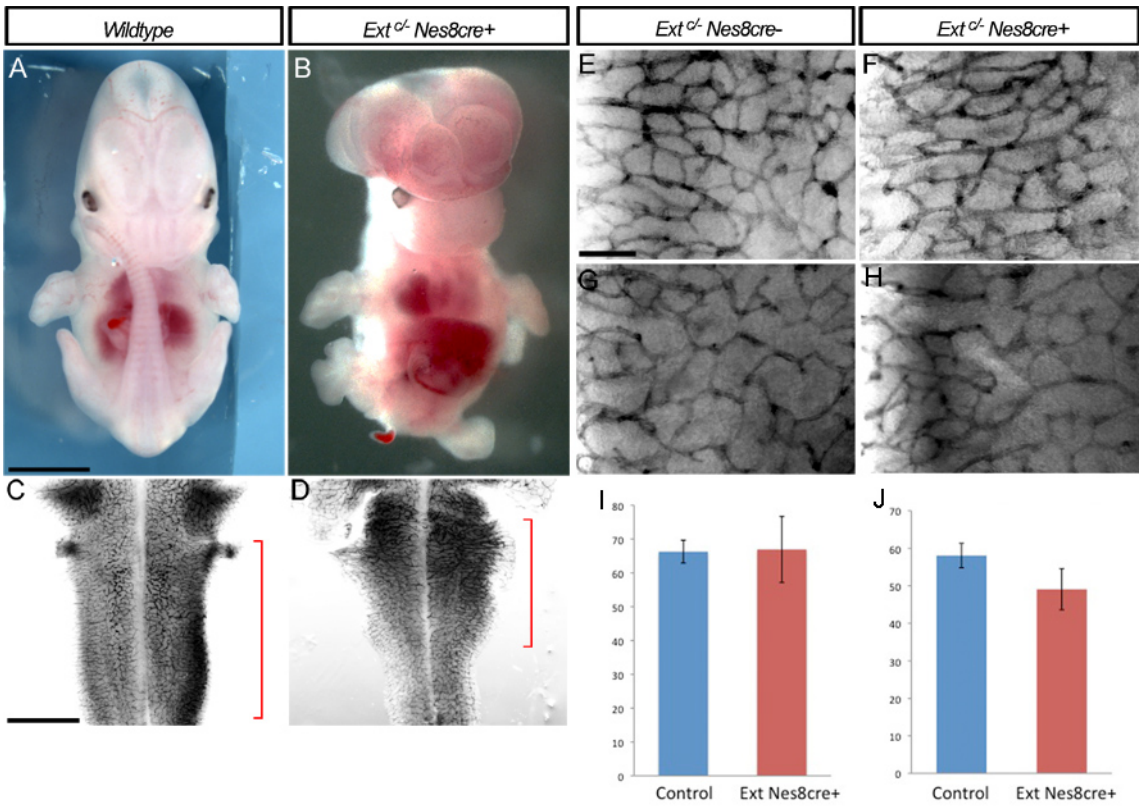

Figure 4.10: Embryos lacking neural-specific HSPGs have severe morphological defects but normal vascular branching.

E12.5 embryos lacking neural progenitor-derived EXT exhibit many morphological defects, including malformed brains that protrude from the head, syndactyly and small tails, compared to wildtype (A,B). Dissected hindbrains (C-F) and cervical spinal cords (G,H) were immunolabelled with PECAM to visualise the vasculature. Hindbrains in *Ext;Nes8Cre* mutants were truncated (red brackets in C compared with D) with no clear midbrain/hindbrain boundary, resulting in altered vessel morphology. Quantification of vessel branching in control and *Ext;Nes8Cre* mutant hindbrains (E,F) and spinal cords (G,H) revealed no significant difference (n=3 each). Scale bars: A,B – 1mm; C,D – 500μm; E,H – 100μm.

4.2.2 HSPGs in VEGF164-driven facial branchiomotor neuron migration

4.2.2.1 Cytoplasmic domain of NRP1 is not essential for VEGF164-driven FBM neuronal migration

In most SEMA-activated NRP1 signalling pathways, a co-receptor is required for signal transduction (Feiner et al., 1997; Schwarz et al., 2008b; Takahashi et al., 1999). In analogy, a co-receptor is thought to be used for VEGF164/NRP1 signalling. However, unpublished observations suggest that VEGF164/NRP1-mediated migration of FBM somata in the hindbrain does not essentially require plexins or either of the VEGF tyrosine kinase receptors (Q. Schwarz & C. Ruhrberg, unpublished data). Quenten Schwarz therefore generated a mouse that retains the transmembrane and ligand-binding domains of NRP1, whilst the cytoplasmic domain is abolished (hereafter referred to as Nrp^{cyto} mutant), to investigate if the intracellular domain of NRP1 itself could transduce signals.

In situ hybridisation with an *Isl1* probe of E12.5 hindbrains to visualise FBM neuronal cell bodies (Fig. 4.11) revealed that there is no migration defect in mice lacking the cytoplasmic domain of NRP1; somata followed the correct migratory path and formed rounded facial motor nuclei on the pial side (Fig. 4.11C,D), as in wildtype (Fig. 4.11A,B). There was a mild migration defect in embryos lacking NRP2 with a few somata segregating from the stream, but facial nuclei still formed properly (Fig. 4.11E,F). My earlier results suggest compensation between the two neuropilin receptors in NCC migration (Figs. 3.11 and 3.12), so to address whether this might account for the lack of phenotype, I analysed FBM migration in hindbrains from embryos lacking both NRP2 and the cytoplasmic domain of NRP1. Compound Nrp^{cyto}/*Nrp2*-null mutants had a mild FBM migration defect, as in embryos lacking NRP2 (Fig. 4.11E,F), but rounded facial motor nuclei formed in the correct location (Fig. 4.11G,H). These results allowed me to conclude that the cytoplasmic domain of NRP1 does not conduct signal transduction in the migration of FBM neuronal cell bodies.

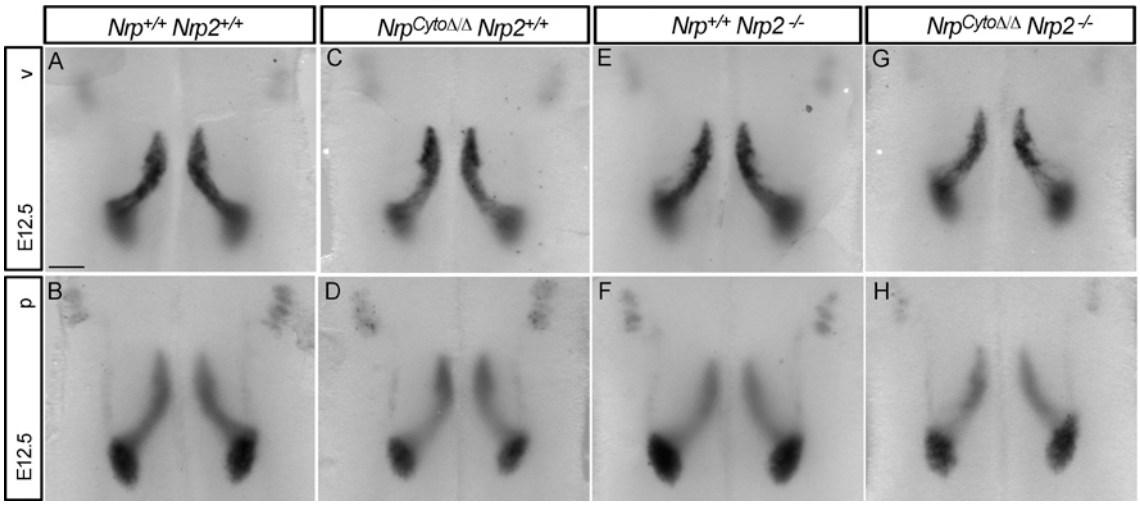

Figure 4.11: The cytoplasmic domain of NRP1 is not required for FBM somata migration.

In situ hybridisation with *Isl1* probe to visualise migrating FBM neuronal cell bodies in hindbrains from E12.5 wildtype, *Nrp2*-null, Nrp^{Cyto}-null or compound Nrp^{Cyto}/*Nrp2*-null embryos. FBM somata migrated in two streams on either side of the midline at r4 on ventricular side (A) to form facial nuclei at r6 on pial side (B) of hindbrains in wildtype embryos (A,B; n=7). No defects in FBM somata migration were observed in Nrp^{Cyto} mutants (C,D; n=2). *Nrp2*-null mutants (E,F; n=5) had variable migration defects with a few somata segregated from the migratory stream. The compound Nrp^{Cyto}*/Nrp2*-null mutant (G,H; n=1) phenocopied the *Nrp2*-null mutants. Hindbrains viewed from the ventricular side (v) and the pial side (p). Scale bar: 200μm.

4.2.2.2 6-O-sulphated HSPGs are involved in VEGF164-driven FBM neuronal migration

HSPGs have been proposed to act as co-receptors for VEGF164 to facilitate binding to its tyrosine kinase receptors and NRP1 in vascular development (for example (Gitay-Goren et al., 1992)), but not for signal transduction. I therefore asked if HSPGs could act as co-receptors for VEGF164/NRP1 signalling in FBM soma migration in the hindbrain. Initially, I assessed whether 6-*O*-sulphated HSPGs are required for this migration, since they have been implicated in VEGF164 signalling in the vasculature of zebrafish (Chen et al., 2005). Quenten Schwarz previously showed that there was no migration defect in mice lacking HS6ST1 (Q. Schwarz & C. Ruhrberg, unpublished data). I analysed mice lacking HS6ST2 using *Isl1 in situ* hybridisation and found that FBM somata in *Hs6st2*-null embryos underwent normal tangential migration, and formed rounded facial motor nuclei on the pial side of the hindbrain (Fig. 4.12C,D), as in wildtype (Fig. 4.12A,B). To assess whether there was compensation between the 6-*O*-sulphotransferases, I next analysed FBM somata migration in mice lacking both HS6ST1 and HS6ST2. In 7/7 compound *Hs6st1/Hs6st2*-null mutants analysed, a developmental delay was observed, consistent with previous findings (Figs. 4.7 and 4.8), and the hindbrains appeared thinner compared to single mutants and controls (not shown). I found defects in FBM somata migration in compound *Hs6st1/Hs6st2*-null mutants, but the phenotype was variable (Fig. 4.13). 2/7 had no defects in FBM soma migration (Fig. 4.13C,D). 4/7 had mild migration defects, with ectopic migratory FBM neurons (Fig. 4.13E) or separation of FBM neurons into distinct streams (Fig. 4.13G), similar to but less severe than *Nrp1* (Schwarz et al., 2004) and $Vegf^{120/120}$ mutants (Fig. 1.9B-E). Both of these types of defects resulted in misshapen facial nuclei on the pial side (Fig. 4.13F,H). 1/7 had severe migration defects; FBM neurons were born in incorrect locations, migrated randomly and crossed at the midline instead of remaining in distinct bilateral populations (Fig. 4.13I). This resulted in severely misshapen facial nuclei (Fig. 4.13J). These hindbrains also had severe morphological defects, and rhombomere boundaries were disrupted (Fig. 4.13I,J). Prior to dissection, I noticed that this embryo had head malformations resembling the E12.5 *Ext;Nes8Cre* mutants (not shown). Therefore, it is not clear if the observed FBM migration defects were a direct consequence of altered VEGF164/NRP1 signalling, or an indirect consequence of abnormal brain architecture.

4.2.2.3 2-O-sulphated HSPGs are required for VEGF164-driven FBM neuronal migration

Because *Hs2st* is expressed in r4 of the E10.5 hindbrain, at the site of origin of FBM neurons (J. Vieira & C. Ruhrberg), I next assessed whether 2-*O*-sulphated HSPGs are required by migrating FBM neurons. *Isl1 in situ* hybridisation revealed a prominent migration defect in *Hs2st*-null embryos at E12.5 (Fig. 4.14C,D). Migrating FBM somata separated into two distinct streams (Fig. 4.14C), resulting in misshapen facial motor nuclei

forming at r6 (Fig. 4.14D) instead of rounded nuclei as in wildtype (Fig. 4.14B). The distance between the trigeminal nuclei and the facial nuclei was significantly shorter in these mutants (brackets in Fig. 4.14B,D; wildtype 633μm ± 4.7 versus mutant 485μm ± 10.1, P = 0.007), as reported for mice lacking VEGF164 (Schwarz et al., 2004). The phenotype was maintained at E14.5 in *Hs2st*-null embryos, when one of the facial motor nuclei was substantially smaller than in wildtype, and the other more dispersed and misshapen compared to wildtype (Fig. 4.14E,F). Facial nuclei in control hindbrains increase in size from E12.5 to E14.5 (Fig. 4.14B,E). At E14.5, mutants had smaller facial nuclei compared to mutants at E12.5, which have large misshapen facial nuclei (Fig. 4.14D,F), raising the possibility that FBM neuronal cell bodies that are ectopically positioned at E12.5 may be lost by apoptosis rather than form the facial nuclei. The phenotypes in these *Hs2st*-null mice at E12.5 and E14.5 are consistent with those described for mice lacking NRP1 or VEGF164 (Fig. 1.9B-E) (Schwarz et al., 2004). Taken together, these results are indicative of an essential requirement for 2-*O*-sulphated HSPGs in VEGF164-driven FBM neuron migration.

4.2.2.4 Syndecan4 is not required for VEGF164-driven FBM neuron migration

Disrupting 2-*O*-sulphated HSPGs in the mouse results in defective FBM neuronal migration in the hindbrain, but whether a specific HSPG is required remains to be elucidated. I had access to mice lacking syndecan4 from collaborators (Prof Mike Simons, Yale University, USA), and since the microarray indicated that *syndecan4* is expressed in the hindbrain (Fig. 4.2), I tested these mice for FBM migration defects. However, no defects were found in an *Isl1 in situ* hybridisation (Fig. 4.15C,D), indicating that syndecan4 is not required for FBM neuron migration. Other candidate HSPGs that might be required for VEGF164-driven FBM migration need to be identified.

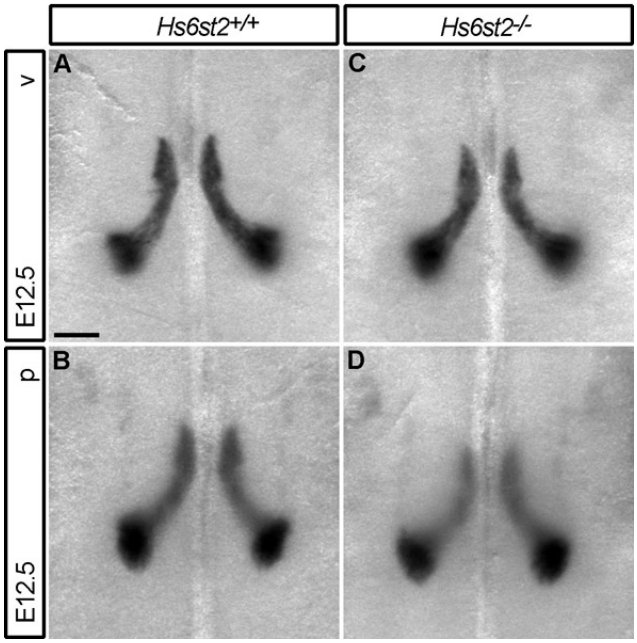

Figure 4.12: FBM somata migrate normally in the absence of HS6ST2.

In situ hybridisation with *Isl1* probe to visualise migrating FBM neuronal cell bodies in hindbrains from E12.5 wildtype (A,B) and *Hs6st2*-null mutant (C,D) embryos. FBM neuronal cell bodies in 4/4 mutant hindbrains migrated in single streams (C) to form correctly shaped facial nuclei (D), as in wildtypes (n=4). v, ventricular side; p, pial side. Scale bar: 200μm.

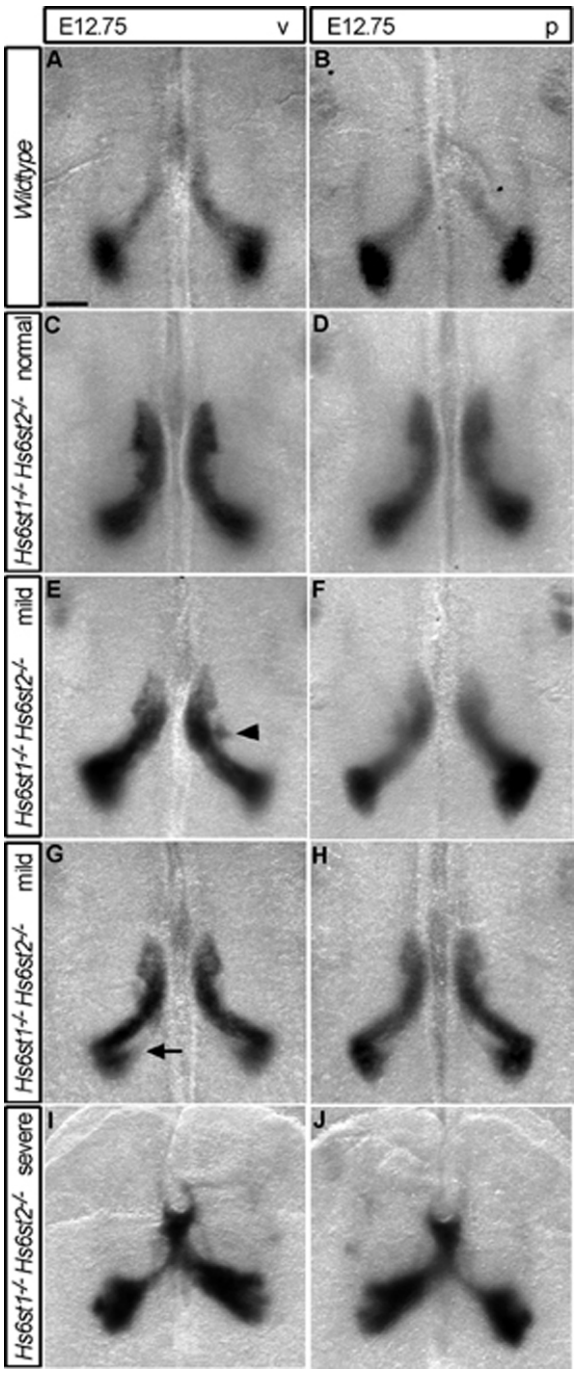

Figure 4.13: FBM somata migration is affected with varying penetrance when both HS6ST1 and HS6ST2 are lost.

In situ hybridisation with *Isl1* probe to visualise migrating FBM neuronal cell bodies in E12.75 hindbrains from wildtype (A,B) and four compound Hs*6st1/Hs6st2*-null mutant (C-J) embryos with varying phenotypes. FBM somata in wildtypes had mostly migrated from r4 on ventricular side (A), and had formed facial nuclei at r6 on pial side (B) of the hindbrain. 2/7 had normal FBM neuron migration (C,D), 4/7 had mild defects in FBM soma migration, such as misplaced clusters of neurons (arrowhead in E) or duplicate streams of cell bodies (arrow in G). Only 1/7 had severe defects in FBM soma migration, including crossing at the midline (I) and misshapen facial nuclei (J). v, ventricular side; p, pial side. Scale bar: 200μm.

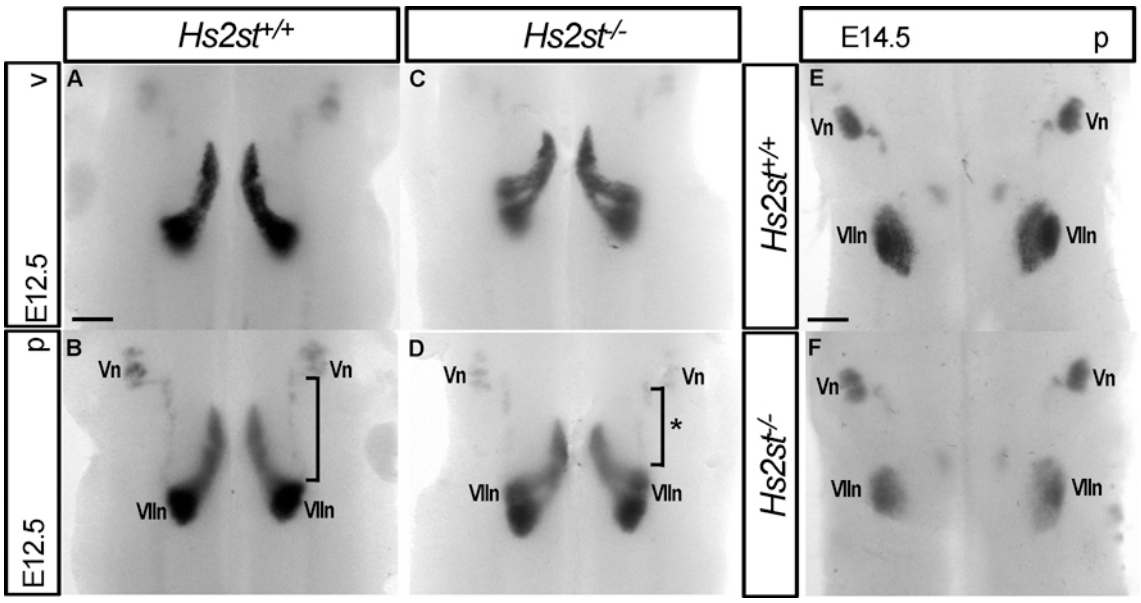

Figure 4.14: Defects in FBM soma migration in the absence of HS2ST.

In situ hybridisation with *Isl1* probe to highlight migratory FBM neuronal cell bodies in E12.5 wildtype (A,B) and *Hs2st*-null (C,D) embryos. FBM cell bodies in 3/3 mutants were misguided (C) and formed multiple facial nuclei (D). Distances between trigeminal nuclei (Vn) and facial nuclei (VIIn) were shorter in 3/3 mutants compared to wildtype (compare brackets in B and D; * $P > 0.05$ in a 2-tailed paired t-test). At E14.5, 3/4 *Hs2st*-null mutants displayed misshapen nuclei compared to wildtype (E,F). v, ventricular side; p, pial side. Scale bar: 200μm.

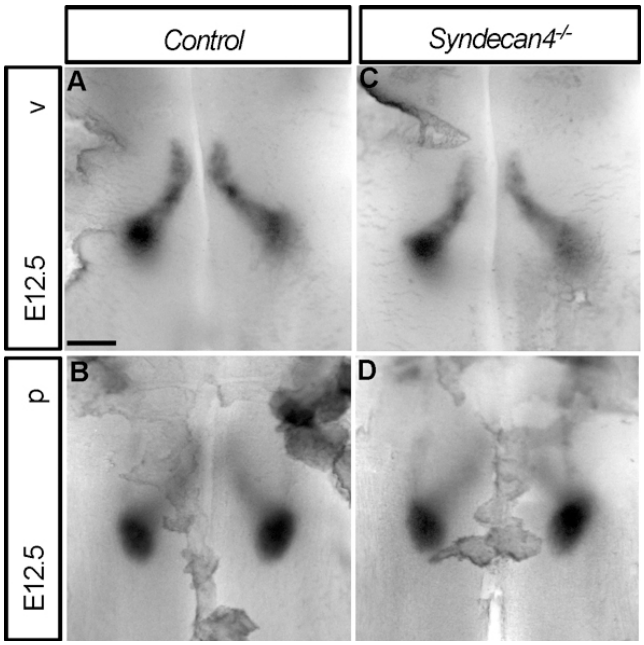

Figure 4.15: Loss of Syndecan4 does not affect FBM neuron migration.

In situ hybridisation with *Isl1* probe to visualise migrating FBM somata in E12.5 wildtype (A,B) and *Syndecan4*-null mutant (C,D). FBM neuronal cell bodies in mutants migrated normally (C) and formed rounded facial nuclei (D; n=2), as in wildtype (B; n=2). v, ventricular side; p, pial side. Scale bar: 200μm.

4.3 Discussion

As I discussed in Chapter 1.2, substantial *in vitro* evidence for HSPGs acting in VEGF164 signalling exists, but there remains a distinct lack of *in vivo* evidence. I have investigated whether specific HS chain patterns are required for VEGF164-driven vascular or neuronal patterning using mice lacking specific HSPG-modifying enzymes.

The microarray analysis showed that *Vegfa* expression was high in the hindbrain (Fig. 4.2), in accordance with its roles in vascular and neuronal patterning (Ruhrberg et al., 2002; Schwarz et al., 2004). Consistent with the possibility that HSPGs are involved in hindbrain development, most HSPG core proteins and their biosynthetic enzymes were expressed in the hindbrain at E11.5 (Fig. 4.2). *Ndst1* and *Hsepi* were expressed at a high level in the hindbrain and have been previously studied. Mice lacking NDST1 have structurally altered HS chains with reductions in *N*-sulphation, epimerisation, 2-*O*-sulphation and 6-*O*-sulphation (Abramsson et al., 2007), however my examination of the published images of pericyte recruitment in these mice revealed no apparent reduction in hindbrain vascular branching. In the same study, mice lacking C5-epimerase had reduced HS epimerisation and 2-*O*-sulphation but increased 6-*O*-sulphation (Abramsson et al., 2007), but again no obvious reduction in vascular branching. *Ndst2* was also expressed at a high level, but *Ndst2*-null mice have no embryonic growth defects or structural HS defects (Forsberg et al., 1999), so are unlikely to have VEGF164 signalling defects. Whether other HSPG modifying enzymes, such as EXT1, EXT2, HS2ST, HS6ST1 or HS6ST2, function in VEGF164 signalling *in vivo* had not been investigated prior to this study.

2-*O*-sulphated HS is essential for VEGF164-driven migration of the FBM neurons (Fig. 4.14), and 6-*O*-sulphated HS is also involved (Fig. 4.13). The fine structure of HS is therefore important for VEGF164 signalling through neuronal NRP1 in FBM neuronal patterning. 2-*O*-sulphation of HS, along with *N*-sulphation, forms the modification backbone upon which 6-*O*- and 3-*O*-sulphation then occurs (Gallagher, 2001) and 2-*O*-sulphated HS chains are a component of all HSPGs. It might be apprehended that 2-*O*-sulphation would be essential in the signalling of HS-binding growth factors, whereas the less common 6-*O*-sulphation would be non-essentially required. However previous observations in embryos lacking HS2ST state that, despite defects in kidney morphogenesis, the CNS and the skeleton, the PNS and cardiovascular system develop normally, and it was therefore suggested that *N*- and 6-*O*-sulphation compensate (Merry and Wilson, 2002). Further investigation is needed to elucidate whether the 2-*O*- and 6-*O*-sulphated HSPGs are required as VEGF164 co-receptors for NRP1 on the FBM neurons or to retain VEGF164 in the environment and present it to its receptors. Disruption of FBM somata migration in mice lacking HSPGs specifically in motor neurons would demonstrate

that HSPGs are required as co-receptors. However, there is currently no genetic mouse model that is sufficient to study this question.

In contrast, HS2ST and HS6ST1 (J. Vieira & C. Ruhrberg, unpublished data) and HS6ST2 (Fig. 4.4) were not essential for VEGF164-driven sprouting angiogenesis in the subventricular vessel plexus. This corroborates with observations in mice lacking NDST1 and C5-epimerase (Abramsson et al., 2007), and suggests that the fine structure of HS is not important in this VEGF164 signalling pathway. Moreover, functional compensation between HS6ST1 and HS6ST2 does not occur to rescue vessel branching (Figs. 4.6 and 4.7) and *Hs6st3* is not upregulated to compensate (Fig. 4.3). The reason for the difference between the requirement for HSPGs in VEGF164 signalling in vascular and neuronal patterning may lie with the receptors. VEGFR1 and VEGFR2 tyrosine kinases act in VEGF164-driven vascular patterning and not in FBM neuronal patterning (Q. Schwarz & C. Ruhrberg, unpublished data). NRP1 is required in both cases: as a co-receptor for VEGFR2 in VEGF164-driven angiogenesis, and as a VEGF164-binding receptor in FBM neuronal migration. Since the cytoplasmic domain of NRP1 is not required (Fig. 4.11), an unknown, but probably HS-binding, co-receptor is required for signal transduction in FBM neuron migration.

As previously described, the Lexicon Pharmaceuticals *Hs6st2* mutant mouse still produced a low level of *Hs6st2* mRNA (Fig. 4.3). This may account for the discrepancies in the analysis of vessel branching between this and the *Hs6st2* mutant mouse from Japan that was used for preliminary studies (J. Vieira & C. Ruhrberg, unpublished data). I found that mice lacking HS6ST1 and HS6ST2 had a developmental delay of 0.25 days, and mice lacking only HS6ST2 were also slightly delayed. The delay would have been difficult to assess in the preliminary experiments since only the heads of the embryos were sent from Japan and staging according to limb development was not possible. The decrease in vessel branching in E12.5 mice lacking HS6ST2 previously (J. Vieira & C. Ruhrberg, unpublished data) and the non-significant decrease I found (Fig. 4.4) could therefore be due to a small developmental delay. At E12.75, vascular remodelling occurs in the hindbrain, which could account for the slightly increased branching in the delayed HS6ST1/HS6ST2 embryos compared to control hindbrains. This would require further investigation in wildtype animals by performing a time-course of subventricular vessel remodelling. On the other hand, the developmental delay and the striking oedema in mice lacking HS6ST1 and HS6ST2 suggest that the Lexicon *Hs6st2* knockout is at least a severe and functional knockdown.

My findings indicate that HS produced in endothelial cells or neural progenitors are not essential for VEGF164-driven sprouting angiogenesis in the brain (Figs. 4.9 and 4.10). The efficiency of the tissue-specific HSPG knockouts was verified, so the lack of phenotype

cannot be explained by inefficient knockdown. However, functional compensation of HSPG production between the two cell types could not be addressed, as the double endothelial/neural CRE knockout was embryonic lethal for reasons that are not yet understood. Alternatively, the lack of vascular defects may be due to pericyte derived HSPGs. Pericytes can produce cell-surface HS that act in *trans* through VEGFR2 to mediate VEGF164-driven angiogenesis (Jakobsson et al., 2006), and HSPGs are required for proper pericyte recruitment and coverage of new vessels (Abramsson et al., 2007). A recent study showed that abolishing HSPG production specifically in pericytes does not lead to a reduction in vessel branching in the CNS, but that pericyte recruitment is affected in the peripheral vasculature of the skin that leads to increased regression of vessels (Stenzel et al., 2009). It is therefore unlikely that pericytes produce HSPGs that are required for VEGF164-driven vessel sprouting *in vivo*, but this could be further investigated by implementation of a double pericyte/endothelial HSPG knockout, for example using *Pdgfrb-Cre* (Foo et al., 2006). Perhaps HSPGs need to be ablated from all cell types in the brain to produce an angiogenesis defect. Alternatively, HSPGs are simply not required for VEGF-A driven developmental angiogenesis.

Vessels in the hindbrains of mice lacking HS-binding VEGF164 are markedly less branched, larger in diameter and have bulbous vessel endings (Ruhrberg et al., 2002). This is caused by loss of the VEGF-A gradient, which is normally created by retention of VEGF isoforms by matrix components. Although VEGF164 binds HS (Houck et al., 1992), it has never been conclusively proven that HSPGs are the molecules that bind VEGF164 and retain it in gradients *in vivo*. None of the HSPG enzyme knockout mice I analysed had phenotypes resembling the vasculature when heparin-binding VEGF-A is lost, which implies that either the loss of HSPGs is compensated for by another matrix component, or that HSPGs are not the matrix component required for the VEGF-A gradients. Embryonic stem cells harvested from mice lacking EXT1 produce no HS but exhibit a stimulated level of chondroitin sulphate production (Lin et al., 2000). This suggests that chondroitin sulphate, another glycosaminoglycan structurally similar to HS, may compensate for the loss of HS. A family of chondroitin sulphate proteoglycans called lecticans are one of the main components of the ECM in the CNS (Yamaguchi, 2000). This raises the possibility that chondroitin sulphate proteoglycans may be expressed by neural progenitors as an alternative to HSPGs in VEGF164 retention *in vivo*. To assess the likelihood of this possibility, expression studies of chondroitin sulphate-modified proteins in the developing brain could be carried out, for example using previously described antibodies (Akatsu et al., 2010). An example of a suitable chondroitin sulphate proteoglycan is NG2, which is found on pericytes and neural progenitor subsets and binds a wide range of proteins,

making it suitable for a role in VEGF164 retention for angiogenesis (for review (Stallcup, 2002).

Early *in vitro* research into VEGF-A binding to its receptors showed that iodinated VEGF165 binds VEGFR2 only in the presence of heparin and that binding is inhibited by unlabelled VEGF165 (Tessler et al., 1994). Subsequent work showed that VEGFR2 binding by iodinated VEGF121 was competed for by unlabelled VEGF165 in the absence of heparin (Gitay-Goren et al., 1996). The authors suggested that iodination and oxidation damage VEGF165 and thereby change its VEGFR2-binding ability, which is restored by heparin (Neufeld et al., 1999). Consistent with this idea, glypican1 binds VEGF165 with high affinity and acts as a chaperone to restore the VEGFR2-binding ability of oxidised VEGF165 (Gengrinovitch et al., 1999). More recently, it was shown that mice lacking glypican1 are born with no defects in appearance, size and lifespan, suggesting no defects in vascular development (Jen et al., 2009). Taken together, these results raise the possibility that HSPGs are required in VEGF165-driven angiogenesis only in situations when VEGF165 has undergone oxidative stress, such as hypoxia, wound repair or inflammation, and not in developmental angiogenesis.

Despite the lack of vascular phenotypes, mice without HS6ST1 and HS6ST2 had severe oedema that might suggest a lymphatic defect (Fig. 4.8), and was also indicative of knockdown of HS6ST1 and HS6ST2 being effective. The oedematous bodies were similar to those of mice lacking VEGF-C, which have apparently normal blood vessel development (Karkkainen et al., 2004). This raises the possibility that HSPG is essential for VEGF-C guided lymphangiogenesis. In support of this idea, VEGF-C binds to NRP1 and NRP2 *in vitro* in an interaction that is enhanced by the presence of heparin (Karpanen et al., 2006). *In vivo*, NRP2 and VEGFR3 interact to mediate the VEGF-C signalling required for the initial steps in lymphatic vascular development (Xu et al., 2010). In zebrafish, lymphangioblasts derive from caudal vein endothelial cells and bud off to form lymphatic vessels (Hogan et al., 2009). The disorganisation in the caudal vein of the zebrafish injected with *Hs6st2* morpholino (Chen et al., 2005) might also be due to lymphangioblasts not budding off to form lymphatic vessels and causing oedema as opposed to blood vasculature defects, as suggested. Alternatively, the oedema could be secondary to vascular stability defects, as previously observed when HSPG production was abolished in pericytes (Stenzel et al., 2009). To address whether pericytes are affected in mice lacking HS6ST1 and HS6ST2, pericyte coverage in the hindbrain vasculature at E12.5 could be assessed using immunolabelling with a pericyte marker and IB4. Investigation into whether lymphatic structure is affected in the mice lacking HS6ST1 and HS6ST2 is also required, which could be attempted by immunolabelling for lymphatic markers such as PROX-1 or LYV-1.

Genes expressed at high levels in the microarray may be suitable candidates for the HSPG involved in neural patterning in the hindbrain. I have shown that syndecan4 is not involved in VEGF164-driven FBM neuronal migration (Fig. 4.15), but there are many other candidates (Fig. 4.2). Of these, glypican-2 is known for its expression on the developing axons and growth cones (Ivins et al., 1997), which explains its high expression in the hindbrain but provides no specific evidence for NRP1 or VEGF164 interaction. Agrin, also expressed at high levels in the developing hindbrain, is required for synaptogenesis in the CNS (Hilgenberg et al., 2002; Smith and Hilgenberg, 2002). Recently, perlecan was found to bind NRP1 (Muthusamy et al., 2010) and had been implicated in VEGF-A guided endothelial cell migration and proliferation (Zoeller et al., 2009). Perlecan may therefore be an ideal candidate for the HSPG essential for VEGF164/NRP1 guided FBM neuron migration, and examination of mice lacking perlecan would clarify this.

5. Final Conclusions and Future Work

5.1 Neuropilins in the developing sympathetic nervous system

In the work described in Chapter 3, I investigated how NRP1 and NRP2 and their SEMA ligands control the early steps in the development of the sympathetic nervous system from sympathetic NCCs in the mouse. I found that the previously described disruption of the sympathetic nervous system when NRP1 signalling is lost is in fact due to defective sympathetic NCC migration and aggregation at the dorsal aorta. My findings are consistent with early *in vitro* work (Eickholt et al., 1999), but contrast with the study that described the sympathetic nervous system phenotype in *Nrp1*-null mice (Kawasaki et al., 2002). The abnormal migration of NCCs results in ectopically placed sympathetic precursors, the fate of which is unaffected since they are able to differentiate into sympathetic neurons, presumably supported by expression of survival factors in their abnormal location. I further showed that the defects in *Nrp1*-deficient mice are independent of vascular abnormalities and are NC cell autonomous.

Consistent with previous work showing that SEMA3F/NRP2 repels sympathetic axons *in vitro* (Giger et al., 2000), my findings indicate that NRP2 signalling guides sympathetic axons *in vivo*. I also show a novel 'back-up' role for NRP2/SEMA3F signalling in sympathetic NCC migration when NRP1 signalling is lost. Future work on expression of NRP1 and NRP2 in ectopic NCCs would answer questions on the mechanism behind this suggestion. For example, is NRP2 switched on in a subset of NCCs in the absence of NRP1? Or is NRP2 is expressed at a low level in a subset of NCCs which are unaffected when NRP1 is lost? It would also be interesting to carry out sympathetic NCC migration studies in the SEMA ligand knockout mice, since there is a possibility that SEMA3A may signal through NRP2 in the absence of NRP1. If this were the case, then removal of SEMA3A would result in a more severe sympathetic NCC migration phenotype than removal of NRP1.

I investigated the pattern of sympathetic innervation in postnatal mice lacking NRP1 in the NC lineage. I found that, consistent with previous findings in mice lacking SEMA3A (Ieda et al., 2007), the distribution of sympathetic fibres in the cardiac wall of mutants is altered. I would like to continue with ECG tracing in live mice lacking NRP1 in the NC lineage, and determine whether they are able to respond properly to situations such as exercise or other stress stimuli. Further, without NRP1 in the NC lineage, the sympathetic innervation of the postnatal dorsal aorta was disrupted. To determine whether blood pressure is affected, studies could be carried out in these mutant mice in the future. I would also like to investigate whether SEMA3A/NRP1 signalling is a specific controller of innervation of vascular sympathetic targets by examining innervation of the carotid arteries versus innervation of the trachea and salivary glands in mice lacking NRP1 in the NC lineage.

Finally, I confirmed that SEMA3G is expressed in major arteries during development as previously described (Kutschera et al., 2011; Taniguchi et al., 2005). Despite this, I found no evidence that SEMA3G is involved in sympathetic development or in postnatal sympathetic axon guidance in the heart or dorsal aorta. The lack of sympathetic axon guidance function could be confirmed by also looking at the carotid arteries, trachea and salivary glands in mice lacking SEMA3G. However, based on my findings and that SEMA3G has been shown to act on smooth muscle cells (Kutschera et al., 2011), I speculate that its *in vivo* function may be vascular.

5.2 HSPGs in VEGF164-driven vascular and neuronal patterning

The aim of the work described in Chapter 4 was to decipher the role that HSPGs play in VEGF164-driven vascular and neuronal patterning in the developing hindbrain. I found no evidence that endothelial or neuronal HSPGs, or 2-*O*- or 6-*O*-sulphated HSPGs, are essential for VEGF164-driven vessel branching in the mouse hindbrain. This suggests that HSPGs are not required for the presentation of VEGF164 to its receptors on endothelial cells to mediate sprouting angiogenesis. However, since HSPGs produced by pericytes can act on endothelial VEGFR2 in *trans* to stimulate angiogenesis (Jakobsson et al., 2006), I would propose an investigation into vascular branching defects in embryos deficient in endothelial and pericyte HSPGs before I conclude that they are not absolutely essential. Since HSPG-modifying enzymes have been suggested to compensate for each other, it would also be an idea to attempt a triple *Hs6st1/Hs6st2/Hs2st* knockout to assess whether vascular branching is affected in the absence of all 2-*O*- and most 6-*O*-sulphation.

My results also suggest that HSPGs are not the matrix molecules essential for the formation of VEGF-A gradients in the ECM that are required for vessel branching, since none of the mouse mutants phenocopied mice lacking heparin-binding VEGF-A (Ruhrberg et al., 2002). Chondroitin sulphates are structurally similar and expressed in the ECM (Yamaguchi, 2000), and therefore may be the alternative VEGF-A binding matrix molecule responsible for retaining it in the ECM. In the microarray, neurocan and versican, two of the lectican family of chondroitin sulphates, were expressed at high levels in the hindbrains, suggesting that they might be candidates. Future investigations into mice lacking the enzymes essential for chondroitin sulphate modifications would add support to this suggestion.

In stark contrast, I found that HSPGs are essential for VEGF164/NRP1 guided migration of FBM neuronal cell bodies, and the pattern of HS sulphation is important. Previous unpublished investigations have shown that VEGFR1 and VEGFR2 are not involved in this process, and I here show that NRP1 itself does not signal intracellularly in this system.

Perhaps the difference in HSPGs requirement between the two systems is due to an unfound NRP1 co-receptor that needs HSPGs. It would be interesting to identify the exact HSPG involved in the process, a possible candidate being perlecan due to its ability to bind NRP1 (Muthusamy et al., 2010). Alternatively, the HSPGs themselves might act as the signal transducing co-receptor, in analogy to the function of plexin/NRP co-receptors.

A particularly interesting finding from these investigations was the potential lymphatic defect in mice lacking 6-*O*-sulphated HS. This requires extensive experimentation before any conclusions to its relevance can be drawn. For example, examination of the structure of the lymphatic vessels in these mutants in comparison to mice lacking VEGF-C, the lymphangiogenesis factor (Karkkainen et al., 2004), might suggest that VEGF-C signalling is HSPG-dependent.

REFERENCES

Abramsson, A., Kurup, S., Busse, M., Yamada, S., Lindblom, P., Schallmeiner, E., Stenzel, D., Sauvaget, D., Ledin, J., Ringvall, M. et al. (2007). Defective N-sulfation of heparan sulfate proteoglycans limits PDGF-BB binding and pericyte recruitment in vascular development. *Genes Dev* **21**, 316-31.

Aikawa, J., Grobe, K., Tsujimoto, M. and Esko, J. D. (2001). Multiple isozymes of heparan sulfate/heparin GlcNAc N-deacetylase/GlcN N-sulfotransferase. Structure and activity of the fourth member, NDST4. *J Biol Chem* **276**, 5876-82.

Akatsu, C., Fongmoon, D., Mizumoto, S., Jacquinet, J. C., Kongtawelert, P., Yamada, S. and Sugahara, K. (2010). Development of a mouse monoclonal antibody against the chondroitin sulfate-protein linkage region derived from shark cartilage. *Glycoconj J* **27**, 387-99.

Albers, K. M., Perrone, T. N., Goodness, T. P., Jones, M. E., Green, M. A. and Davis, B. M. (1996). Cutaneous overexpression of NT-3 increases sensory and sympathetic neuron number and enhances touch dome and hair follicle innervation. *J Cell Biol* **134**, 487-97.

Alfandari, D., Cousin, H. and Marsden, M. (2010). Mechanism of Xenopus cranial neural crest cell migration. *Cell Adh Migr* **4**, 553-60.

Anderson, D. J., Carnahan, J. F., Michelsohn, A. and Patterson, P. H. (1991). Antibody markers identify a common progenitor to sympathetic neurons and chromaffin cells in vivo and reveal the timing of commitment to neuronal differentiation in the sympathoadrenal lineage. *J Neurosci* **11**, 3507-19.

Andres, R., Forgie, A., Wyatt, S., Chen, Q., de Sauvage, F. J. and Davies, A. M. (2001). Multiple effects of artemin on sympathetic neurone generation, survival and growth. *Development* **128**, 3685-95.

Ashikari-Hada, S., Habuchi, H., Kariya, Y. and Kimata, K. (2005). Heparin regulates vascular endothelial growth factor165-dependent mitogenic activity, tube formation, and its receptor phosphorylation of human endothelial cells. Comparison of the effects of heparin and modified heparins. *J Biol Chem* **280**, 31508-15.

Asmus, S. E., Parsons, S. and Landis, S. C. (2000). Developmental changes in the transmitter properties of sympathetic neurons that innervate the periosteum. *J Neurosci* **20**, 1495-504.

Atha, D. H., Lormeau, J. C., Petitou, M., Rosenberg, R. D. and Choay, J. (1985). Contribution of monosaccharide residues in heparin binding to antithrombin III. *Biochemistry* **24**, 6723-9.

Auclair, F., Valdes, N. and Marchand, R. (1996). Rhombomere-specific origin of branchial and visceral motoneurons of the facial nerve in the rat embryo. *J Comp Neurol* **369**, 451-61.

Belmadani, A., Tran, P. B., Ren, D., Assimacopoulos, S., Grove, E. A. and Miller, R. J. (2005). The chemokine stromal cell-derived factor-1 regulates the migration of sensory neuron progenitors. *J Neurosci* **25**, 3995-4003.

Britsch, S., Li, L., Kirchhoff, S., Theuring, F., Brinkmann, V., Birchmeier, C. and Riethmacher, D. (1998). The ErbB2 and ErbB3 receptors and their ligand, neuregulin-1, are essential for development of the sympathetic nervous system. *Genes Dev* **12**, 1825-36.

Bronner-Fraser, M. (1986). Analysis of the early stages of trunk neural crest migration in avian embryos using monoclonal antibody HNK-1. *Dev Biol* **115**, 44-55.

Bullock, S. L., Fletcher, J. M., Beddington, R. S. and Wilson, V. A. (1998). Renal agenesis in mice homozygous for a gene trap mutation in the gene encoding heparan sulfate 2-sulfotransferase. *Genes Dev* **12**, 1894-906.

Cai, H. and Reed, R. R. (1999). Cloning and characterization of neuropilin-1-interacting protein: a PSD-95/Dlg/ZO-1 domain-containing protein that interacts with the cytoplasmic domain of neuropilin-1. *J Neurosci* **19**, 6519-27.

Cao, J. M., Chen, L. S., KenKnight, B. H., Ohara, T., Lee, M. H., Tsai, J., Lai, W. W., Karagueuzian, H. S., Wolf, P. L., Fishbein, M. C. et al. (2000a). Nerve sprouting and sudden cardiac death. *Circ Res* **86**, 816-21.

Cao, J. M., Fishbein, M. C., Han, J. B., Lai, W. W., Lai, A. C., Wu, T. J., Czer, L., Wolf, P. L., Denton, T. A., Shintaku, I. P. et al. (2000b). Relationship between regional cardiac hyperinnervation and ventricular arrhythmia. *Circulation* **101**, 1960-9.

Cariboni, A., Davidson, K., Rakic, S., Maggi, R., Parnavelas, J. G. and Ruhrberg, C. (2011). Defective gonadotropin-releasing hormone neuron migration in mice lacking SEMA3A signalling through NRP1 and NRP2: implications for the aetiology of hypogonadotropic hypogonadism. *Hum Mol Genet* **20**, 336-44.

Carmeliet, P., Ferreira, V., Breier, G., Pollefeyt, S., Kieckens, L., Gertsenstein, M., Fahrig, M., Vandenhoeck, A., Harpal, K., Eberhardt, C. et al. (1996). Abnormal blood vessel development and lethality in embryos lacking a single VEGF allele. *Nature* **380**, 435-9.

Carney, T. J., Dutton, K. A., Greenhill, E., Delfino-Machin, M., Dufourcq, P., Blader, P. and Kelsh, R. N. (2006). A direct role for Sox10 in specification of neural crest-derived sensory neurons. *Development* **133**, 4619-30.

Chai, Y., Jiang, X., Ito, Y., Bringas, P., Jr., Han, J., Rowitch, D. H., Soriano, P., McMahon, A. P. and Sucov, H. M. (2000). Fate of the mammalian cranial neural crest during tooth and mandibular morphogenesis. *Development* **127**, 1671-9.

Chalasani, S. H., Sabelko, K. A., Sunshine, M. J., Littman, D. R. and Raper, J. A. (2003). A chemokine, SDF-1, reduces the effectiveness of multiple axonal repellents and is required for normal axon pathfinding. *J Neurosci* **23**, 1360-71.

Chen, E., Stringer, S. E., Rusch, M. A., Selleck, S. B. and Ekker, S. C. (2005). A unique role for 6-O sulfation modification in zebrafish vascular development. *Dev Biol* **284**, 364-76.

Chen, H., Chedotal, A., He, Z., Goodman, C. S. and Tessier-Lavigne, M. (1997). Neuropilin-2, a novel member of the neuropilin family, is a high affinity receptor for the semaphorins Sema E and Sema IV but not Sema III. *Neuron* **19**, 547-59.

Cheng, Y., Cheung, M., Abu-Elmagd, M. M., Orme, A. and Scotting, P. J. (2000). Chick sox10, a transcription factor expressed in both early neural crest cells and central nervous system. *Brain Res Dev Brain Res* **121**, 233-41.

Cheung, M. and Briscoe, J. (2003). Neural crest development is regulated by the transcription factor Sox9. *Development* **130**, 5681-93.

Cheung, M., Chaboissier, M. C., Mynett, A., Hirst, E., Schedl, A. and Briscoe, J. (2005). The transcriptional control of trunk neural crest induction, survival, and delamination. *Dev Cell* **8**, 179-92.

Chow, L. T., Chow, S. S., Anderson, R. H. and Gosling, J. A. (1993). Innervation of the human cardiac conduction system at birth. *Br Heart J* **69**, 430-5.

Cochard, P., Goldstein, M. and Black, I. B. (1978). Ontogenetic appearance and disappearance of tyrosine hydroxylase and catecholamines in the rat embryo. *Proc Natl Acad Sci U S A* **75**, 2986-90.

Colley, K. J. (1997). Golgi localization of glycosyltransferases: more questions than answers. *Glycobiology* **7**, 1-13.

Cornell, R. A. and Eisen, J. S. (2005). Notch in the pathway: the roles of Notch signaling in neural crest development. *Semin Cell Dev Biol* **16**, 663-72.

Crick, S. J., Wharton, J., Sheppard, M. N., Royston, D., Yacoub, M. H., Anderson, R. H. and Polak, J. M. (1994). Innervation of the human cardiac conduction system. A quantitative immunohistochemical and histochemical study. *Circulation* **89**, 1697-708.

David, G., Bai, X. M., Van der Schueren, B., Cassiman, J. J. and Van den Berghe, H. (1992). Developmental changes in heparan sulfate expression: in situ detection with mAbs. *J Cell Biol* **119**, 961-75.

De Bellard, M. E., Rao, Y. and Bronner-Fraser, M. (2003). Dual function of Slit2 in repulsion and enhanced migration of trunk, but not vagal, neural crest cells. *J Cell Biol* **162**, 269-79.

De Calisto, J., Araya, C., Marchant, L., Riaz, C. F. and Mayor, R. (2005). Essential role of non-canonical Wnt signalling in neural crest migration. *Development* **132**, 2587-97.

de Lange, W. J., Halabi, C. M., Beyer, A. M. and Sigmund, C. D. (2008). Germ line activation of the Tie2 and SMMHC promoters causes noncell-specific deletion of floxed alleles. *Physiol Genomics* **35**, 1-4.

de Vries, C., Escobedo, J. A., Ueno, H., Houck, K., Ferrara, N. and Williams, L. T. (1992). The fms-like tyrosine kinase, a receptor for vascular endothelial growth factor. *Science* **255**, 989-91.

De Vries, L., Lou, X., Zhao, G., Zheng, B. and Farquhar, M. G. (1998). GIPC, a PDZ domain containing protein, interacts specifically with the C terminus of RGS-GAIP. *Proc Natl Acad Sci U S A* **95**, 12340-5.

Debby-Brafman, A., Burstyn-Cohen, T., Klar, A. and Kalcheim, C. (1999). F-Spondin, expressed in somite regions avoided by neural crest cells, mediates inhibition of distinct somite domains to neural crest migration. *Neuron* **22**, 475-88.

Dottori, M., Gross, M. K., Labosky, P. and Goulding, M. (2001). The winged-helix transcription factor Foxd3 suppresses interneuron differentiation and promotes neural crest cell fate. *Development* **128**, 4127-38.

Duband, J.-L. (2006). Neural crest delamination and migration: integrating regulations of cell interactions, locomotion, survival and fate. In *Neural Crest Induction and Differentiation*, vol. 589 (ed. J.-P. Saint-Jeannet), pp. 45-77. New York, U.S.A.: Springer Science & Landes Bioscience.

Eickholt, B. J., Mackenzie, S. L., Graham, A., Walsh, F. S. and Doherty, P. (1999). Evidence for collapsin-1 functioning in the control of neural crest migration in both trunk and hindbrain regions. *Development* **126**, 2181-9.

Enomoto, H., Crawford, P. A., Gorodinsky, A., Heuckeroth, R. O., Johnson, E. M., Jr. and Milbrandt, J. (2001). RET signaling is essential for migration, axonal growth and axon guidance of developing sympathetic neurons. *Development* **128**, 3963-74.

Erickson, C. A., Duong, T. D. and Tosney, K. W. (1992). Descriptive and experimental analysis of the dispersion of neural crest cells along the dorsolateral path and their entry into ectoderm in the chick embryo. *Dev Biol* **151**, 251-72.

Ernsberger, U., Patzke, H., Tissier-Seta, J. P., Reh, T., Goridis, C. and Rohrer, H. (1995). The expression of tyrosine hydroxylase and the transcription factors cPhox-2 and Cash-1: evidence for distinct inductive steps in the differentiation of chick sympathetic precursor cells. *Mech Dev* **52**, 125-36.

Esko, J. D. and Selleck, S. B. (2002). Order out of chaos: assembly of ligand binding sites in heparan sulfate. *Annu Rev Biochem* **71**, 435-71.

Fantin, A., Maden, C. H. and Ruhrberg, C. (2009). Neuropilin ligands in vascular and neuronal patterning. *Biochem Soc Trans* **37**, 1228-32.

Feiner, L., Koppel, A. M., Kobayashi, H. and Raper, J. A. (1997). Secreted chick semaphorins bind recombinant neuropilin with similar affinities but bind different subsets of neurons in situ. *Neuron* **19**, 539-45.

Ferrara, N. (2000). VEGF: an update on biological and therapeutic aspects. *Curr Opin Biotechnol* **11**, 617-24.

Flamme, I., Frolich, T. and Risau, W. (1997). Molecular mechanisms of vasculogenesis and embryonic angiogenesis. *J Cell Physiol* **173**, 206-10.

Foo, S. S., Turner, C. J., Adams, S., Compagni, A., Aubyn, D., Kogata, N., Lindblom, P., Shani, M., Zicha, D. and Adams, R. H. (2006). Ephrin-B2 controls cell motility and adhesion during blood-vessel-wall assembly. *Cell* **124**, 161-73.

Forsberg, E., Pejler, G., Ringvall, M., Lunderius, C., Tomasini-Johansson, B., Kusche-Gullberg, M., Eriksson, I., Ledin, J., Hellman, L. and Kjellen, L. (1999). Abnormal mast cells in mice deficient in a heparin-synthesizing enzyme. *Nature* **400**, 773-6.

Francis, S. E., Goh, K. L., Hodivala-Dilke, K., Bader, B. L., Stark, M., Davidson, D. and Hynes, R. O. (2002). Central roles of alpha5beta1 integrin and fibronectin in vascular development in mouse embryos and embryoid bodies. *Arterioscler Thromb Vasc Biol* **22**, 927-33.

Fujisawa, H., Takagi, S. and Hirata, T. (1995). Growth-associated expression of a membrane protein, neuropilin, in Xenopus optic nerve fibers. *Dev Neurosci* **17**, 343-9.

Gallagher, J. T. (2001). Heparan sulfate: growth control with a restricted sequence menu. *J Clin Invest* **108**, 357-61.

Gammill, L. S. and Bronner-Fraser, M. (2003). Neural crest specification: migrating into genomics. *Nat Rev Neurosci* **4**, 795-805.

Gammill, L. S., Gonzalez, C., Gu, C. and Bronner-Fraser, M. (2006). Guidance of trunk neural crest migration requires neuropilin 2/semaphorin 3F signaling. *Development* **133**, 99-106.

Gao, Y., Li, M., Chen, W. and Simons, M. (2000). Synectin, syndecan-4 cytoplasmic domain binding PDZ protein, inhibits cell migration. *J Cell Physiol* **184**, 373-9.

Garcia-Garcia, M. J. and Anderson, K. V. (2003). Essential role of glycosaminoglycans in Fgf signaling during mouse gastrulation. *Cell* **114**, 727-37.

Gengrinovitch, S., Berman, B., David, G., Witte, L., Neufeld, G. and Ron, D. (1999). Glypican-1 is a VEGF165 binding proteoglycan that acts as an extracellular chaperone for VEGF165. *J Biol Chem* **274**, 10816-22.

Gerhardt, H., Golding, M., Fruttiger, M., Ruhrberg, C., Lundkvist, A., Abramsson, A., Jeltsch, M., Mitchell, C., Alitalo, K., Shima, D. et al. (2003). VEGF guides angiogenic sprouting utilizing endothelial tip cell filopodia. *J Cell Biol* **161**, 1163-77.

Gerhardt, H., Ruhrberg, C., Abramsson, A., Fujisawa, H., Shima, D. and Betsholtz, C. (2004). Neuropilin-1 is required for endothelial tip cell guidance in the developing central nervous system. *Dev Dyn* **231**, 503-9.

Gerova, M., Gero, J., Dolezel, S. and Blazkova-Huzulakova, I. (1973). Sympathetic control of canine abdominal aorta. *Circ Res* **33**, 149-59.

Giger, R. J., Cloutier, J. F., Sahay, A., Prinjha, R. K., Levengood, D. V., Moore, S. E., Pickering, S., Simmons, D., Rastan, S., Walsh, F. S. et al. (2000). Neuropilin-2 is required in vivo for selective axon guidance responses to secreted semaphorins. *Neuron* **25**, 29-41.

Gitay-Goren, H., Cohen, T., Tessler, S., Soker, S., Gengrinovitch, S., Rockwell, P., Klagsbrun, M., Levi, B. Z. and Neufeld, G. (1996). Selective binding of VEGF121 to one of the three vascular endothelial growth factor receptors of vascular endothelial cells. *J Biol Chem* **271**, 5519-23.

Gitay-Goren, H., Soker, S., Vlodavsky, I. and Neufeld, G. (1992). The binding of vascular endothelial growth factor to its receptors is dependent on cell surface-associated heparin-like molecules. *J Biol Chem* **267**, 6093-8.

Glebova, N. O. and Ginty, D. D. (2004). Heterogeneous requirement of NGF for sympathetic target innervation in vivo. *J Neurosci* **24**, 743-51.

Gluzman-Poltorak, Z., Cohen, T., Herzog, Y. and Neufeld, G. (2000). Neuropilin-2 is a receptor for the vascular endothelial growth factor (VEGF) forms VEGF-145 and VEGF-165 [corrected]. *J Biol Chem* **275**, 18040-5.

Goldman, D. C., Bailey, A. S., Pfaffle, D. L., Al Masri, A., Christian, J. L. and Fleming, W. H. (2009a). BMP4 regulates the hematopoietic stem cell niche. *Blood* **114**, 4393-401.

Goldman, D. C., Donley, N. and Christian, J. L. (2009b). Genetic interaction between Bmp2 and Bmp4 reveals shared functions during multiple aspects of mouse organogenesis. *Mech Dev* **126**, 117-27.

Gridley, T. (2006). The long and short of it: somite formation in mice. *Dev Dyn* **235**, 2330-6.

Groysman, M., Shoval, I. and Kalcheim, C. (2008). A negative modulatory role for rho and rho-associated kinase signaling in delamination of neural crest cells. *Neural Dev* **3**, 27.

Gu, C., Limberg, B. J., Whitaker, G. B., Perman, B., Leahy, D. J., Rosenbaum, J. S., Ginty, D. D. and Kolodkin, A. L. (2002). Characterization of neuropilin-1 structural features that confer binding to semaphorin 3A and vascular endothelial growth factor 165. *J Biol Chem* **277**, 18069-76.

Gu, C., Rodriguez, E. R., Reimert, D. V., Shu, T., Fritzsch, B., Richards, L. J., Kolodkin, A. L. and Ginty, D. D. (2003). Neuropilin-1 conveys semaphorin and VEGF signaling during neural and cardiovascular development. *Dev Cell* **5**, 45-57.

Gu, C., Yoshida, Y., Livet, J., Reimert, D. V., Mann, F., Merte, J., Henderson, C. E., Jessell, T. M., Kolodkin, A. L. and Ginty, D. D. (2005). Semaphorin 3E and plexin-D1 control vascular pattern independently of neuropilins. *Science* **307**, 265-8.

Habuchi, H., Miyake, G., Nogami, K., Kuroiwa, A., Matsuda, Y., Kusche-Gullberg, M., Habuchi, O., Tanaka, M. and Kimata, K. (2003). Biosynthesis of heparan sulphate with diverse structures and functions: two alternatively spliced forms of human heparan sulphate 6-O-sulphotransferase-2 having different expression patterns and properties. *Biochem J* **371**, 131-42.

Habuchi, H., Nagai, N., Sugaya, N., Atsumi, F., Stevens, R. L. and Kimata, K. (2007). Mice deficient in heparan sulfate 6-O-sulfotransferase-1 exhibit defective heparan sulfate

biosynthesis, abnormal placentation, and late embryonic lethality. *J Biol Chem* **282**, 15578-88.

Habuchi, H., Tanaka, M., Habuchi, O., Yoshida, K., Suzuki, H., Ban, K. and Kimata, K. (2000). The occurrence of three isoforms of heparan sulfate 6-O-sulfotransferase having different specificities for hexuronic acid adjacent to the targeted N-sulfoglucosamine. *J Biol Chem* **275**, 2859-68.

Hacker, U., Nybakken, K. and Perrimon, N. (2005). Heparan sulphate proteoglycans: the sweet side of development. *Nat Rev Mol Cell Biol* **6**, 530-41.

Hagner-McWhirter, A., Hannesson, H. H., Campbell, P., Westley, J., Roden, L., Lindahl, U. and Li, J. P. (2000). Biosynthesis of heparin/heparan sulfate: kinetic studies of the glucuronyl C5-epimerase with N-sulfated derivatives of the Escherichia coli K5 capsular polysaccharide as substrates. *Glycobiology* **10**, 159-71.

HajMohammadi, S., Enjyoji, K., Princivalle, M., Christi, P., Lech, M., Beeler, D., Rayburn, H., Schwartz, J. J., Barzegar, S., de Agostini, A. I. et al. (2003). Normal levels of anticoagulant heparan sulfate are not essential for normal hemostasis. *J Clin Invest* **111**, 989-99.

Han, C., Yan, D., Belenkaya, T. Y. and Lin, X. (2005). Drosophila glypicans Dally and Dally-like shape the extracellular Wingless morphogen gradient in the wing disc. *Development* **132**, 667-79.

He, Z. and Tessier-Lavigne, M. (1997). Neuropilin is a receptor for the axonal chemorepellent Semaphorin III. *Cell* **90**, 739-51.

Hemavathy, K., Ashraf, S. I. and Ip, Y. T. (2000). Snail/slug family of repressors: slowly going into the fast lane of development and cancer. *Gene* **257**, 1-12.

Herzog, Y., Kalcheim, C., Kahane, N., Reshef, R. and Neufeld, G. (2001). Differential expression of neuropilin-1 and neuropilin-2 in arteries and veins. *Mech Dev* **109**, 115-9.

Hilgenberg, L. G., Ho, K. D., Lee, D., O'Dowd, D. K. and Smith, M. A. (2002). Agrin regulates neuronal responses to excitatory neurotransmitters in vitro and in vivo. *Mol Cell Neurosci* **19**, 97-110.

Hogan, B. M., Bos, F. L., Bussmann, J., Witte, M., Chi, N. C., Duckers, H. J. and Schulte-Merker, S. (2009). Ccbe1 is required for embryonic lymphangiogenesis and venous sprouting. *Nat Genet* **41**, 396-8.

Honma, Y., Araki, T., Gianino, S., Bruce, A., Heuckeroth, R., Johnson, E. and Milbrandt, J. (2002). Artemin is a vascular-derived neurotropic factor for developing sympathetic neurons. *Neuron* **35**, 267-82.

Houck, K. A., Leung, D. W., Rowland, A. M., Winer, J. and Ferrara, N. (1992). Dual regulation of vascular endothelial growth factor bioavailability by genetic and proteolytic mechanisms. *J Biol Chem* **267**, 26031-7.

Hu, Z., Wang, C., Xiao, Y., Sheng, N., Chen, Y., Xu, Y., Zhang, L., Mo, W., Jing, N. and Hu, G. (2009). NDST1-dependent heparan sulfate regulates BMP signaling and internalization in lung development. *J Cell Sci* **122**, 1145-54.

Huber, K. (2006). The sympathoadrenal cell lineage: specification, diversification, and new perspectives. *Dev Biol* **298**, 335-43.

Ieda, M., Fukuda, K., Hisaka, Y., Kimura, K., Kawaguchi, H., Fujita, J., Shimoda, K., Takeshita, E., Okano, H., Kurihara, Y. et al. (2004). Endothelin-1 regulates cardiac sympathetic innervation in the rodent heart by controlling nerve growth factor expression. *J Clin Invest* **113**, 876-84.

Ieda, M., Kanazawa, H., Kimura, K., Hattori, F., Ieda, Y., Taniguchi, M., Lee, J. K., Matsumura, K., Tomita, Y., Miyoshi, S. et al. (2007). Sema3a maintains normal heart rhythm through sympathetic innervation patterning. *Nat Med* **13**, 604-12.

Ikenouchi, J., Matsuda, M., Furuse, M. and Tsukita, S. (2003). Regulation of tight junctions during the epithelium-mesenchyme transition: direct repression of the gene expression of claudins/occludin by Snail. *J Cell Sci* **116**, 1959-67.

Inatani, M., Irie, F., Plump, A. S., Tessier-Lavigne, M. and Yamaguchi, Y. (2003). Mammalian brain morphogenesis and midline axon guidance require heparan sulfate. *Science* **302**, 1044-6.

Ito, T., Kagoshima, M., Sasaki, Y., Li, C., Udaka, N., Kitsukawa, T., Fujisawa, H., Taniguchi, M., Yagi, T., Kitamura, H. et al. (2000). Repulsive axon guidance molecule Sema3A inhibits branching morphogenesis of fetal mouse lung. *Mech Dev* **97**, 35-45.

Ivins, J. K., Litwack, E. D., Kumbasar, A., Stipp, C. S. and Lander, A. D. (1997). Cerebroglycan, a developmentally regulated cell-surface heparan sulfate proteoglycan, is expressed on developing axons and growth cones. *Dev Biol* **184**, 320-32.

Jakobsson, L., Kreuger, J., Holmborn, K., Lundin, L., Eriksson, I., Kjellen, L. and Claesson-Welsh, L. (2006). Heparan sulfate in trans potentiates VEGFR-mediated angiogenesis. *Dev Cell* **10**, 625-34.

Jen, Y. H., Musacchio, M. and Lander, A. D. (2009). Glypican-1 controls brain size through regulation of fibroblast growth factor signaling in early neurogenesis. *Neural Dev* **4**, 33.

Jia, L., Cheng, L. and Raper, J. (2005). Slit/Robo signaling is necessary to confine early neural crest cells to the ventral migratory pathway in the trunk. *Dev Biol* **282**, 411-21.

Jiang, Y., Liu, M. T. and Gershon, M. D. (2003). Netrins and DCC in the guidance of migrating neural crest-derived cells in the developing bowel and pancreas. *Dev Biol* **258**, 364-84.

Kagoshima, M. and Ito, T. (2001). Diverse gene expression and function of semaphorins in developing lung: positive and negative regulatory roles of semaphorins in lung branching morphogenesis. *Genes Cells* **6**, 559-71.

Kalcheim, C. and Teillet, M. A. (1989). Consequences of somite manipulation on the pattern of dorsal root ganglion development. *Development* **106**, 85-93.

Karkkainen, M. J., Haiko, P., Sainio, K., Partanen, J., Taipale, J., Petrova, T. V., Jeltsch, M., Jackson, D. G., Talikka, M., Rauvala, H. et al. (2004). Vascular endothelial growth factor C is required for sprouting of the first lymphatic vessels from embryonic veins. *Nat Immunol* **5**, 74-80.

Karpanen, T., Heckman, C. A., Keskitalo, S., Jeltsch, M., Ollila, H., Neufeld, G., Tamagnone, L. and Alitalo, K. (2006). Functional interaction of VEGF-C and VEGF-D with neuropilin receptors. *FASEB J* **20**, 1462-72.

Kasemeier-Kulesa, J. C., Kulesa, P. M. and Lefcort, F. (2005). Imaging neural crest cell dynamics during formation of dorsal root ganglia and sympathetic ganglia. *Development* **132**, 235-45.

Kasemeier-Kulesa, J. C., McLennan, R., Romine, M. H., Kulesa, P. M. and Lefcort, F. (2010). CXCR4 controls ventral migration of sympathetic precursor cells. *J Neurosci* **30**, 13078-88.

Kawakami, A., Kitsukawa, T., Takagi, S. and Fujisawa, H. (1996). Developmentally regulated expression of a cell surface protein, neuropilin, in the mouse nervous system. *J Neurobiol* **29**, 1-17.

Kawasaki, T., Bekku, Y., Suto, F., Kitsukawa, T., Taniguchi, M., Nagatsu, I., Nagatsu, T., Itoh, K., Yagi, T. and Fujisawa, H. (2002). Requirement of neuropilin 1-mediated Sema3A signals in patterning of the sympathetic nervous system. *Development* **129**, 671-80.

Kawasaki, T., Kitsukawa, T., Bekku, Y., Matsuda, Y., Sanbo, M., Yagi, T. and Fujisawa, H. (1999). A requirement for neuropilin-1 in embryonic vessel formation. *Development* **126**, 4895-902.

Kelsh, R. N. (2006). Sorting out Sox10 functions in neural crest development. *Bioessays* **28**, 788-98.

Keynes, R. J. and Stern, C. D. (1984). Segmentation in the vertebrate nervous system. *Nature* **310**, 786-9.

Kisanuki, Y. Y., Hammer, R. E., Miyazaki, J., Williams, S. C., Richardson, J. A. and Yanagisawa, M. (2001). Tie2-Cre transgenic mice: a new model for endothelial cell-lineage analysis in vivo. *Dev Biol* **230**, 230-42.

Kitsukawa, T., Shimizu, M., Sanbo, M., Hirata, T., Taniguchi, M., Bekku, Y., Yagi, T. and Fujisawa, H. (1997). Neuropilin-semaphorin III/D-mediated chemorepulsive signals play a crucial role in peripheral nerve projection in mice. *Neuron* **19**, 995-1005.

Kitsukawa, T., Shimono, A., Kawakami, A., Kondoh, H. and Fujisawa, H. (1995). Overexpression of a membrane protein, neuropilin, in chimeric mice causes anomalies in the cardiovascular system, nervous system and limbs. *Development* **121**, 4309-18.

Kolodkin, A. L., Levengood, D. V., Rowe, E. G., Tai, Y. T., Giger, R. J. and Ginty, D. D. (1997). Neuropilin is a semaphorin III receptor. *Cell* **90**, 753-62.

Kos, R., Reedy, M. V., Johnson, R. L. and Erickson, C. A. (2001). The winged-helix transcription factor FoxD3 is important for establishing the neural crest lineage and repressing melanogenesis in avian embryos. *Development* **128**, 1467-79.

Krispin, S., Nitzan, E., Kassem, Y. and Kalcheim, C. (2010). Evidence for a dynamic spatiotemporal fate map and early fate restrictions of premigratory avian neural crest. *Development* **137**, 585-95.

Krull, C. E., Lansford, R., Gale, N. W., Collazo, A., Marcelle, C., Yancopoulos, G. D., Fraser, S. E. and Bronner-Fraser, M. (1997). Interactions of Eph-related receptors and ligands confer rostrocaudal pattern to trunk neural crest migration. *Curr Biol* **7**, 571-80.

Kubota, Y., Morita, T. and Ito, K. (1996). New monoclonal antibody (4E9R) identifies mouse neural crest cells. *Dev Dyn* **206**, 368-78.

Kulesa, P. M., Lefcort, F. and Kasemeier-Kulesa, J. C. (2009). The migration of autonomic precursor cells in the embryo. *Auton Neurosci* **151**, 3-9.

Kuriyama, S. and Mayor, R. (2008). Molecular analysis of neural crest migration. *Philos Trans R Soc Lond B Biol Sci* **363**, 1349-62.

Kusche, M. and Lindahl, U. (1990). Biosynthesis of heparin. O-sulfation of D-glucuronic acid units. *J Biol Chem* **265**, 15403-9.

Kutschera, S., Weber, H., Weick, A., De Smet, F., Genove, G., Takemoto, M., Prahst, C., Riedel, M., Mikelis, C., Baulande, S. et al. (2011). Differential Endothelial Transcriptomics Identifies Semaphorin 3G as a Vascular Class 3 Semaphorin. *Arterioscler Thromb Vasc Biol* **31**, 151-9.

Lamanna, W. C., Baldwin, R. J., Padva, M., Kalus, I., Ten Dam, G., van Kuppevelt, T. H., Gallagher, J. T., von Figura, K., Dierks, T. and Merry, C. L. (2006). Heparan sulfate 6-O-endosulfatases: discrete in vivo activities and functional co-operativity. *Biochem J* **400**, 63-73.

Leighton, P. A., Mitchell, K. J., Goodrich, L. V., Lu, X., Pinson, K., Scherz, P., Skarnes, W. C. and Tessier-Lavigne, M. (2001). Defining brain wiring patterns and mechanisms through gene trapping in mice. *Nature* **410**, 174-9.

Li, J. P., Gong, F., Hagner-McWhirter, A., Forsberg, E., Abrink, M., Kisilevsky, R., Zhang, X. and Lindahl, U. (2003). Targeted disruption of a murine glucuronyl C5-epimerase gene results in heparan sulfate lacking L-iduronic acid and in neonatal lethality. *J Biol Chem* **278**, 28363-6.

Lidholt, K. and Lindahl, U. (1992). Biosynthesis of heparin. The D-glucuronosyl- and N-acetyl-D-glucosaminyltransferase reactions and their relation to polymer modification. *Biochem J* **287 (Pt 1)**, 21-9.

Liem, K. F., Jr., Tremml, G., Roelink, H. and Jessell, T. M. (1995). Dorsal differentiation of neural plate cells induced by BMP-mediated signals from epidermal ectoderm. *Cell* **82**, 969-79.

Lin, X. (2004). Functions of heparan sulfate proteoglycans in cell signaling during development. *Development* **131**, 6009-21.

Lin, X., Wei, G., Shi, Z., Dryer, L., Esko, J. D., Wells, D. E. and Matzuk, M. M. (2000). Disruption of gastrulation and heparan sulfate biosynthesis in EXT1-deficient mice. *Dev Biol* **224**, 299-311.

Lind, T., Tufaro, F., McCormick, C., Lindahl, U. and Lidholt, K. (1998). The putative tumor suppressors EXT1 and EXT2 are glycosyltransferases required for the biosynthesis of heparan sulfate. *J Biol Chem* **273**, 26265-8.

Lindahl, U., Kusche, M., Lidholt, K. and Oscarsson, L. G. (1989). Biosynthesis of heparin and heparan sulfate. *Ann N Y Acad Sci* **556**, 36-50.

Lindblom, P., Gerhardt, H., Liebner, S., Abramsson, A., Enge, M., Hellstrom, M., Backstrom, G., Fredriksson, S., Landegren, U., Nystrom, H. C. et al. (2003). Endothelial PDGF-B retention is required for proper investment of pericytes in the microvessel wall. *Genes Dev* **17**, 1835-40.

Lo, L. C., Johnson, J. E., Wuenschell, C. W., Saito, T. and Anderson, D. J. (1991). Mammalian achaete-scute homolog 1 is transiently expressed by spatially restricted subsets of early neuroepithelial and neural crest cells. *Genes Dev* **5**, 1524-37.

Long, J. B., Jay, S. M., Segal, S. S. and Madri, J. A. (2009). VEGF-A and Semaphorin3A: modulators of vascular sympathetic innervation. *Dev Biol* **334**, 119-32.

Luo, G., Hofmann, C., Bronckers, A. L., Sohocki, M., Bradley, A. and Karsenty, G. (1995). BMP-7 is an inducer of nephrogenesis, and is also required for eye development and skeletal patterning. *Genes Dev* **9**, 2808-20.

Luo, Y., Raible, D. and Raper, J. A. (1993). Collapsin: a protein in brain that induces the collapse and paralysis of neuronal growth cones. *Cell* **75**, 217-27.

Makita, T., Sucov, H. M., Gariepy, C. E., Yanagisawa, M. and Ginty, D. D. (2008). Endothelins are vascular-derived axonal guidance cues for developing sympathetic neurons. *Nature* **452**, 759-63.

Mamluk, R., Gechtman, Z., Kutcher, M. E., Gasiunas, N., Gallagher, J. and Klagsbrun, M. (2002). Neuropilin-1 binds vascular endothelial growth factor 165, placenta growth factor-2, and heparin via its b1b2 domain. *J Biol Chem* **277**, 24818-25.

Marko, S. B. and Damon, D. H. (2008). VEGF promotes vascular sympathetic innervation. *Am J Physiol Heart Circ Physiol* **294**, H2646-52.

Matsuda, I., Fukaya, M., Nakao, H., Nakao, K., Matsumoto, H., Mori, K., Watanabe, M. and Aiba, A. (2010). Development of the somatosensory cortex, the cerebellum, and the main olfactory system in Semaphorin 3F knockout mice. *Neurosci Res* **66**, 321-9.

Matthews, H. K., Marchant, L., Carmona-Fontaine, C., Kuriyama, S., Larrain, J., Holt, M. R., Parsons, M. and Mayor, R. (2008). Directional migration of neural crest cells in vivo is regulated by Syndecan-4/Rac1 and non-canonical Wnt signaling/RhoA. *Development* **135**, 1771-80.

McCormick, C., Duncan, G., Goutsos, K. T. and Tufaro, F. (2000). The putative tumor suppressors EXT1 and EXT2 form a stable complex that accumulates in the Golgi apparatus and catalyzes the synthesis of heparan sulfate. *Proc Natl Acad Sci U S A* **97**, 668-73.

McLennan, R. and Kulesa, P. M. (2007). In vivo analysis reveals a critical role for neuropilin-1 in cranial neural crest cell migration in chick. *Dev Biol* **301**, 227-39.

McPherson, C. E., Varley, J. E. and Maxwell, G. D. (2000). Expression and regulation of type I BMP receptors during early avian sympathetic ganglion development. *Dev Biol* **221**, 220-32.

Merry, C. L., Bullock, S. L., Swan, D. C., Backen, A. C., Lyon, M., Beddington, R. S., Wilson, V. A. and Gallagher, J. T. (2001). The molecular phenotype of heparan sulfate in the Hs2st-/- mutant mouse. *J Biol Chem* **276**, 35429-34.

Merry, C. L. and Wilson, V. A. (2002). Role of heparan sulfate-2-O-sulfotransferase in the mouse. *Biochim Biophys Acta* **1573**, 319-27.

Mitchell, K. J., Pinson, K. I., Kelly, O. G., Brennan, J., Zupicich, J., Scherz, P., Leighton, P. A., Goodrich, L. V., Lu, X., Avery, B. J. et al. (2001). Functional analysis of secreted and transmembrane proteins critical to mouse development. *Nat Genet* **28**, 241-9.

Mitchell, P. J., Timmons, P. M., Hebert, J. M., Rigby, P. W. and Tjian, R. (1991). Transcription factor AP-2 is expressed in neural crest cell lineages during mouse embryogenesis. *Genes Dev* **5**, 105-19.

Monsoro-Burq, A. H., Wang, E. and Harland, R. (2005). Msx1 and Pax3 cooperate to mediate FGF8 and WNT signals during Xenopus neural crest induction. *Dev Cell* **8**, 167-78.

Morikawa, Y., D'Autreaux, F., Gershon, M. D. and Cserjesi, P. (2007). Hand2 determines the noradrenergic phenotype in the mouse sympathetic nervous system. *Dev Biol* **307**, 114-26.

Morikawa, Y., Zehir, A., Maska, E., Deng, C., Schneider, M. D., Mishina, Y. and Cserjesi, P. (2009). BMP signaling regulates sympathetic nervous system development through Smad4-dependent and -independent pathways. *Development* **136**, 3575-84.

Morin, X., Cremer, H., Hirsch, M. R., Kapur, R. P., Goridis, C. and Brunet, J. F. (1997). Defects in sensory and autonomic ganglia and absence of locus coeruleus in mice deficient for the homeobox gene Phox2a. *Neuron* **18**, 411-23.

Muthusamy, A., Cooper, C. R. and Gomes, R. R., Jr. (2010). Soluble perlecan domain i enhances vascular endothelial growth factor-165 activity and receptor phosphorylation in human bone marrow endothelial cells. *BMC Biochem* **11**, 43.

Nadanaka, S. and Kitagawa, H. (2008). Heparan sulphate biosynthesis and disease. *J Biochem* **144**, 7-14.

Nagy, A. (2000). Cre recombinase: the universal reagent for genome tailoring. *Genesis* **26**, 99-109.

Nakata, K., Nagai, T., Aruga, J. and Mikoshiba, K. (1998). Xenopus Zic family and its role in neural and neural crest development. *Mech Dev* **75**, 43-51.

Nakaya, Y. and Sheng, G. (2008). Epithelial to mesenchymal transition during gastrulation: an embryological view. *Dev Growth Differ* **50**, 755-66.

Nasevicius, A., Larson, J. and Ekker, S. C. (2000). Distinct requirements for zebrafish angiogenesis revealed by a VEGF-A morphant. *Yeast* **17**, 294-301.

Neufeld, G., Cohen, T., Gengrinovitch, S. and Poltorak, Z. (1999). Vascular endothelial growth factor (VEGF) and its receptors. *FASEB J* **13**, 9-22.

Neufeld, G., Kessler, O. and Herzog, Y. (2002). The interaction of Neuropilin-1 and Neuropilin-2 with tyrosine-kinase receptors for VEGF. *Adv Exp Med Biol* **515**, 81-90.

Newgreen, D. F., Gibbins, I. L., Sauter, J., Wallenfels, B. and Wutz, R. (1982). Ultrastructural and tissue-culture studies on the role of fibronectin, collagen and glycosaminoglycans in the migration of neural crest cells in the fowl embryo. *Cell Tissue Res* **221**, 521-49.

Nuwayhid, N., Glaser, J. H., Johnson, J. C., Conrad, H. E., Hauser, S. C. and Hirschberg, C. B. (1986). Xylosylation and glucuronosylation reactions in rat liver Golgi apparatus and endoplasmic reticulum. *J Biol Chem* **261**, 12936-41.

Osborne, N. J., Begbie, J., Chilton, J. K., Schmidt, H. and Eickholt, B. J. (2005). Semaphorin/neuropilin signaling influences the positioning of migratory neural crest cells within the hindbrain region of the chick. *Dev Dyn* **232**, 939-49.

Park, J. E., Keller, G. A. and Ferrara, N. (1993). The vascular endothelial growth factor (VEGF) isoforms: differential deposition into the subepithelial extracellular matrix and bioactivity of extracellular matrix-bound VEGF. *Mol Biol Cell* **4**, 1317-26.

Pattyn, A., Morin, X., Cremer, H., Goridis, C. and Brunet, J. F. (1999). The homeobox gene Phox2b is essential for the development of autonomic neural crest derivatives. *Nature* **399**, 366-70.

Peirson, S. N., Butler, J. N. and Foster, R. G. (2003). Experimental validation of novel and conventional approaches to quantitative real-time PCR data analysis. *Nucleic Acids Res* **31**, e73.

Petersen, P. H., Zou, K., Hwang, J. K., Jan, Y. N. and Zhong, W. (2002). Progenitor cell maintenance requires numb and numblike during mouse neurogenesis. *Nature* **419**, 929-34.

Pikas, D. S., Eriksson, I. and Kjellen, L. (2000). Overexpression of different isoforms of glucosaminyl N-deacetylase/N-sulfotransferase results in distinct heparan sulfate N-sulfation patterns. *Biochemistry* **39**, 4552-8.

Pratt, T., Conway, C. D., Tian, N. M., Price, D. J. and Mason, J. O. (2006). Heparan sulphation patterns generated by specific heparan sulfotransferase enzymes direct distinct aspects of retinal axon guidance at the optic chiasm. *J Neurosci* **26**, 6911-23.

Raab, S., Beck, H., Gaumann, A., Yuce, A., Gerber, H. P., Plate, K., Hammes, H. P., Ferrara, N. and Breier, G. (2004). Impaired brain angiogenesis and neuronal apoptosis induced by conditional homozygous inactivation of vascular endothelial growth factor. *Thromb Haemost* **91**, 595-605.

Ragland, J. W. and Raible, D. W. (2004). Signals derived from the underlying mesoderm are dispensable for zebrafish neural crest induction. *Dev Biol* **276**, 16-30.

Raman, R., Venkataraman, G., Ernst, S., Sasisekharan, V. and Sasisekharan, R. (2003). Structural specificity of heparin binding in the fibroblast growth factor family of proteins. *Proc Natl Acad Sci U S A* **100**, 2357-62.

Randall, W. C., Szentivanyi, M., Pace, J. B., Wechsler, J. S. and Kaye, M. P. (1968). Patterns of sympathetic nerve projections onto the canine heart. *Circ Res* **22**, 315-23.

Rapraeger, A. C., Krufka, A. and Olwin, B. B. (1991). Requirement of heparan sulfate for bFGF-mediated fibroblast growth and myoblast differentiation. *Science* **252**, 1705-8.

Reissmann, E., Ernsberger, U., Francis-West, P. H., Rueger, D., Brickell, P. M. and Rohrer, H. (1996). Involvement of bone morphogenetic protein-4 and bone morphogenetic protein-7 in the differentiation of the adrenergic phenotype in developing sympathetic neurons. *Development* **122**, 2079-88.

Rickmann, M., Fawcett, J. W. and Keynes, R. J. (1985). The migration of neural crest cells and the growth of motor axons through the rostral half of the chick somite. *J Embryol Exp Morphol* **90**, 437-55.

Ringvall, M., Ledin, J., Holmborn, K., van Kuppevelt, T., Ellin, F., Eriksson, I., Olofsson, A. M., Kjellen, L. and Forsberg, E. (2000). Defective heparan sulfate biosynthesis and neonatal lethality in mice lacking N-deacetylase/N-sulfotransferase-1. *J Biol Chem* **275**, 25926-30.

Risau, W. (1997). Mechanisms of angiogenesis. *Nature* **386**, 671-4.

Robinson, C. J., Mulloy, B., Gallagher, J. T. and Stringer, S. E. (2006). VEGF165-binding sites within heparan sulfate encompass two highly sulfated domains and can be liberated by K5 lyase. *J Biol Chem* **281**, 1731-40.

Rossignol, M., Gagnon, M. L. and Klagsbrun, M. (2000). Genomic organization of human neuropilin-1 and neuropilin-2 genes: identification and distribution of splice variants and soluble isoforms. *Genomics* **70**, 211-22.

Rovasio, R. A., Delouvee, A., Yamada, K. M., Timpl, R. and Thiery, J. P. (1983). Neural crest cell migration: requirements for exogenous fibronectin and high cell density. *J Cell Biol* **96**, 462-73.

Ruhrberg, C., Gerhardt, H., Golding, M., Watson, R., Ioannidou, S., Fujisawa, H., Betsholtz, C. and Shima, D. T. (2002). Spatially restricted patterning cues provided by heparin-binding VEGF-A control blood vessel branching morphogenesis. *Genes Dev* **16**, 2684-98.

Ruiz de Almodovar, C., Coulon, C., Salin, P. A., Knevels, E., Chounlamountri, N., Poesen, K., Hermans, K., Lambrechts, D., Van Geyte, K., Dhondt, J. et al. (2010). Matrix-binding vascular endothelial growth factor (VEGF) isoforms guide granule cell migration in the cerebellum via VEGF receptor Flk1. *J Neurosci* **30**, 15052-66.

Safaiyan, F., Lindahl, U. and Salmivirta, M. (2000). Structural diversity of N-sulfated heparan sulfate domains: distinct modes of glucuronyl C5 epimerization, iduronic acid 2-O-sulfation, and glucosamine 6-O-sulfation. *Biochemistry* **39**, 10823-30.

Sahay, A., Molliver, M. E., Ginty, D. D. and Kolodkin, A. L. (2003). Semaphorin 3F is critical for development of limbic system circuitry and is required in neurons for selective CNS axon guidance events. *J Neurosci* **23**, 6671-80.

Sakai, D., Suzuki, T., Osumi, N. and Wakamatsu, Y. (2006). Cooperative action of Sox9, Snail2 and PKA signaling in early neural crest development. *Development* **133**, 1323-33.

Santiago, A. and Erickson, C. A. (2002). Ephrin-B ligands play a dual role in the control of neural crest cell migration. *Development* **129**, 3621-32.

Schilling, T. F. and Kimmel, C. B. (1994). Segment and cell type lineage restrictions during pharyngeal arch development in the zebrafish embryo. *Development* **120**, 483-94.

Schmidt, C. (2008). The role of Wnt signalling in the development of somites and neural crest. Berlin: Springer.

Schmidt, C., McGonnell, I. M., Allen, S., Otto, A. and Patel, K. (2007). Wnt6 controls amniote neural crest induction through the non-canonical signaling pathway. *Dev Dyn* **236**, 2502-11.

Schneider, C., Wicht, H., Enderich, J., Wegner, M. and Rohrer, H. (1999). Bone morphogenetic proteins are required in vivo for the generation of sympathetic neurons. *Neuron* **24**, 861-70.

Schwarz, Q., Gu, C., Fujisawa, H., Sabelko, K., Gertsenstein, M., Nagy, A., Taniguchi, M., Kolodkin, A. L., Ginty, D. D., Shima, D. T. et al. (2004). Vascular endothelial growth factor controls neuronal migration and cooperates with Sema3A to pattern distinct compartments of the facial nerve. *Genes Dev* **18**, 2822-34.

Schwarz, Q., Maden, C. H., Davidson, K. and Ruhrberg, C. (2009a). Neuropilin-mediated neural crest cell guidance is essential to organise sensory neurons into segmented dorsal root ganglia. *Development* **136**, 1785-9.

Schwarz, Q., Maden, C. H., Vieira, J. M. and Ruhrberg, C. (2009b). Neuropilin 1 signaling guides neural crest cells to coordinate pathway choice with cell specification. *Proc Natl Acad Sci U S A* **106**, 6164-9.

Schwarz, Q. and Ruhrberg, C. (2010). Neuropilin, you gotta let me know: should I stay or should I go? *Cell Adh Migr* **4**, 61-6.

Schwarz, Q., Vieira, J. M., Howard, B., Eickholt, B. J. and Ruhrberg, C. (2008a). Neuropilin 1 and 2 control cranial gangliogenesis and axon guidance through neural crest cells. *Development* **135**, 1605-13.

Schwarz, Q., Waimey, K. E., Golding, M., Takamatsu, H., Kumanogoh, A., Fujisawa, H., Cheng, H. J. and Ruhrberg, C. (2008b). Plexin A3 and plexin A4 convey semaphorin signals during facial nerve development. *Dev Biol* **324**, 1-9.

Sedita, J., Izvolsky, K. and Cardoso, W. V. (2004). Differential expression of heparan sulfate 6-O-sulfotransferase isoforms in the mouse embryo suggests distinctive roles during organogenesis. *Dev Dyn* **231**, 782-94.

Selever, J., Liu, W., Lu, M. F., Behringer, R. R. and Martin, J. F. (2004). Bmp4 in limb bud mesoderm regulates digit pattern by controlling AER development. *Dev Biol* **276**, 268-79.

Shah, N. M., Groves, A. K. and Anderson, D. J. (1996). Alternative neural crest cell fates are instructively promoted by TGFbeta superfamily members. *Cell* **85**, 331-43.

Shworak, N. W., Liu, J., Petros, L. M., Zhang, L., Kobayashi, M., Copeland, N. G., Jenkins, N. A. and Rosenberg, R. D. (1999). Multiple isoforms of heparan sulfate D-glucosaminyl 3-O-sulfotransferase. Isolation, characterization, and expression of human cdnas and identification of distinct genomic loci. *J Biol Chem* **274**, 5170-84.

Smith, M. A. and Hilgenberg, L. G. (2002). Agrin in the CNS: a protein in search of a function? *Neuroreport* **13**, 1485-95.

Soker, S., Fidder, H., Neufeld, G. and Klagsbrun, M. (1996). Characterization of novel vascular endothelial growth factor (VEGF) receptors on tumor cells that bind VEGF165 via its exon 7-encoded domain. *J Biol Chem* **271**, 5761-7.

Soker, S., Takashima, S., Miao, H. Q., Neufeld, G. and Klagsbrun, M. (1998). Neuropilin-1 is expressed by endothelial and tumor cells as an isoform-specific receptor for vascular endothelial growth factor. *Cell* **92**, 735-45.

Southard-Smith, E. M., Kos, L. and Pavan, W. J. (1998). Sox10 mutation disrupts neural crest development in Dom Hirschsprung mouse model. *Nat Genet* **18**, 60-4.

Stallcup, W. B. (2002). The NG2 proteoglycan: past insights and future prospects. *J Neurocytol* **31**, 423-35.

Stenzel, D., Nye, E., Nisancioglu, M., Adams, R. H., Yamaguchi, Y. and Gerhardt, H. (2009). Peripheral mural cell recruitment requires cell-autonomous heparan sulfate. *Blood* **114**, 915-24.

Steventon, B., Araya, C., Linker, C., Kuriyama, S. and Mayor, R. (2009). Differential requirements of BMP and Wnt signalling during gastrulation and neurulation define two steps in neural crest induction. *Development* **136**, 771-9.

Takahashi, T., Fournier, A., Nakamura, F., Wang, L. H., Murakami, Y., Kalb, R. G., Fujisawa, H. and Strittmatter, S. M. (1999). Plexin-neuropilin-1 complexes form functional semaphorin-3A receptors. *Cell* **99**, 59-69.

Takahashi, T., Nakamura, F., Jin, Z., Kalb, R. G. and Strittmatter, S. M. (1998). Semaphorins A and E act as antagonists of neuropilin-1 and agonists of neuropilin-2 receptors. *Nat Neurosci* **1**, 487-93.

Takashima, S., Kitakaze, M., Asakura, M., Asanuma, H., Sanada, S., Tashiro, F., Niwa, H., Miyazaki Ji, J., Hirota, S., Kitamura, Y. et al. (2002). Targeting of both mouse neuropilin-1 and neuropilin-2 genes severely impairs developmental yolk sac and embryonic angiogenesis. *Proc Natl Acad Sci U S A* **99**, 3657-62.

Taneyhill, L. A., Coles, E. G. and Bronner-Fraser, M. (2007). Snail2 directly represses cadherin6B during epithelial-to-mesenchymal transitions of the neural crest. *Development* **134**, 1481-90.

Taniguchi, M., Masuda, T., Fukaya, M., Kataoka, H., Mishina, M., Yaginuma, H., Watanabe, M. and Shimizu, T. (2005). Identification and characterization of a novel member of murine semaphorin family. *Genes Cells* **10**, 785-92.

Taniguchi, M., Yuasa, S., Fujisawa, H., Naruse, I., Saga, S., Mishina, M. and Yagi, T. (1997). Disruption of semaphorin III/D gene causes severe abnormality in peripheral nerve projection. *Neuron* **19**, 519-30.

Terman, B. I., Dougher-Vermazen, M., Carrion, M. E., Dimitrov, D., Armellino, D. C., Gospodarowicz, D. and Bohlen, P. (1992). Identification of the KDR tyrosine kinase as a receptor for vascular endothelial cell growth factor. *Biochem Biophys Res Commun* **187**, 1579-86.

Tessler, S., Rockwell, P., Hicklin, D., Cohen, T., Levi, B. Z., Witte, L., Lemischka, I. R. and Neufeld, G. (1994). Heparin modulates the interaction of VEGF165 with soluble and cell associated flk-1 receptors. *J Biol Chem* **269**, 12456-61.

Tsarovina, K., Pattyn, A., Stubbusch, J., Muller, F., van der Wees, J., Schneider, C., Brunet, J. F. and Rohrer, H. (2004). Essential role of Gata transcription factors in sympathetic neuron development. *Development* **131**, 4775-86.

Vieira, J. M., Schwarz, Q. and Ruhrberg, C. (2007). Selective requirements for NRP1 ligands during neurovascular patterning. *Development* **134**, 1833-43.

Villanueva, S., Glavic, A., Ruiz, P. and Mayor, R. (2002). Posteriorization by FGF, Wnt, and retinoic acid is required for neural crest induction. *Dev Biol* **241**, 289-301.

Waimey, K. E., Huang, P. H., Chen, M. and Cheng, H. J. (2008). Plexin-A3 and plexin-A4 restrict the migration of sympathetic neurons but not their neural crest precursors. *Dev Biol* **315**, 448-58.

Walz, A., Feinstein, P., Khan, M. and Mombaerts, P. (2007). Axonal wiring of guanylate cyclase-D-expressing olfactory neurons is dependent on neuropilin 2 and semaphorin 3F. *Development* **134**, 4063-72.

Wang, C. K., Omi, M., Ferrari, D., Cheng, H. C., Lizarraga, G., Chin, H. J., Upholt, W. B., Dealy, C. N. and Kosher, R. A. (2004). Function of BMPs in the apical ectoderm of the developing mouse limb. *Dev Biol* **269**, 109-22.

Wang, H. U. and Anderson, D. J. (1997). Eph family transmembrane ligands can mediate repulsive guidance of trunk neural crest migration and motor axon outgrowth. *Neuron* **18**, 383-96.

Wang, L., Mukhopadhyay, D. and Xu, X. (2006). C terminus of RGS-GAIP-interacting protein conveys neuropilin-1-mediated signaling during angiogenesis. *FASEB J* **20**, 1513-5.

Wang, Q., Fang, W. H., Krupinski, J., Kumar, S., Slevin, M. and Kumar, P. (2008). Pax genes in embryogenesis and oncogenesis. *J Cell Mol Med* **12**, 2281-94.

West, D. C., Rees, C. G., Duchesne, L., Patey, S. J., Terry, C. J., Turnbull, J. E., Delehedde, M., Heegaard, C. W., Allain, F., Vanpouille, C. et al. (2005). Interactions of multiple heparin binding growth factors with neuropilin-1 and potentiation of the activity of fibroblast growth factor-2. *J Biol Chem* **280**, 13457-64.

Weston, J. A. (1991). Sequential segregation and fate of developmentally restricted intermediate cell populations in the neural crest lineage. *Curr Top Dev Biol* **25**, 133-53.

Wilson, Y. M., Richards, K. L., Ford-Perriss, M. L., Panthier, J. J. and Murphy, M. (2004). Neural crest cell lineage segregation in the mouse neural tube. *Development* **131**, 6153-62.

Wu, J., Saint-Jeannet, J. P. and Klein, P. S. (2003). Wnt-frizzled signaling in neural crest formation. *Trends Neurosci* **26**, 40-5.

Wuenschell, C. W., Mori, N. and Anderson, D. J. (1990). Analysis of SCG10 gene expression in transgenic mice reveals that neural specificity is achieved through selective derepression. *Neuron* **4**, 595-602.

Xia, G., Chen, J., Tiwari, V., Ju, W., Li, J. P., Malmstrom, A., Shukla, D. and Liu, J. (2002). Heparan sulfate 3-O-sulfotransferase isoform 5 generates both an antithrombin-binding site and an entry receptor for herpes simplex virus, type 1. *J Biol Chem* **277**, 37912-9.

Xu, Y., Yuan, L., Mak, J., Pardanaud, L., Caunt, M., Kasman, I., Larrivee, B., Del Toro, R., Suchting, S., Medvinsky, A. et al. (2010). Neuropilin-2 mediates VEGF-C-induced lymphatic sprouting together with VEGFR3. *J Cell Biol* **188**, 115-30.

Yabe, T., Hata, T., He, J. and Maeda, N. (2005). Developmental and regional expression of heparan sulfate sulfotransferase genes in the mouse brain. *Glycobiology* **15**, 982-93.

Yamaguchi, Y. (2000). Lecticans: organizers of the brain extracellular matrix. *Cell Mol Life Sci* **57**, 276-89.

Yanowitz, F., Preston, J. B. and Abildskov, J. A. (1966). Functional distribution of right and left stellate innervation to the ventricles. Production of neurogenic electrocardiographic changes by unilateral alteration of sympathetic tone. *Circ Res* **18**, 416-28.

Yasuda, T., Mundy, C., Kinumatsu, T., Shibukawa, Y., Shibutani, T., Grobe, K., Minugh-Purvis, N., Pacifici, M. and Koyama, E. (2010). Sulfotransferase Ndst1 is Needed for Mandible and TMJ Development. *J Dent Res*.

Yayon, A., Klagsbrun, M., Esko, J. D., Leder, P. and Ornitz, D. M. (1991). Cell surface, heparin-like molecules are required for binding of basic fibroblast growth factor to its high affinity receptor. *Cell* **64**, 841-8.

Yazdani, U. and Terman, J. R. (2006). The semaphorins. *Genome Biol* **7**, 211.

Zoeller, J. J., Whitelock, J. M. and Iozzo, R. V. (2009). Perlecan regulates developmental angiogenesis by modulating the VEGF-VEGFR2 axis. *Matrix Biol* **28**, 284-91.

LIST OF SUPPORTING PUBLICATIONS

Schwarz, Q., Maden, C. H., Davidson, K. and Ruhrberg, C. (2009). Neuropilin-mediated neural crest cell guidance is essential to organise sensory neurons into segmented dorsal root ganglia. *Development* **136**, 1785-9.

Schwarz, Q., Maden, C. H., Vieira, J. M. and Ruhrberg, C. (2009). Neuropilin 1 signaling guides neural crest cells to coordinate pathway choice with cell specification. *Proc Natl Acad Sci U S A* **106**, 6164-9.

Fantin, A., Maden, C. H. and Ruhrberg, C. (2009). Neuropilin ligands in vascular and neuronal patterning. *Biochem Soc Trans* **37**, 1228-32.